



12-2000

Development of aliphatic polyketone fibers by melt spinning and drawing

Pankaj Gupta

Follow this and additional works at: https://trace.tennessee.edu/utk_gradthes

Recommended Citation

Gupta, Pankaj, "Development of aliphatic polyketone fibers by melt spinning and drawing. " Master's Thesis, University of Tennessee, 2000.
https://trace.tennessee.edu/utk_gradthes/9329

This Thesis is brought to you for free and open access by the Graduate School at TRACE: Tennessee Research and Creative Exchange. It has been accepted for inclusion in Masters Theses by an authorized administrator of TRACE: Tennessee Research and Creative Exchange. For more information, please contact trace@utk.edu.

To the Graduate Council:

I am submitting herewith a thesis written by Pankaj Gupta entitled "Development of aliphatic polyketone fibers by melt spinning and drawing." I have examined the final electronic copy of this thesis for form and content and recommend that it be accepted in partial fulfillment of the requirements for the degree of Master of Science, with a major in Polymer Engineering.

J. E. Spruiell, Major Professor

We have read this thesis and recommend its acceptance:

Gajannan Bhat, K. Kit

Accepted for the Council:

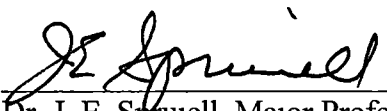
Carolyn R. Hodges

Vice Provost and Dean of the Graduate School

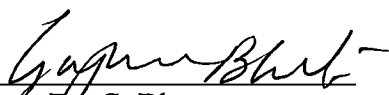
(Original signatures are on file with official student records.)

To the Graduate Council

I am submitting herewith a dissertation written by Pankaj Gupta entitled "Development of Aliphatic Polyketone Fibers by Melt Spinning and Drawing." I have examined the final copy of this dissertation for form and content and recommend that it be accepted in partial fulfillment of the requirements for the degree of Master of Science, with a major in Polymer Engineering

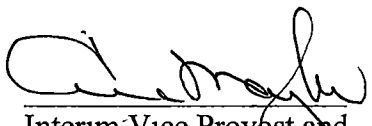

Dr. J. E. Spruiell, Major Professor

We have read this dissertation
and recommend its acceptance


Dr. G. Bhat


Dr. K. Kit

Accepted for the Council


Interim Vice Provost and
Dean of the Graduate School

**DEVELOPMENT OF ALIPHATIC POLYKETONE
FIBERS BY MELT SPINNING AND DRAWING**

A Thesis

Presented for the

Master of Science

Degree

The University of Tennessee, Knoxville

Pankaj Gupta

December, 2000

ACKNOWLEDGEMENTS

I would like to thank my advisor, Dr J E. Spruiell, whose guidance and expertise helped me through with this work. Thanks goes to Shell Chemical Company for funding and materials used in this study. Special thanks go to John Flood and JeriAnne Schulte who provided much help and encouragement.

I would like to thank Mike Neil, Greg Jones and Doug Fielden for their technical support and to Phillips Inc., who were kind enough to provide the x-ray intensity scans for some of my samples. And most of all, I thank my parents and friends for their love and support.

ABSTRACT

Aliphatic polyketones are a class of perfectly alternating co- and ter-polymers that have ethylene and carbon monoxide as the main repeat units. In the terpolymer, a small amount of propylene is added to improve the chain flexibility and to reduce the melting point.

Melt spinning followed by drawing of polyketones yields filaments that have high tensile strength that could be used for industrial applications such as tire cords. Polyketones as resins have extremely good chemical, hydrolytic, barrier and mechanical properties. In this study an attempt is made to investigate whether these polymers could be formed into a high-tenacity industrial grade fiber. Spinning and post spinning operations like drawing and heat setting have been optimized so that the resulting fibers have good mechanical properties. Characterization of the filaments was done using a number of techniques to study the structure development of the fibers with drawing. The purpose of this study was, therefore, to optimize the processing conditions and thereafter investigate the structure-property relationship of both the copolymer and the terpolymer fibers. The effects of molecular weight, propylene content, draw ratio and draw temperatures on the structure were also investigated.

Four different grades of aliphatic polyketones were investigated in this study. The melt spun as-spun copolymer fibers have both α and β phases at room temperature. The high draw ratio copolymer fibers have predominantly the α phase. The terpolymer fibers have β phase at all temperatures and preparation conditions.

The lattice parameters were measured for one of the terpolymer grades and they are in agreement with those obtained by other authors. The melting behavior of the as spun samples of both the co and terpolymer samples show a bi-modal peak distribution.

Birefringence and WAXS analysis indicate an increase in the orientation with draw ratio for all the sample grades. Microfibrillar structure develops with increasing draw ratio. This was also corroborated by the two-point small angle x-ray scattering contour plots. However, at high draw ratios the meridian peaks in the SAXS contour plots weaken indicating an increase in the order in the non-crystalline regions. A strong correlation was found between the orientation and tensile strength and modulus of the fibers. Fibers having tenacity in the range of 9-11 gpd were obtained. Another notable feature is the retention of their strength at elevated temperatures. It was observed that these fibers retain 85-90 % of their original strength till a temperature of 125 °C. The terpolymer fibers were comparatively stronger than the copolymer fibers both in terms of strength and modulus.

TABLE OF CONTENTS

Chapter	Page
1. Introduction	1
2. Review of Literature	4
2.1 History	4
2.2 Classification	5
2.3 Synthesis	5
2.3.1 Non-Alternating Ethylene/ Carbon monoxide copolymers	5
2.3.2 Alternating Ethylene/Carbon monoxide copolymers ..	7
2.3.2.1 Catalyst System	7
2.3.2.2 Polymerization Mechanism	9
2.4 Crystal Structure	14
2.5 Polymorphism	17
2.6 Morphology	17
2.7 Properties	19
2.7.1 Fundamental Properties	19
2.7.2 Material Properties	20
2.8 Processability	22
2.9 Decomposition	22
2.10 Preparation of polyketone fibers	23
3. Materials, Processing and Characterization	25
3.1 Materials	25

3.2	Processing	26
3.2.1	Melt spinning	26
3.2.2	Drawing	28
3.3	Characterization Techniques	31
3.3.1	X-Ray Scattering	31
3.3.1.1	Wide Angle X-Ray diffraction (WAXD).	31
3.3.1.2	Small Angle X-Ray diffraction	35
3.3.2	Orientation	35
3.3.2.1	Axial Orientation Functions	35
3.3.2.2	Birefringence	43
3.3.3	Thermal Analysis	44
3.3.4	Tensile Testing	45
3.3.4.1	Elevated Temperature Tensile Testing	45
3.3.5	Thermal Shrinkage	46
3.3.6	Electron Microscopy	47
3.3.7	Sonic Modulus	47
4.	Results and Discussion	50
4.1	Temperature Dependence of Drawing	50
4.2	Crystal Phases	52
4.3	Thermal Properties	58
4.4	Crystallinity	68
4.5	Crystalline Orientation	71

4 6	Birefringence and Amorphous Orientation	75
4 7	Lattice Cell Parameters	80
4 8	SEM Results	81
4.9	SAXS Results	83
4.10	Variation in Cryatlite size with Draw Ratio	92
4.11	Structure Development on drawing	92
4.12	Mechanical Properties	95
4 12 1	Tensile Properties at room temperature	95
4.12 2	Tensile Properties at Elevated Temperatures	103
5.	Conclusions	110
	References	113
Appendices		
1.	Calculation of the Residence time	120
2	Calculation of $\langle \cos^2 \phi_{c,z} \rangle$	123
3	Calculation of unit cell dimensions	126
Vita		129

LIST OF TABLES

Table	Page
2 1	Crystal unit cell descriptions for PK-C ₂ , PK-C ₂ /C ₃ & HDPE [33] 15
2.2	Fundamental Properties of aliphatic polyketones in comparison to other semi-crystalline polymers [35] 20
2.3	Typical Mechanical Properties of PK and other semi-crystalline polymers [35]. 21
3.1	Processing conditions for PK fibers (as used by Shell) 28
3 2	Drawing Conditions for PK-C ₂ & PK-C ₂ /C ₃ 30
4 1	Optimum Temperatures and maximum draw ratios for different polyketone grades 51
4.2	Volume and weight fractions of a and b phases in CLMW 54
4.3	Estimation of % Propylene in Terpolymer samples 68
4 4	Comparison of unit cell parameter with Lommerts and Chatani's values. 81
4 5	Long Period and Lamellar thickness with draw ratio 91
4 6	Long Period, Lamellar thickness and 002 crystallite size data of THMW. 92
4 7	Crystallite size data for the 210 crystal planes 93
4 8	Comparison of high-strength tire cord fibers with PK-C ₂ /C ₃ 103
A3 1	X-ray data for different crystal planes in oriented THMP fiber 126
A3.2	Computed lattice cell constants for oriented, THMP fiber 128

LIST OF FIGURES

Figure	Page
2.1 Structure of high productivity Shell type catalyst [5].....	9
2.2 Polymerization mechanism as proposed by Sen [20].....	10
2.3 Polymerization mechanism as proposed by Drent et al. [3]	12
2.4 Polymerization mechanism as proposed by Zhao et al. [27]	13
2.5 α & β unit cell structures of PK-C ₂	16
2.6 Calculated diffraction patterns of a (top) and b (bottom) forms, corresponding to copolymer and terpolymer respectively [34].....	18
3.1 Schematic of the Fincor-2 stage Drawing Apparatus; B Bobbin, G Guide; I, II & III three sets of rollers, T. Tensioner & W. Winder	29
3.2 WAXD in reflection and transmission modes [43]	32
3.3 WAXD flat plate film pattern showing diffraction peaks in an oriented PK-C ₂ /C ₃ fiber [47] ($\alpha = 0^\circ$)	34
3.4 Structure of oriented partially crystalline polymers from a) cold stretched, not annealed b) annealed after stretching L. Long Period [44]	36
3.5 Stein's coordinate system for specifying orientation modes in orthorhombic polymers [45]	38
3.6 (<i>hkl</i>) plane normal oriented at a latitude α or co-latitude ϕ in the sphere of reflection [46]	39
3.7 Equatorial 2θ scan of an oriented PK-C ₂ /C ₃ fiber ($\alpha = 0^\circ$).....	42
3.8 Schematic representation of Sonic modulus apparatus	48

4.1	Plot of DR Vs Temperature for different PK grades	51
4.2	Equatorial 2 θ scans of CLMW and THMW	53
4.3	Equatorial 2 θ scans of different draw ratio samples of CLMW ...	53
4.4	Equatorial 2 θ scans of different draw ratio samples of THMW	56
4.5	Equatorial 2 θ scans of different draw ratio samples of THMP	56
4.6	WAXD Flat Plate patterns of high draw ratio fibers	57
4.7	Variation of Melting point, T _m , with Draw Ratio, DR	59
4.8	DSC scans of as-spun filaments	60
4.9	DSC scans of CLMW and THMP	62
4.10	DSC scans of THMW as-spun filaments at different scan rates showing the disappearance of bi-modal melting behavior at higher scan rates	65
4.11	Variation of a) ΔH and b) peak temperatures with DSC scan rates, THMW	66
4.12	Plot of T _m Vs % Propylene	67
4.13	Variation of % Crystallinity with draw ratio, DR	70
4.14	WAXD Flat plate patterns of CLMW & THMP	72
4.15	WAXD Flat plate patterns of TLMW & THMW	73
4.16	F _{c,z} Vs DR, calculated using 110 & 210 peak intensity distribution ...	74
4.17	F _{c,z} Vs DR, calculated using 002 peak intensity distribution	74
4.18	α Vs 2 θ diffraction scan of an oriented PK- C ₂ /C ₃	76
4.19	Development of orientation with draw ratio	77
4.20	Plot of Amorphous orientation, F _{am} , with draw ratio, DR	79

4.21	Thermal shrinkage of fibers Vs draw ratio for different grades.....	79
4.22	SEM photographs of peel and fracture surfaces of CLMW ..	82
4.23	SEM photographs of peel and fracture surfaces of THMW	84
4.24	SEM photographs of peel and fracture surfaces of TLMW ..	85
4.25	SEM photographs of peel and fracture surfaces of THMP	86
4.26	SAXS Contour plots of THMW & TLMW	87
4.27	SAXS Contour plots of THMP & CLMW ..	88
4.28	Proposed Fiber model for polyketone terpolymer fibers	96
4.29	A typical stress strain curve of polyketone fibers (THMW)	98
4.30	Development of Tenacity with draw ratio	99
4.31	Variation of tenacity with orientation as measured by optical birefringence	99
4.32	Development of a) Tensile modulus and b) Sonic modulus with draw ratio	101
4.33	Plot of % strain at break with draw ratio	102
4.34	Plot of Tenacity Vs Temperature	104
4.35	Plot of Modulus with Temperature	105
4.36	Plot of % Strain at break with Temperature	106
4.37	MTS Gripping system showing the extra Δl that goes unaccounted in the tensile test	109

CHAPTER 1

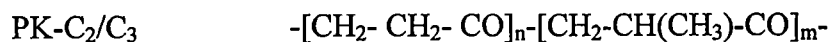
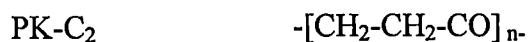
INTRODUCTION

In the second half of the 20th century, the use of polymers in our daily life has grown tremendously. Polymers are used in different forms and for a wide range of applications. Noticeable among these are the synthetic and man-made polymers that have found applications in not only the textile and apparel sector but also in a lot of industrial usages like tire cords, reinforcing and structural agents, barrier films, food and packaging industry, automotive parts, etc. With increasing competition and a demand for better performance materials, development of new polymeric materials is a major activity.

New catalyst systems have provided the opportunity to produce new polymers with a better set of properties. Some of these developments have been or are in the process of being commercialized depending on the economic feasibility of their synthesis and processing. Once new materials are synthesized, their processing needs to be optimized to be able to maximize their properties. The process of making fibers from polymers generally involves spinning, wherein the polymer is extruded through a spinneret to form fibers under suitable shear rates and temperatures, and drawing, which involves plastic stretching of the material to enhance its strength and modulus. There are other allied processes too, but spinning followed by drawing are the major processes by which commercially available polymers are formed into fibers.

Different polymeric synthetic fibers are available in the market – examples include Nylon 6 & 66, polyethylene terephthalate (PET), polyethylene (PE) and polypropylene (PP) [1]. Recently, a new class of palladium bidentate catalysts have been developed that can be used for the production of perfectly alternating polyolefin polyketones [2,3].

The first generation aliphatic polyketones were perfectly alternating copolymers of carbon monoxide and ethylene. These were (and are) high melting, high strength and high stiffness polymers with excellent chemical, thermal, tribological and barrier properties [4]. However, their high melting temperature and relative instability of the melt limits their application in extrusion melt processing methods. To ease the stability problem and reduce the melting temperature a third monomer – propylene was randomly substituted for ethylene in the alternating chain. The proportion of propylene is generally less than 10-12 % by weight [5]. The termonomer modifies the crystallinity of the polymer, broadens its melt-processing window, and improves its resilience and ductility. The commercially available copolymer has a melting temperature of about 255-260°C, and with increasing propylene content in the terpolymer the melting point decreases. The terpolymer available under the trade name CARILON[®] has a melting temperature of 220°C with glass transition occurring at 15°C. Its density is 1.24 g/cm³ at room temperature and 1.00 g/cm³ in the melt [7]. Like most other semi-crystalline polymers, polyketone is opaque in the solid state, except in films. For the sake of simplicity the copolymer and the terpolymer will be, henceforth, referred to as PK-C₂ and PK-C₂/C₃, where:



Recent attempts have shown that the polyketone copolymer (PK-C₂) and terpolymer (PK-C₂/C₃) fibers with high tenacity could be produced by gel spinning and drawing [6]. High performance fibers produced this way have tenacities as high as 2.8 GPa. However, gel spinning is a prolonged and expensive process with considerable environmental concerns. Preliminary studies in our laboratory and at Shell Chemical Company have been successful in producing high tenacity fibers by melt spinning of PK-C₂ & PK-C₂/C₃ followed by drawing. Copeland and Spruiell [42, 47] have investigated melt spinning of low and high molecular weight polyketone terpolymer. The present work is a continuation of the collaborative work with Shell to investigate the melt processing and production of high tenacity fibers from aliphatic polyketones. The materials investigated include not only the low melting terpolymer (as used by Copeland) but also a high melting terpolymer and the copolymer.

Since the processing conditions and parameters have a significant affect on the fiber properties, an attempt is made to study the optimum conditions of fiber melt spinning to produce fibers that will be suitable for commercial use. The aim of this work is to produce high tenacity fibers by melt spinning and by post-spinning drawing and to characterize the resulting fibers in order to ascertain the effect of different process variables such as draw ratio, draw temperature, propylene content and molecular weight on structure, orientation, mechanical and thermal properties of the resulting fibers

CHAPTER 2

REVIEW OF LITERATURE

2.1 History

The first copolymerization of ethylene and carbon monoxide was reported by Farben-fabriken Bayer under harsh conditions (230°C and 2000 atm) [8]. It was later studied independently by Reppe [9] and Brubaker (Dupont) [10] under substantially milder conditions. Reppe obtained only oligomers that were exclusively alternating ethylene-carbon monoxide sequences whereas Brubaker and co-workers obtained non-alternating copolymers of ethylene and carbon monoxide. Subsequent efforts to develop catalysts derived from group VIII transition metal-complexes to produce linear and alternating copolymers failed to arouse interest because of their economic unviability. In the 1980s, interest was renewed when Drent and coworkers (at Shell) developed a new class of highly efficient homogeneous palladium catalyst systems for the production of perfectly alternating copolymers of ethylene and carbon monoxide. Following this, Shell announced the commercial availability of ethylene/propylene/carbon monoxide terpolymers under the trade name of Carilon[®]. This decision followed 20 years of intensive research and developmental work, resulting in more than 200 patents. Properties of Carilon[®] are comparable to those of engineering polymers like nylon and polyacetal.

2.2 Classification

Depending on the classification, there are two main families of ethylene/carbon monoxide copolymers:

1. **Non-alternating copolymers:** these contain less than 50 mol % CO and have the general chemical structure as shown below:



2. **Alternating copolymers:** these have a perfect alternating structure, thus having 50 mol % of CO and olefin, respectively. In this, terpolymers have acquired great practical importance, the structures are provided below:

Copolymer:



Terpolymer:



2.3 Synthesis

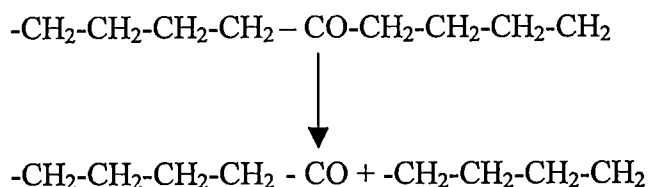
2.3.1 Non-alternating Ethylene/Carbon monoxide copolymers

Non-alternating, random copolymers with a CO content less than 50 mol % have been obtained mainly by a free-radical mechanism or with γ -ray irradiation [11,12] The polymerization is carried out in bulk or in an inert solvent like benzene, cyclohexane or a saturated hydrocarbon. High temperatures (135°C – 200°C) and high pressures (100-1000 atm) have to be used for the process. Copolymers with molecular weight up to 8000 have been obtained depending on reaction conditions. Pressure,

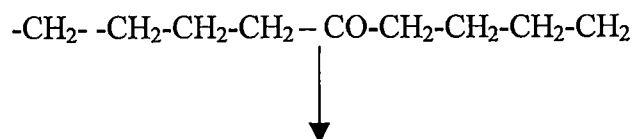
composition of the reaction mixture, temperature and nature of the solvent greatly influence the composition, yield, molecular weight and other properties of the polymer. The copolymers thus obtained have low molecular weights and low yields. Physically, these exist as low molecular weight liquids to crystalline solids. The properties are strongly dependent on the CO content. In comparison to the structure of polyethylene, the insertion of CO into the main chain has the effect of making the *a* axis longer and the *b* axis shorter. The main chain shows a planar zigzag conformation with carbonyl groups alternating in opposite directions

Non alternating copolymers are photodegradable, due to the presence of a photodegradable CO moiety. If the CO content is less than 2-3 mol %, the product maintains the properties of LDPE, while able to degrade under exposure to UV radiation to form shorter and weaker chains. At room temperature, chain cleavage is induced by UV radiation and follows a Norrish II type process with the formation of methyl and vinyl end groups [13,14]. Norrish I and Norrish II degradation processes are sketched below.

Norrish I



Norrish II





Arco, Dow, Dupont and Union Carbide are currently marketing these kinds of polymer products

2.3.2 Alternating Ethylene/Carbon monoxide copolymers

2.3.2.1 Catalyst system

The oligomerization of ethylene and carbon monoxide by transition metal catalysts has been observed since 1941 [8]. In the 1970s, several Group VIII-metal compounds were found to be catalytically active in the synthesis of strictly alternating ethylene-carbon monoxide copolymers. The copolymerization experiments were carried out at 100-200°C under a total gas pressure of 100-200 atm. These catalyst systems were capable of producing high molecular weight and strictly alternating copolymers, however their activities were low, and industrial interest was rather limited. A considerable improvement in the catalyst systems was accomplished when a new class of catalyst was discovered and patented by Shell [2,3], constituting a technological breakthrough concerning molecular weight and productivity. Such a class is based on ternary system: (1) a palladium salt of a (preferably) carboxy acid, (2) a phosphorous or nitrogen bidentate base, (3) an anion of a acid, preferably an organic acid. An oxidant like 1,4-benzoquinone is also present in many catalytic systems. A standard high-productivity catalyst is typically formed in situ by the mixing of palladium (II) salts like $\{\text{Pd}(\text{MeCO}_2)_2\}$ or $[\text{Pd}(\text{CF}_3\text{CO}_2)_2]$ with a bidentate phosphorous- or nitrogen-donor chelating ligand ($\text{Pd}/\text{ligand} = 1 \text{ mol}/\text{mol}$), a strong non hydrohalogenic acid

(like trifluoroacetic or p-toluenesulphonic acid) or the anionic part of the acid as cocatalyst. The active form of such catalysts are bidentate Pd complexes with P or N ligands [15]. The active form of such catalysts is supposed to have the structure as shown in Figure 2.1, capable of cleaving the olefinic bond and incorporating CO molecules. Usually the reaction is carried out in a batch stirred reactor, preferably at 70-90°C and 50-60 bar, operating in methanol and adding the appropriate mixture of monomers. Because carbon monoxide which constitutes 50 % by weight of the polymer, is a cheap monomer, these copolymers are potentially the lowest cost bulk plastic that can be made.

Several parameters can influence the polymerization reaction. In order to achieve a high catalytic activity, the more efficient catalyst systems should have two common characteristics a neutral ligand able of suitable bidentate coordination and an anion having a weak or non-coordinating attitude towards the metal center in order to be displaced from the coordination sphere by an incoming nucleophilic molecule. The choice of ligands can significantly influence the structure of the copolymer and its properties as well as the copolymerization yields. Also the nature of solvent brings about an influence on polymerization rates [16].

2.3.2.2 Polymerization Mechanism

The first interpretation of the mechanism was proposed by Sen [17-20] as sketched in Figure 2.2. It consists of the alternate insertion of CO and olefin into a

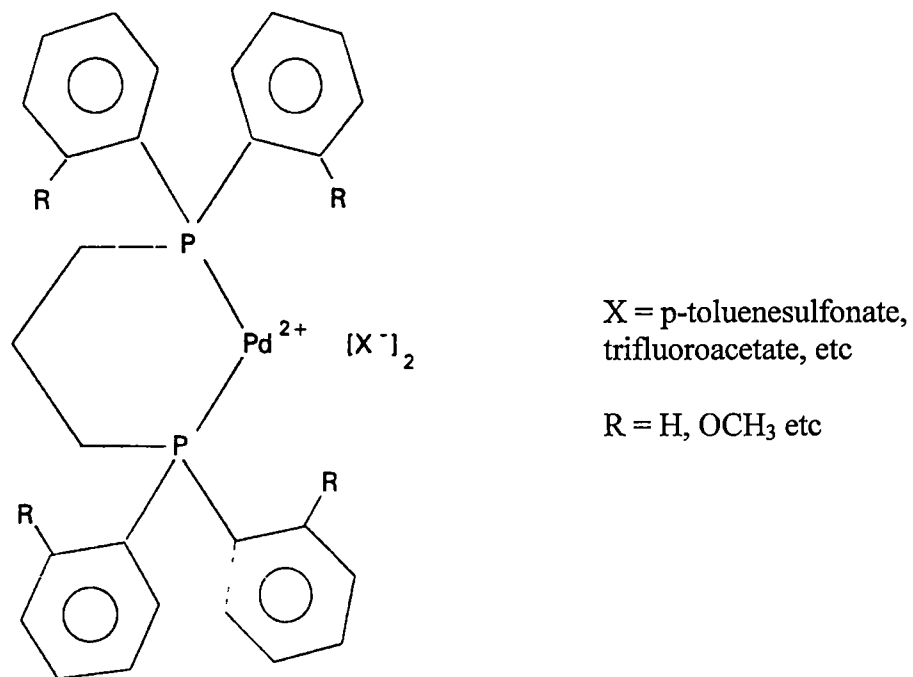


Figure 2.1 Structure of high productivity Shell type catalyst.

Source Sommazi, A & Garbassi, F., *Prog Polym Sci*, 22, 1547 (1997).

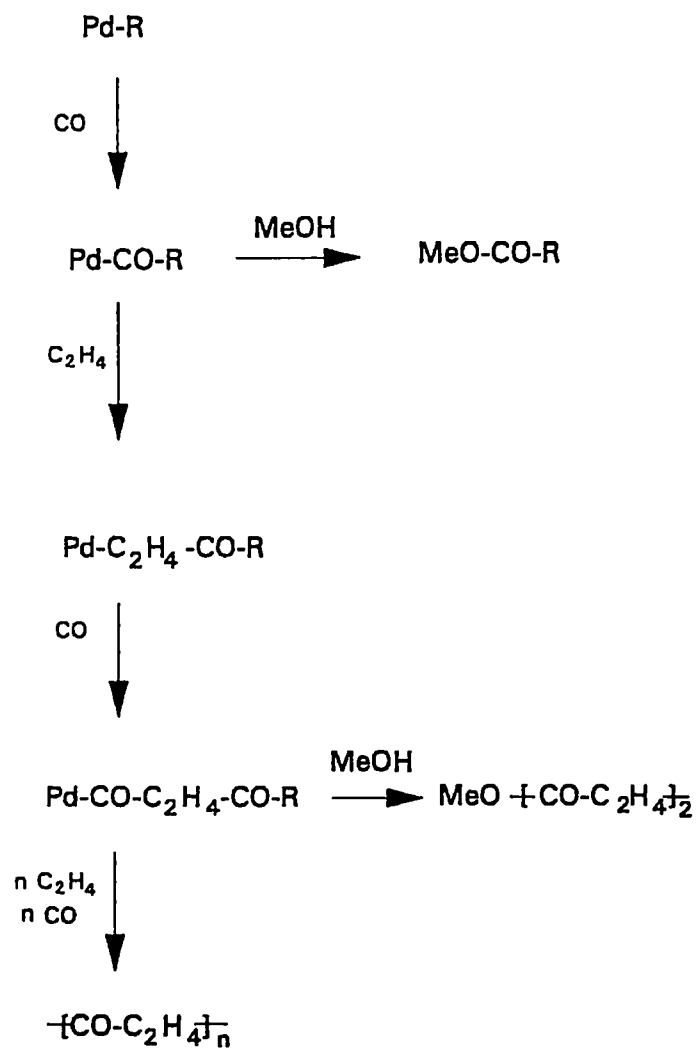


Figure 2.2 Polymerization mechanism as proposed by Sen

Source Sen, A., *Adv Polym Sci.*, 73/74, 125 (1986).

preformed Pd-alkyl bond CO is expected to bind more readily to Pd(II) because it's a better π -acid than olefins and has a greater tendency to insert into the metal-alkyl bonds than olefins. Consequently, alternation is achieved by the simple fact that CO insertion is preferred for the alkyl bond, whereas olefin insertion is preferred on the subsequent Pd-acyl bond. The latter acts as the rate-determining step. The above reaction is described for a catalytic system consisting of $[\text{Pd}(\text{PPh}_3)_n(\text{CH}_3\text{CN})_{4-n}](\text{BF}_4)_2$, where $n = 1-3$, carried out in a non-coordinating system like CHCl_3 or CHCl_2 [21].

A similar mechanism has been proposed by Drent [3], as shown in Figure 2.3. The activation step involves the reaction of Palladium complex with methanol (solvent of reaction), to give a palladium methoxy species. After this, the insertion of CO to give a palladium carbomethoxy species is considered the favored direction of initiation. Next, insertion of coordinated ethylene into the carbomethoxy group takes place to give a palladium dimethylenecarbomethoxy species. Subsequent alternating insertions of ethylene into metal-acyl bonds [22-24] and carbon monoxide [25, 26] into metal-alkyl bonds generated the polyketone. Propagation competes with the termination that occurs with the reaction with methanol. Chain transfer occurs with the formation of keto-ester, diester and diketone terminated macromolecules.

Further insight into the polymerization mechanism has been recently provided by Zhao and Chien [27] using the catalyst complex $[\text{Ph}_2\text{P}(\text{CH}_2)_3\text{PPh}_2]\text{Pd}(\text{CH}_3\text{CN})_2(\text{BF}_4)_2$. This does not require the presence of a protonic acid as coinitiator. A simplified mechanism scheme is reported in Figure 2.4.

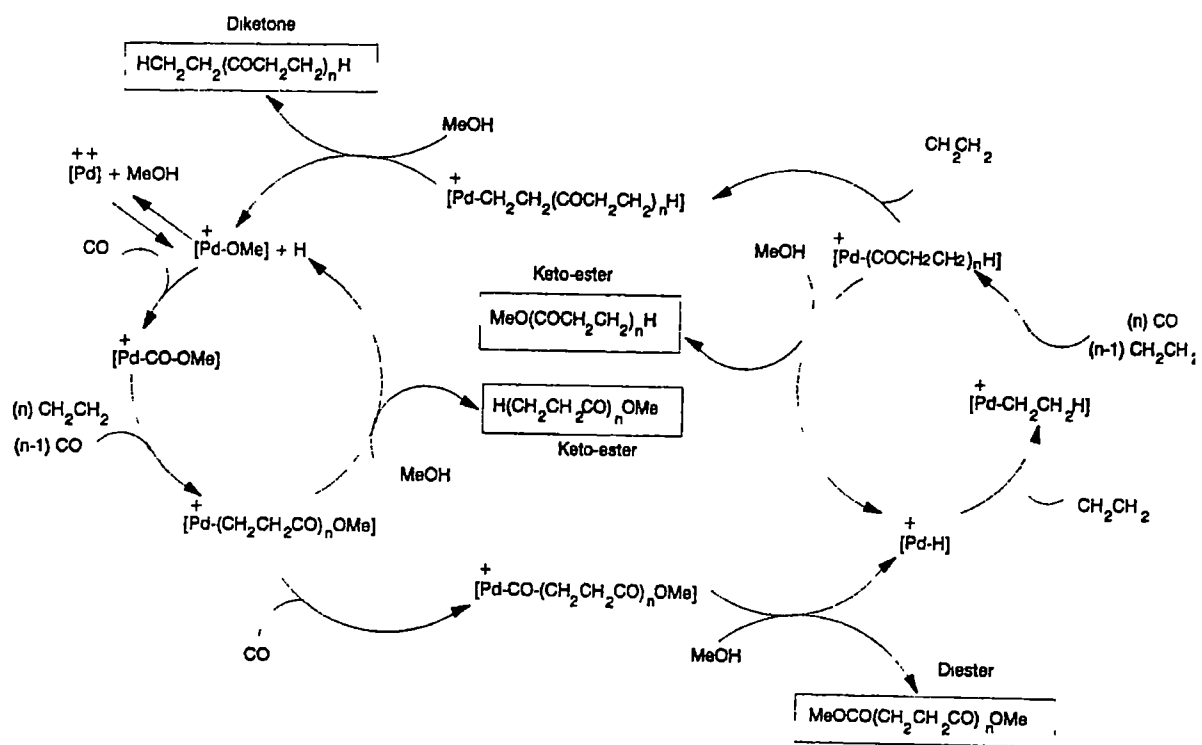


Figure 2.3 Polymerization mechanism as proposed by Drent et al.

Source Drent, E, van Broekhoven, J A M & Doyle, M J., *J Organomet Chem.*,

417, 235 (1991)

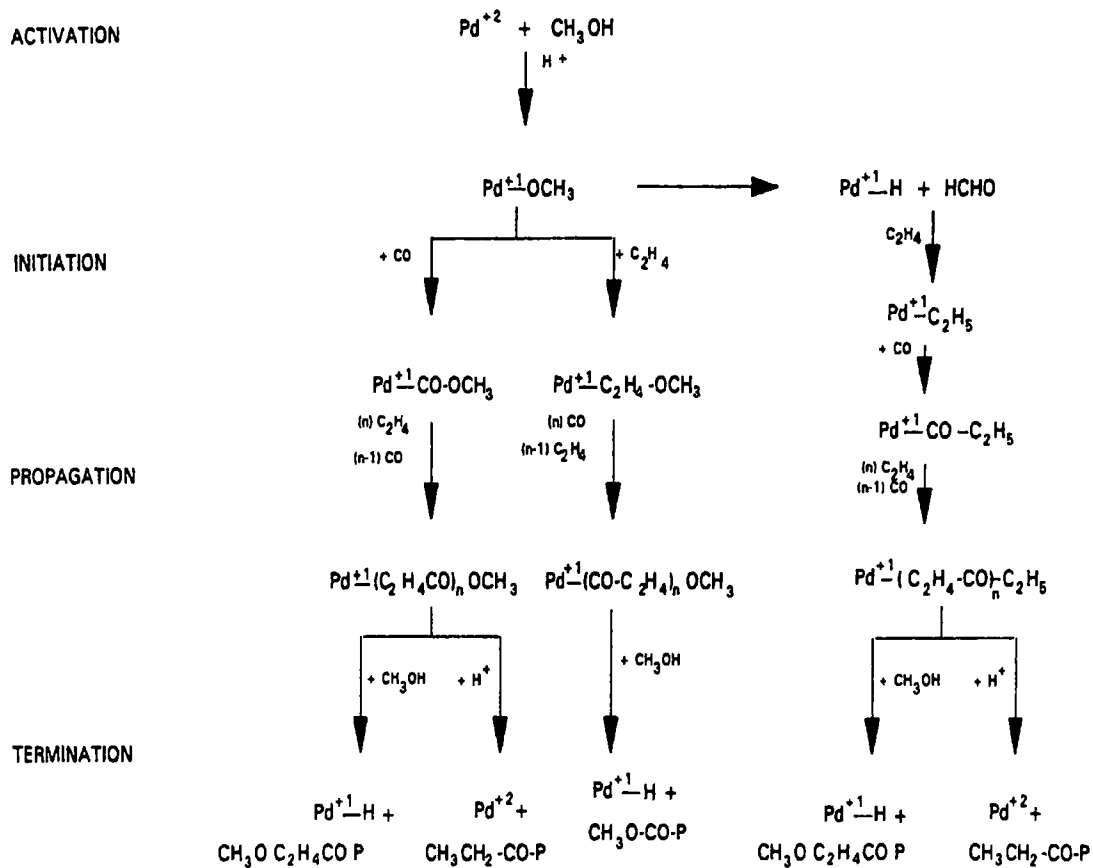


Figure 2.4 Polymerization mechanism as proposed by Zhao et al [27]

Source Zhao, A. X. & Chien, J. C. W., *J Polym Sci Polym Chem*, **30**, 2735 (1992)

Activation involves transformation of the catalyst by methanol so that CO or olefin insertion is made possible. There are two propagation steps: CO insertion into a Pd-alkyl bond and alkene insertion into a Pd-acyl bond. Termination occurs mainly by reaction of methanol with a propagating species, producing a terminal chain and a new initiating species (chain transfer process). In a recent paper [28], a new mechanism for the polymerization of propylene with carbon monoxide has been proposed, involving Pd-carbene species for the high stereoregularity of the copolymerization and the formation of spiroketal repeat units instead of the linear polymer. Further insight into the propylene-carbon monoxide polymerization mechanism has been made by Wong and Drent [29], proposing that the initiation occurs via palladium hydride species, probably formed by a water-gas shift reaction, and the chain termination preferably via protonolysis of palladium alkyl bonds. In fact, in contrast to the ethylene/CO copolymer, which shows a 1.1 ratio of ketone and ester end groups, the propylene/CO copolymer does not contain ester end groups.

2.4 Crystal Structure

For both the terpolymer and the copolymer, the unit cells are orthorhombic with a polymer chain at each corner and one in the center [30, 31]. There are four monomer repeat units per unit cell and the polymer chain conformation is extended planar zigzag (all trans). Polyketones are polymorphic in nature and there are two unit cells that can exist. These are described in Table 2.1. The predominant β form, first reported by Chatani et al [30], for polyketone copolymers with a significant number of molecular

Table 2.1 Crystal unit cell descriptions for PK-C2, PK-C2/C3 & HDPE [33]

Polymer	Unit cell	Space Group	Unit cell dimensions (Å)	Crystal density g/cm ³
PK (α form)	orthorhombic	Pbnm	a = 6.91 b = 5.12 c = 7.6	1.382
PK (β form)	orthorhombic	Pnam	a = 7.97 b = 4.76 c = 7.57	1.297
HDPE	orthorhombic	Pnam	a = 7.40 b = 4.93 c = 2.53	1.01

defects in the polymer chain has a lower density of 1.297 g/cm³, space group Pnam and dimensions a = 7.97 Å, b = 4.76 Å & c = 7.57 Å. The α form has a higher density by virtue of its better packing, about 78 %, the highest for any organic polymer. The difference between the α and β forms can be described by an increase in the angle between the bc plane and the planes of the polymer chains from 26° to 40° (for α and β respectively). This is accomplished by a rotation of the center chain about the c axis through an angle of 180° and a slight rotation of the chains at the corners of the unit cell. Figure 2.5 shows the two different unit cell structures. For the α structure, all carbonyl dipoles point in about the same direction at equal height z, whereas in the β structure the dipole of the carbonyl group of the corner and the center chain point in different directions. Therefore the packing in the α structure is very effective. The cross sectional area of the unit cell perpendicular to the fiber axis amounts to 35.2 Å²,

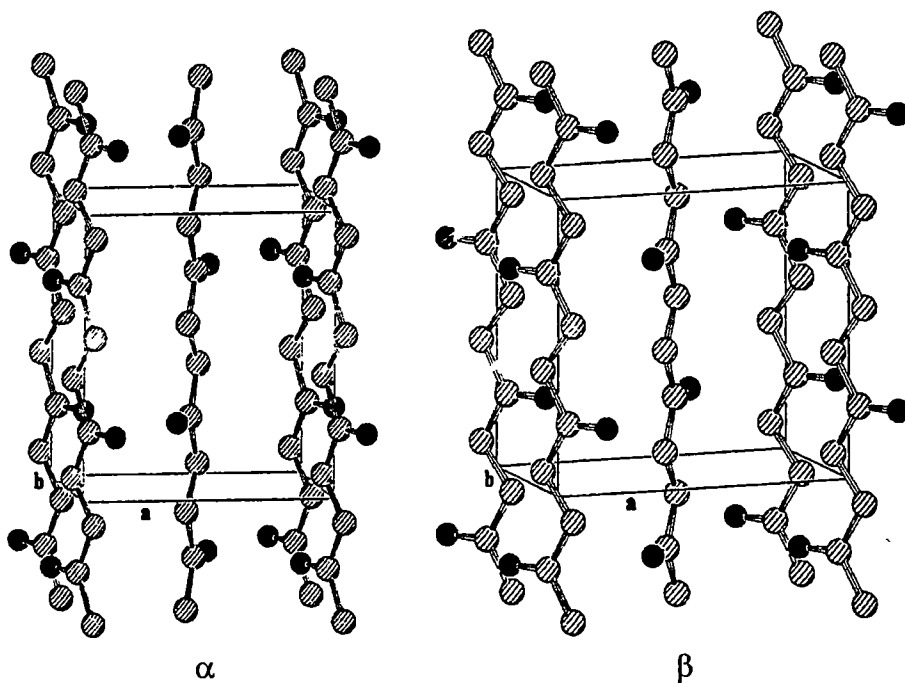


Figure 2.5 α & β unit cell structures of PK-C₂

Source. Klop, E. A., Lommerts, B. J., Veurink, J, Aerts, J. & Van Puijenbroek, R. R.,
J Polym Sci Part B Polym Phys, **33**, 315 (1995)

which is even smaller than for a polyethylene unit cell (36.2 \AA^2) [32]. The β structure is less dense than the α structure, as is obvious from an increased cross section area of 37.9 \AA^2 [31]. The intermolecular distances are smaller in the β structure.

2.5 Polymorphism

Alternating polyketones exhibit polymorphism and, depending on temperature, composition, applied stress, or kinetic factors, crystallize in an orthorhombic α or β form. In drawn fibers of perfectly alternating PK-C₂ at room temperature only the α form exists [34]. A reversible temperature-induced α - β transition occurs at 110-125°C that is accompanied by a 10 % change in crystalline density. The methyl groups in the terpolymer are built into the crystal lattice as defects. With more than 5 mol % of propylene the terpolymer fibers crystallize exclusively in the β form. Below this level the α/β ratio (at room temperature) increases with decreasing amounts of propylene. Figure 2.6 shows the calculated diffraction patterns of α and β forms [34]. The relative shift of the (200) and (210) peaks as the temperature-induced phase transformation takes place is visible in the scans. This helps in concluding the type of phase present in a polyketone polymer sample.

2.6 Morphology

At the 5-50 μm level, the semi crystalline structure of the terpolymer is spherulitic. Unlike the well-defined structures of Nylon 66, the spherulites are less well

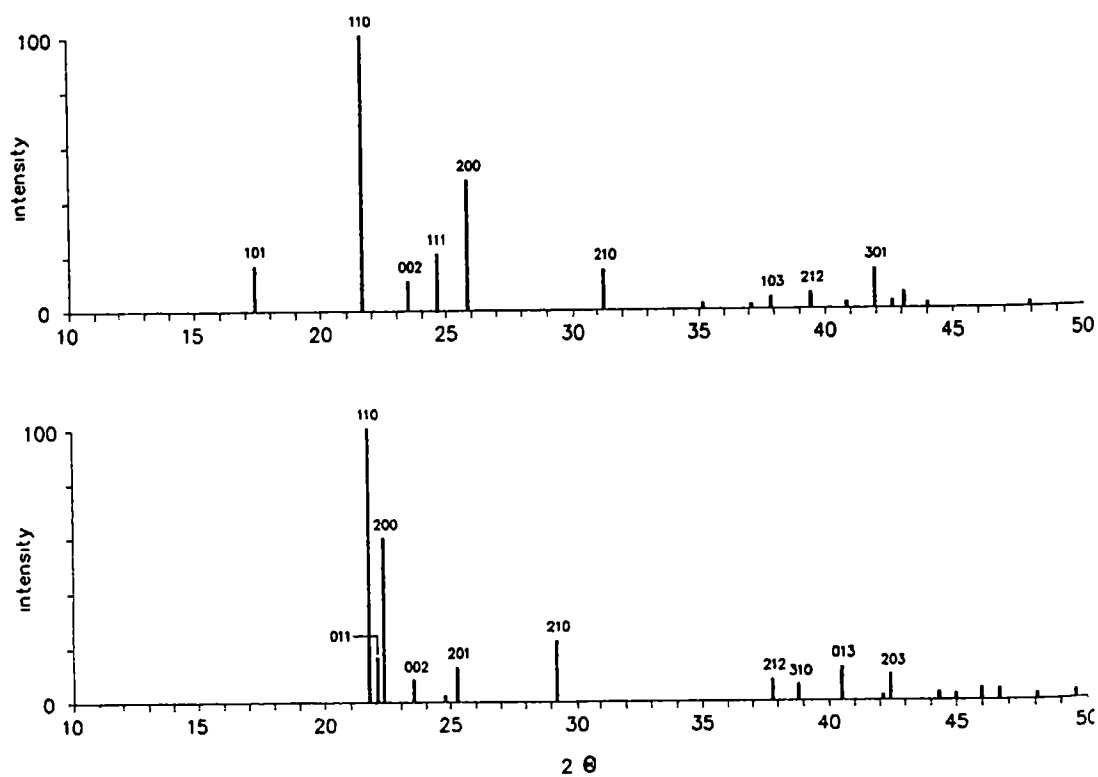


Figure 2.6 Calculated diffraction patterns of α (top) and β (bottom) forms, corresponding to copolymer and terpolymer respectively.

Source Klop, E. A , Lommerts, B. J., Veurink, J, Aerts, J. & Van Puijenbroek, R. R.,
J Polym Sci Part B Polym Phys , **33**, 315 (1995).

defined and are “entangled”, as described by Flood et. al [33]. The copolymer semi-crystalline structure is similar to the terpolymer structure, however, hedrites or partially formed spherulites dominate. Again the hedrite structure was described as “entangled”. Experimental measurements for the determination of the Avrami exponents have concluded a value of three for the terpolymer, indicating a spherulitic type of crystal growth. The values for the copolymer are dependent on the crystallization temperature. For crystallization temperatures from 227.5-235 °C, the Avrami exponent ranged from 2.3 – 3.0, indicating two dimensional and spherical growth. For crystallization temperatures from 217.5 to 222.5 °C the Avrami exponent ranged from 1.5-2.4, indicating two-dimensional crystal growth.

2.7 Properties

2.7.1 Fundamental Properties

The linear, symmetrical and low cross-sectional chain profile allows PK polymers to crystallize readily PK polymers exhibit higher thermal transitions, in the range of other semi-crystalline engineering thermoplastics, with melting points as high as 260°C and a glass transition temperature between 15 and 20 °C, Table 2.2.

The replacement of one third of the methylene groups in PE for carbonyl groups in PK results in high cohesive forces via dipole interactions. These forces contribute to dense chain packing, in the amorphous phase as demonstrated by low fractional free volumes (FFV) of PK polymers (refer to Table 2.2) These strong inter

Table 2.2 Fundamental properties of aliphatic polyketones and comparison to other semi-crystalline polymers [35]

Polymer	T _m (°C)	T _g (°C)	Crystallinity (%)	Crystal density (g/cm ³)	Amorphous Density (g/cm ³)	Cohesive energy density (J/cm ³)	FFV @ room temperature
PK-C ₂	260	15-20	45-55	1.383	1.25	540-840	0.068
PK-C ₂ /C ₃	220	15-20	30-40	1.297	1.21	540-840	0.097
HDPE	135	-80 to -30	70-90	1.0	0.855	250-300	0.189
PEEK	340	144	24-48	1.4	1.265	530-570	0.108
PA6	220	45	30-45	1.23	1.08	770	0.142
PA66	265	45-57	33-44	1.24	1.09	770	0.110
PET	265	60-85	0-50	1.515	1.335	400-480	0.148
POM	175	-38 to -22	64-69	1.506	1.25	440-510	0.107

chain attractions, combined with the relative flexibility of the polymer backbone contribute to a broad and useful range of physical, mechanical and barrier properties

2.7.2 Material Properties

Table 2.3 lists some of the properties of typical polyketone polymers compared to a range of other semi-crystalline polymers. The high thermal properties of PK polymers allows the excellent properties that are maintained over a wide range of temperatures. Heat distortion temperatures (HDT) show PK polymers resist deformation under 64 psi load at temperatures surpassing 100°C [35]. They show high impact strength with a brittle-ductile transition at as low as -40°C [36].

Table 2.3 Typical Mechanical Properties of PK and other semi-crystalline polymers [35]

Polymer	Modulus (GPa)	Strength (MPa)	Yield Strain (%)	Break Strain (%)	HDT (°C)	Notched Izod (J/m)
PK-C ₂	2.3	85	40	90	180	294
PK-C ₂ /C ₃	1.5	60	25	300	105	240
HDPE	1.1	27	10	600	55	100-400
PEEK	3.6	93	5	50	160	80
PA66	1.3	59	25	300	70	110
PA12	1.1	45	5	350	50	150
PBT	2.3	54	4	300	54	55
POM	2.9	65	15	40	135	75

PK polymers have good moisture and chemical resistance. The moisture absorption is only about 0.5% of its weight and the only known solvent at room temperature is hexafluoroisopropanol. They resist degradation and swelling when in contact with a wide range of consumer, industrial and automotive chemicals including solvents, fuels, lubricants and aggressive aqueous environments such as salts and weak acids and bases.

Dense chain packing and polarity allow PK polymers to combine chemical resistance with excellent barrier properties [38] such as to hydrocarbon vapors and gases such as oxygen [37].

These show high tensile yield stress, and they can withstand repeated loading and flexing without being adversely affected. Elongations up to 10% result in no permanent deformation. Further, they demonstrate excellent fatigue [39] and creep

resistance. PK polymers possess exceptional wear properties, low noise generation in gears, bearings and other moving type applications.

2.8 Processability

Polyketones exhibit a melt viscosity that is moderately dependent on shear stress and temperature. The shear-thinning behavior of aliphatic polyketones can be described by the Ellis model and the temperature dependence can be described by the Andrade equation with a flow activation energy of 25 KJ/mol [40]. Their flow behavior makes them suitable for injection molding, blow molding, extrusion and rotational molding. Short cycle times characterize polyketone molding as a result of rapid mold filling combined with rapid crystallization.

Another typical aspect of polyketone melt rheology is that melt viscosity tends to increase gradually with residence time in the melt as aldol condensation proceeds slowly at melt temperatures leading to molecular weight advancement, long-chain branching and eventually to cross linking. If residence time becomes excessive (>20-40 minutes depending upon temperature), degradation as melt fracture, gel formation and crosslinking takes place.

2.9 Decomposition

The presence of carbonyl chromophore makes polyketones prone to photodegradation by UV radiation. In the alternating polyketones both Norrish I & II processes together with photo-oxidation are responsible for chain cleavage [13]

The thermal decomposition process is rather complex, due to the presence of complex groups. Thermolysis of PK-C₂ gives CO, ethylene and water as the pyrolysis products, all emanating from radicals formed by chain scission [41]. Further, these polymers undergo crosslinking (aldol reactions) when maintained at high temperatures (250 – 280 °C) even at relatively short times. Therefore, an efficient stabilization is mandatory for their melt processability. The use of stabilizers like phenolic compounds, aromatic amines, substituted pyrazolinones, alkylate benzoquinones and dihydrocarbyl carbamates is reported in the literature [5]

2.10 Preparation of polyketone fibers

Lommerts was successful in carrying out the solution spinning of polyketones to yield high tenacity polyketone (PK-C₂) fibers [6]. Copolymer resin used for his study had an intrinsic viscosity (m-cresol, 25°C) from 4.6 to 6.1 dL/g, corresponding to a molecular weight of 300,000 to 420,000 g/mol.

A homogenized semi-dilute solution (9-15 wt%) in phenol with a small amount of acetone added to prevent interference of solvent crystallization with the fiber formation process was utilized for dry-jet-wet spinning at 70°C. The solution was extruded through 250 µm capillaries into an acetone cooling/coagulation bath, maintained at -5°C and wound on bobbins at a speed of 1m/min. Subsequently, the washed and dried fibers were subjected to tensile drawing at elevated temperatures. The maximum attainable draw ratio was limited to 26, though above a draw ratio of 17, cracks begin to appear in the material. The fibers were characterized and tested to

ascertain the development of properties with draw ratio. It was noticed that the drawability of PK-C₂ increases with temperature, and with increasing draw ratio there is an increase in the tensile properties – tenacity and modulus. The maximum tensile strength attained was 3.8-3.9 GPa and the initial modulus depends on the drawing temperature.

Copeland and Spruiell [42] have melt spun low molecular weight PK-C₂/C₃ that has 6 mol % propylene. The resins, provided by Shell, were dried under vacuum for 6-8 hours at 60°C and then melt spun into filaments having diameter ranging from 65-85 µm. Melt spinning was done in a four zone heating extruder with a twelve hole spinneret. The zone temperatures were kept at 220, 240, 236 and 250°C and a mass throughput of 0.84g/min/hole was achieved. The total residence time of the resin in the extruder was about 10-12 minutes. Winding take-up speeds were kept at about 344-495 m/min. Subsequently, two zone drawing was performed at different temperatures. The maximum attainable draw ratio was around 5X. Characterization of the fibers confirmed the presence of a predominant β form in the terpolymer (6 mol-% propylene) with the orientation development similar to that in the solution spinning process. As expected, the tensile properties showed an increase with draw ratio and so did the density indicating an increase in the % crystallinity. A maximum tensile strength of 687 MPa and a Young's modulus of 16 GPa were reported.

CHAPTER 3

MATERIALS, PROCESSING AND CHARACTERIZATION

3.1 Materials

The polymers used in this study were supplied by Shell Chemical Laboratory. As-spun and drawn filaments of the following grades were supplied

1 A low molecular weight terpolymer (**TLMW**)

A 1.1 LVN, nominal 60 melt flow, 220 °C melting point terpolymer with a nominal M_w of 40,000 and polydispersity index of 2.32.

2 A higher molecular weight terpolymer (**THMW**)

A1.5 LVN, nominal 15 melt flow, 220 °C melting point terpolymer with a nominal M_w of 80,000 and polydispersity index of 2.99

3 A higher melting point terpolymer (**THMP**)

A 1.5 LVN, 240 °C melting point terpolymer and smaller propylene mole % than other terpolymer materials (MW data not available at present)

4 A low molecular weight copolymer (**CLMW**)

A 1.2 LVN, nominal 60 melt flow, 255 °C melting point copolymer with a nominal M_w of 40,000 and polydispersity index of 3.09

Polymer pellets of TLMW, THMW & THMP were supplied for melt spinning

3.2 Processing

3.2.1 Melt Spinning

Due to the unstable nature of polyketone melts, preliminary investigations of the residence time in the extruder were carried out. To get a rough estimate, a high molecular weight PE, 30 MFR at 190 °C (supplied by Shell, also used for purging the extruder before and after the polyketone spinning in the regular melt spinning setup), was extruded through a Randcastle microtruder with a screw of ¼” in diameter and L/D of 20. The temperature profile was kept the same as that to be used for polyketone. The zone temperatures were 200, 220, 240 & 240 °C in the first, second, third and fourth zones respectively. After the temperatures attained equilibrium, the polymer was fed so that a throughput of 3.5 g/min was achieved. In the steady state, a trace amount of colored PE was added. Time for this colored polymer to appear at the exit was noticed experimentally and compared to the one calculated theoretically based on the barrel and screw characteristics. It was found that the colored PE took about 50 seconds to appear at the spinneret exit after it was fed through the hopper. However, it took about 10 minutes to flush out the colored granules completely from the extruder. Since the amount of the colored PE was extremely small, any time that may have taken to feed the hopper can be neglected.

Based on the extruder characteristics and other approximations, the estimated residence time calculated was about 0.998 minutes, which is in good agreement with the observed value. This gave us confidence as to the extension of this principle to larger extruders where an experimental observation using the colored polymer will not

be practical as it would take a long time to flush out the material. Hence approximations used for Randcastle microtruder were extended for the regular 1" screw extruder and residence times were calculated. It was found that the residence time of PE (same as that used in Randcastle) at throughput of 3 g/min/hole was 3 minutes (Appendix 1). However, in the Randcastle, the total time to flush out the colored polymer was about 10 minutes, so that for a 1" screw extruder this will be much larger. Hence to keep the overall residence time smaller, it was decided to have higher throughput rates, of the order of 4 g/min/hole or more.

Before spinning, the PK-C₂/C₃ pellets were dried overnight at 80°C and stored in dry atmosphere. The zone temperatures were kept at 230, 240 & 240°C for the first second and third zone in a 3-zone extruder. An 8-hole spinneret was used. High Mass throughput rate of about 4g/min/hole was accomplished at a backpressure of 1000-1500 psi and the extrudate in the form of 8 filaments was obtained. However, the winding of this extrudate could not be done because the filaments broke well before reaching the winder. This was due to a very long spin line, because of which the fragile filaments could not bear the tension arising due to the pull of gravity. Further attempts to modify and shorten the spin-line could not be achieved because of time constraints. The as-spun filament samples provided by Shell were used for subsequent study.

The filaments provided by Shell were also prepared using similar conditions that we had used. In addition to as-spun bobbins, Shell also supplied fibers that had been drawn subsequently in a single- or two-stage oven drawing process. The

conditions for the copolymer and the terpolymer processing to make fibers are listed in Table 3.1.

3.2.2 Drawing

As seen in Table 3.1, Shell provided us with samples that were already drawn in a single- or two-stage oven draw process. However, we drew the as-spun filaments (provided by Shell) on a Fincor 2-stage, temperature controlled continuous drawing setup, in order to investigate the optimum drawing conditions for this type of drawing equipment. The schematic of the drawing equipment is shown in Figure 3.1.

Filaments were unwound from the bobbin B, passed over a guide G and wound (4-5 turns are given to avoid any slippage) on the heated rollers. For a single-zone draw process only two sets of rollers are used (I & II), but for a two-zone draw process

Table 3.1 Processing conditions for PK fibers (as used by Shell)

	Copolymer	Terpolymer
Extruder Temperature (°C)	-	235-250
Die diameter (mm)	0.7	0.5-0.7
# of fibers	32	32-64
OVEN DRAW CONDITIONS		
Oven Temperature (°C)	250	230
Draw Ratio (1 or 2 stage draw)	5-7	5-10.5
RELAXATION CONDITIONS		
Oven temperature (°C)	-	210
Draw ratio	-	0.97

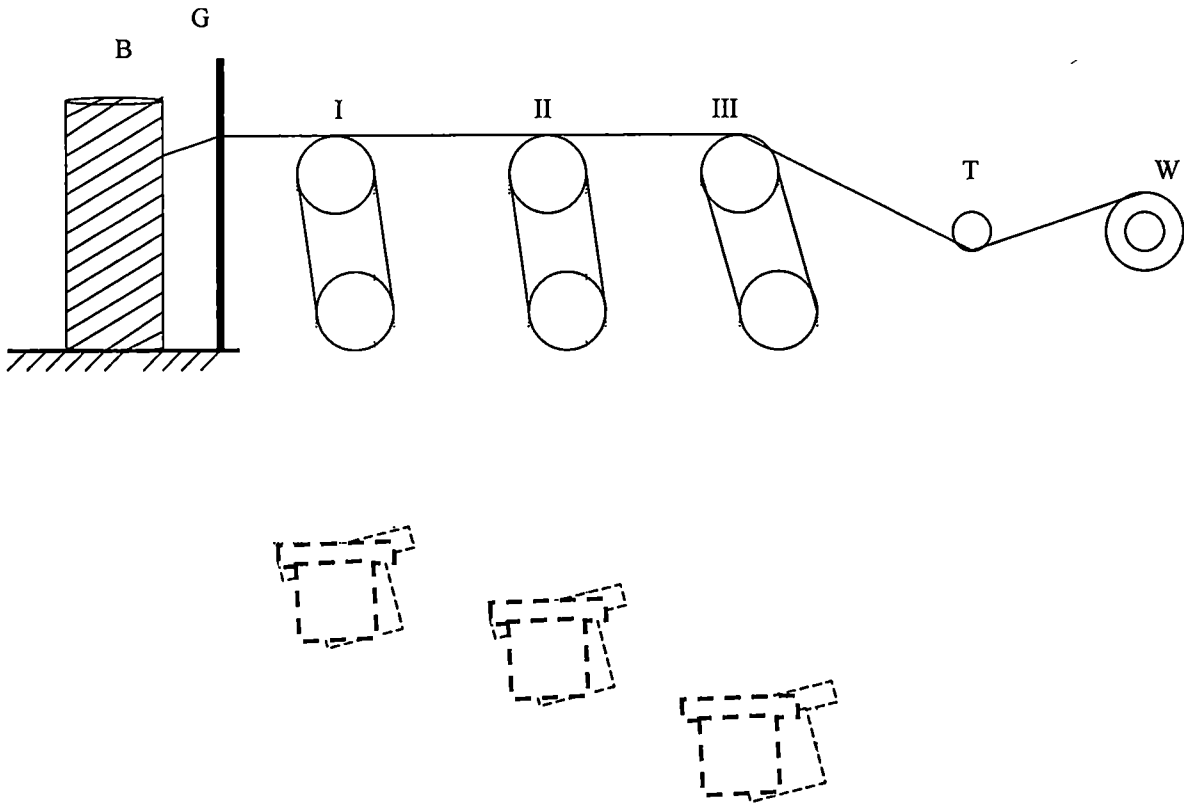


Figure 3.1 Schematic of the Fincor-2 stage Drawing Apparatus; B: Bobbin; G: guide; I, II & III: three sets of heated rollers; T: Tensioner & W: Winder.

all the three sets of rollers were used. Each successive set of rollers rotates at a higher speed than the previous one and is displaced horizontally as well, as seen in the Top view. This prevents any sloughing off of the filaments from the edges of the metallic surfaces of the rollers. The temperature of the three sets can be controlled, though the third set of rollers was generally kept at room temperature. A tensioner T, helps maintain a constant tension so that the winding is done uniformly.

The temperatures of drawing are shown in Table 3.2. The temperature of the first set of rollers was maintained at values ranging from 110-220 °C for copolymer and 110-190 °C for the terpolymer. The temperature of the second set of rollers was held at about 10°C above the temperature of the first set of rollers. The third set of rollers was maintained at room temperature. Temperature calibration of the roller sets was done using a hand held probe. It was found that both the rolls in a set were held at the same temperature after equilibrium was reached. The probe temperature readings also indicated that the temperature panel readings on the drawing set up were way off. Consequently, the hand held probe was used to determine the actual temperature as well as for calibration. The first set of rolls is rotated at the minimum speed i e , at a

Table 3.2 Drawing conditions for PK-C₂ & PK-C₂/C₃.

	Drawing Temperatures			DR Range	Roll I speed (m/min)
	T _I (°C)	T _{II} (°C)	T _{III} (°C)		
Copolymer	110-220	T _I + 10	25	3-8	8
Terpolymer	110-190	T _I + 10	25	3-8	8

linear speed of 8 m/min. The third set of rollers was maintained at a speed that would give the desired total draw ratio. The second roller set was kept at a speed between the two, usually closer to that of the third set than the first, so that the major part of drawing took place in the first draw-zone. The drawn samples were subsequently wound on bobbins, labeled and stored.

3.3 Characterization Techniques

3.3.1 X-Ray Scattering

3.3.1.1 Wide Angle X-Ray Diffraction (WAXD)

Diffraction in general occurs only when the wavelength of the radiation is of the same order of magnitude as the repeat distance between the scattering centers. This requirement follows from the Bragg's Law:

$$n\lambda/2d = \sin \theta,$$

where the incident beam, the normal to the reflecting plane and the diffracted beam are always coplanar and the angle between the reflected and the transmitted beam is always 2θ .

A wide-angle flat plate diffraction photograph of a polycrystalline specimen with characteristic radiation consists of concentric Debye rings [43]. The equipment consists of a x-ray beam falling on the specimen such that the transmission or reflection patterns could be recorded on a photosensitive film, Figure 3.2. In our case the photographs were obtained in the transmission mode.

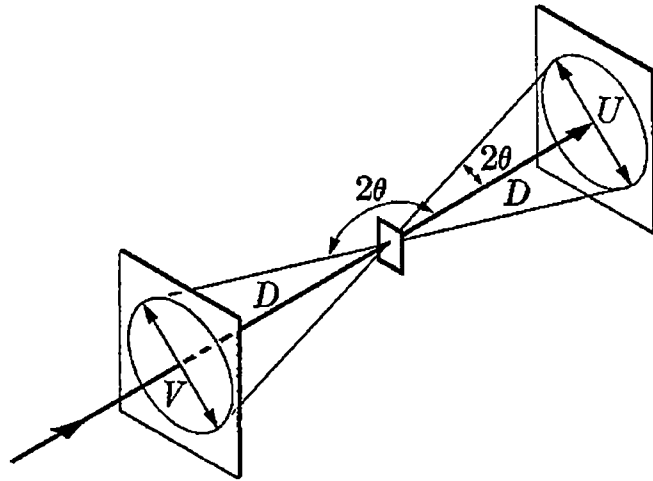


Figure 3.2 Flat plate WAXD in reflection and transmission modes

Source: Cullity, B. D., "Elements of X-Ray Diffraction", second ed., Addison – Wesley Pub. Company, Inc., 176 (1978)

If the individual crystals in the specimen are completely random, then complete concentric rings are obtained. For a specimen having preferred orientation, these Debye rings are of non-uniform intensity around the circumference (if preferred orientation is slight) or actually discontinuous (if there is a high degree of preferred orientation). In the latter case, certain portions of the Debye rings are missing because the orientations that would reflect to those parts of the ring are simply not present in the specimen. Non uniform Debye rings can therefore be taken as conclusive evidence for preferred orientation and by analyzing the non-uniformity we can determine the kind and degree of preferred orientation. The individual crystals in a fiber are so oriented that the same crystallographic direction $[uvw]$ in most of the crystals is parallel or nearly parallel to the fiber axis. This is called the fiber texture. For highly oriented fibers, where nearly all the crystals are aligned along the fiber axis, the Debye rings are reduced to discontinuous rings or spots. This gives a qualitative determination of crystalline orientation of the specimen.

An example of a flat plate pattern for a highly oriented THMW is shown in Figure 3.3. This pattern was indexed by Copeland [44]. The WAXD diffractometer technique was also used to obtain 2θ and azimuthal scans. The 2θ scans, which give the intensity of the reflected x-ray radiation as a function of 2θ , were used to determine the baseline that is used to eliminate the background in the orientation analysis. These were obtained on the Rigaku X-Ray Diffractometer (D/MAX-IA), in the reflection mode. The azimuthal scans are used to determine the crystalline orientation, described later in another section. These were also obtained using the

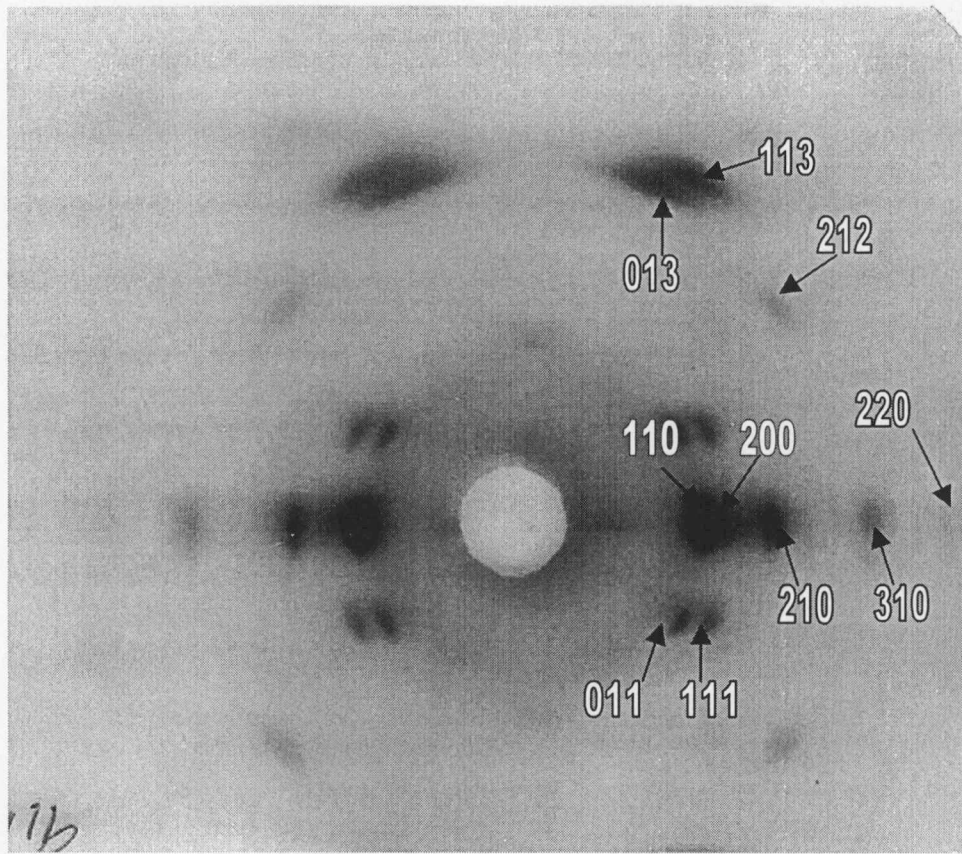


Figure 3.3 WAXD flat plate film pattern showing diffraction peaks in an oriented PK-C₂/C₃ fiber ($\alpha = 0^\circ$).

Rigaku Diffractometer in the transmission mode. X-rays used for the study were produced using a copper target and filtered by a monochromatic nickel filter to give the CuK_α radiation with a wavelength of 1.5418 Å [43].

3.3.1.2 Small Angle X-Ray Diffraction

Small angle x-ray measurements are made to ascertain the structure of lamellar, semi-crystalline polymers. The long period, L , which is the distance between the centers of the adjacent lamellae (high electron density regions), is calculated using Bragg's Law as follows:

$$L = \frac{\lambda}{2 \sin \theta}$$

where θ is the Bragg angle of diffraction. Figure 3.4 shows the long period, L , in semi-crystalline polymer [45]

3.3.2 Orientation

3.3.2.1 Axial Orientation functions

P. H. Hermans originated the concept of an orientation function to specify the degree of axial orientation in fibers. The initial efforts were for a single-phase system, but it was soon realized that most fibers consist of both crystalline and amorphous phases. This led to the specification of two orientation-functions: one for the amorphous phase and the other for the crystalline phase. Desper and Stein [46] extended Hermans' treatment for axial orientation by setting up three equations to

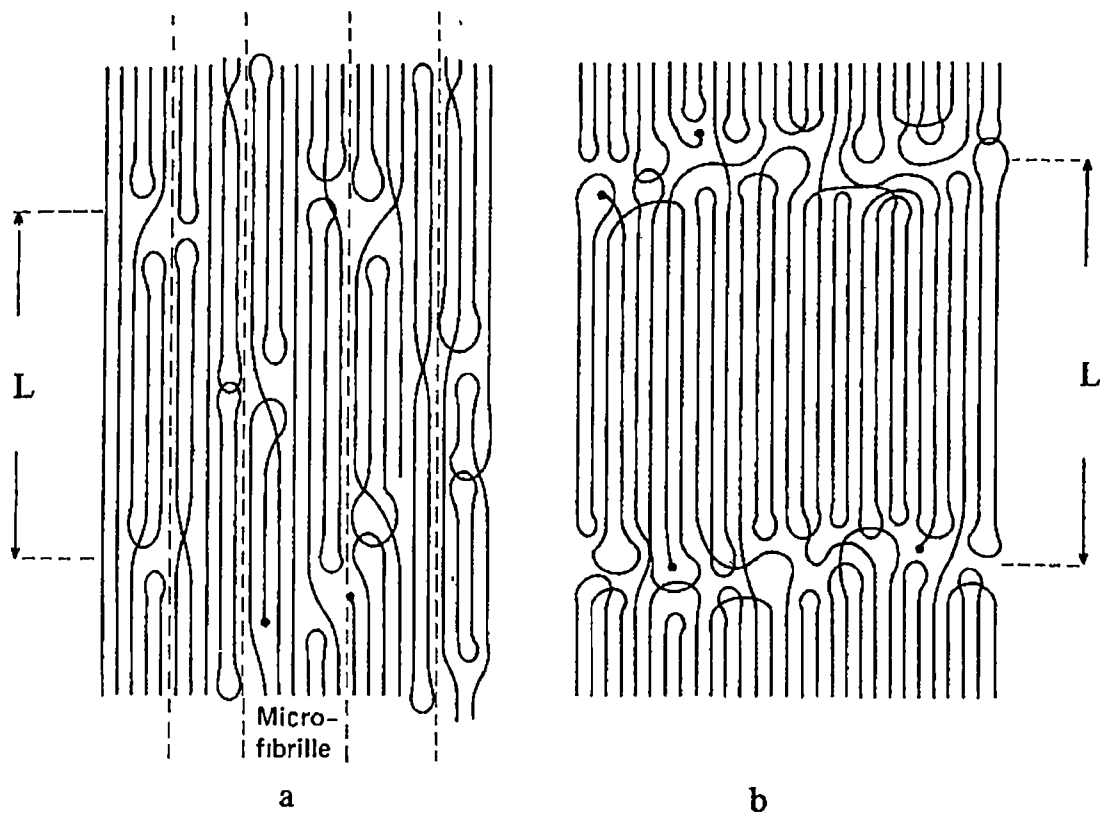


Figure 3.4 Structure of oriented partially crystalline polymers from a) cold stretched, not annealed sample b) annealed after stretching. L: Long Period.

Source: Kamf, G , "Characterization of Plastics by Physical Methods", Hanser Pub., Macmillin, NY, 107 (1986).

specify the degree of orientation of each of the crystal axes with respect to the reference direction Z:

$$f_{a,z} = 1/2 (3 \langle \cos^2 \phi_{a,z} \rangle - 1), \quad (3.1)$$

$$f_{b,z} = 1/2 (3 \langle \cos^2 \phi_{b,z} \rangle - 1), \quad (3.2)$$

$$f_{c,z} = 1/2 (3 \langle \cos^2 \phi_{c,z} \rangle - 1) \quad (3.3)$$

The corresponding geometry is shown in Figure 3.5. If the crystallographic axes are orthogonal,

$$\cos^2 \phi_{a,z} + \cos^2 \phi_{b,z} + \cos^2 \phi_{c,z} = 1 \quad (3.4)$$

From which it follows that

$$f_{a,z} + f_{b,z} + f_{c,z} = 0 \quad (3.5)$$

These results show that only two of the orientation functions are needed to specify the orientation.

For the crystalline phase, numerical values of the mean-square cosines can be calculated from the distribution of plane normals in an appropriate pole figure or directly from the fully corrected intensity distribution $I(\phi, \beta)$, obtained from the wide angle azimuthal x-ray scan. From Figure 3.6, in the case of axial orientation about Z the total number of (hkl) plane normals oriented at given latitude α or co-latitude ϕ is independent of the value of β . Thus the total number of plane normals at a given value of ϕ is proportional to the circumference of the circle of radius r , which is given by $\sin \phi$. Thus to obtain $\langle \cos^2 \phi_{hkl,z} \rangle$ averaged over the entire surface of the orientation sphere, it is necessary to weight $I_{hkl}(\phi, \beta)$ by $\sin \phi$. Thus:

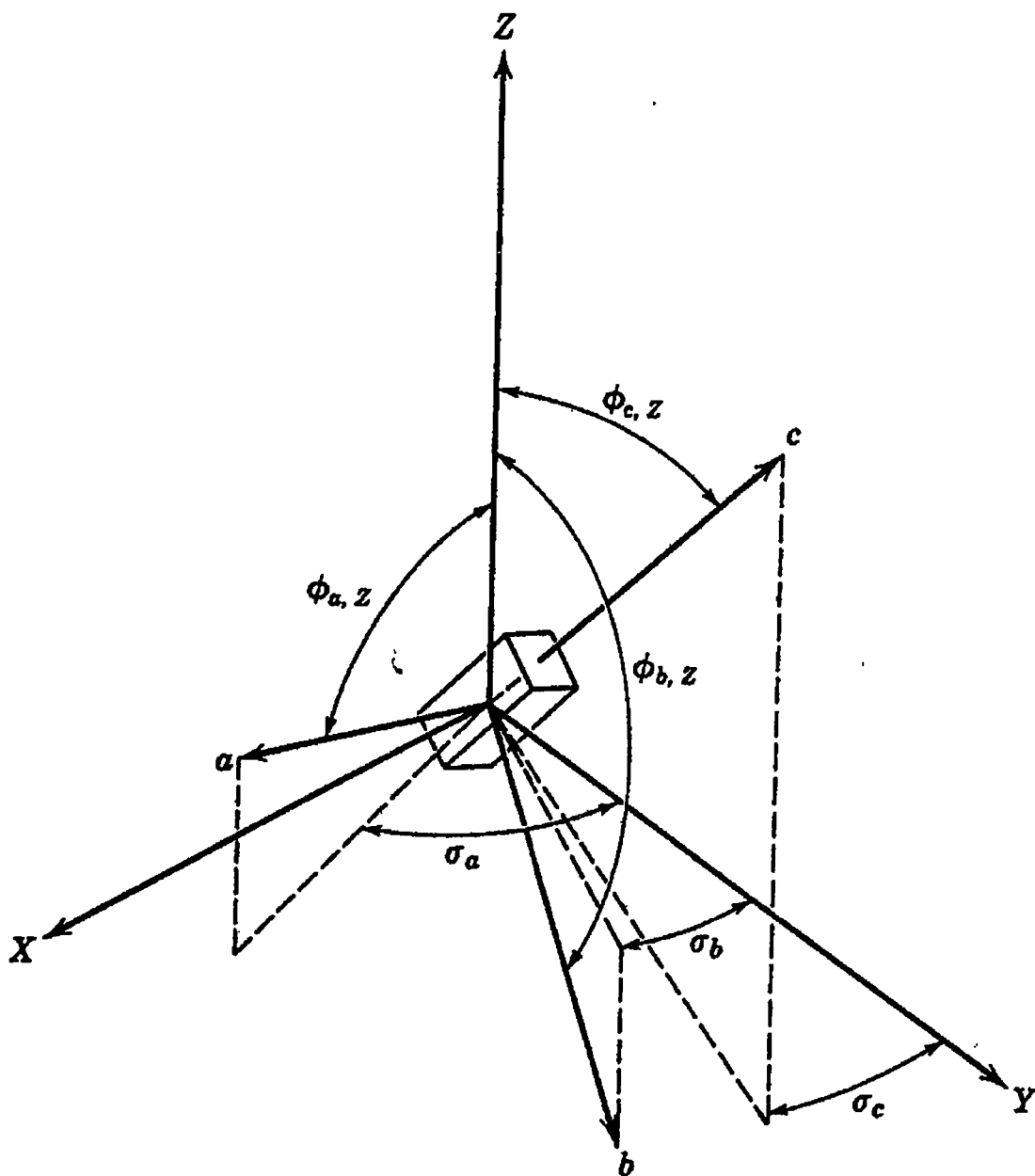


Figure 3.5 Stein's coordinate system for specifying orientation modes in orthorhombic polymers.

Source. Alexander, L. E., "X-Ray Diffraction Methods in Polymer-Science", Robert E. Krieger Pub. Company, NY, 242 (1969)

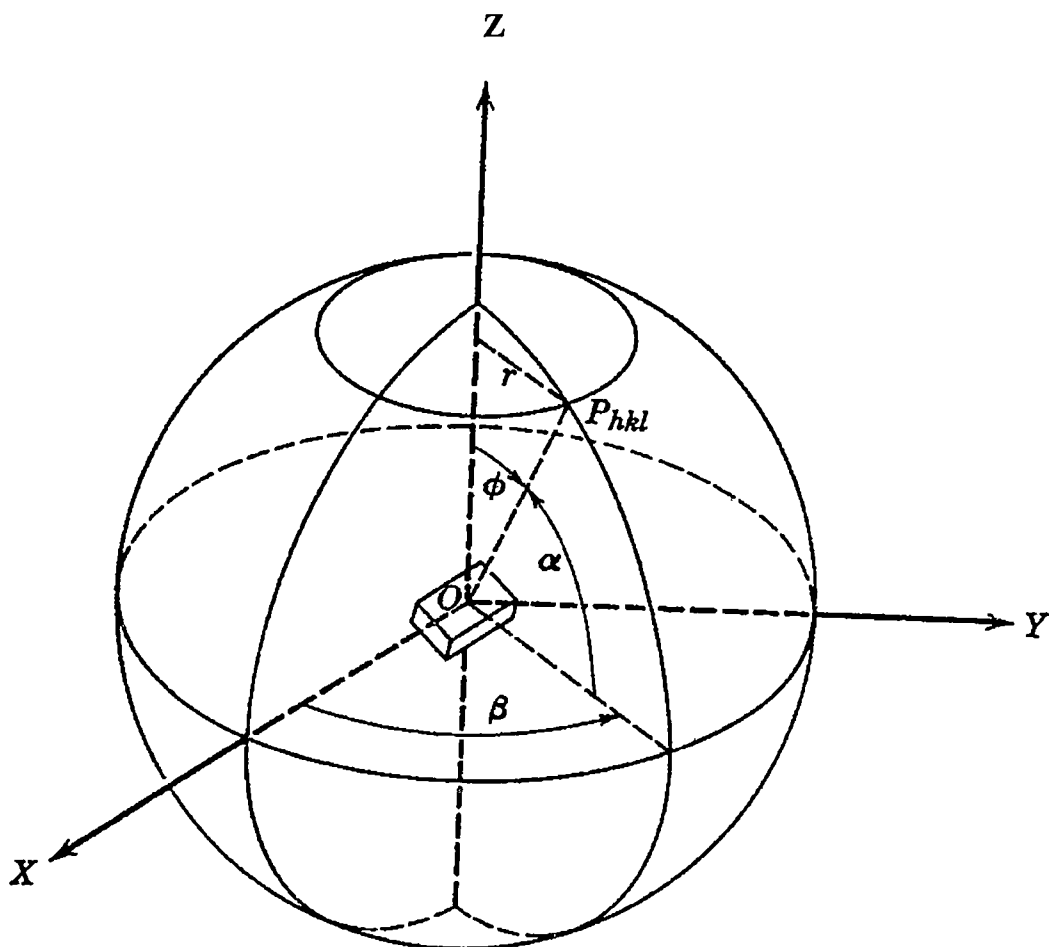


Figure 3.6 (hkl) plane normal oriented at a latitude α or co-latitude ϕ in the sphere of reflection

Source Alexander, L. E., "X-Ray Diffraction Methods in Polymer-Science", Robert E Krieger Pub. Company, NY, 244 (1969)

$$\langle \cos^2 \phi_{hkl,z} \rangle = \frac{\int_0^{\pi/2} I(\phi) \cos^2 \phi \sin \phi \, d\phi}{\int_0^{\pi/2} I(\phi) \sin \phi \, d\phi} \quad (3.6)$$

where

$$I(\phi) = \int_0^{\pi/2} I(\phi, \beta) \, d\beta. \quad (3.7)$$

The diffracted intensities from axially oriented specimens are independent of β , thus simplifying the intensity measurements and requiring only the integration in Equation 3.6 to be performed. If there are $00l$ crystal planes in the fiber, then the azimuthal intensity distribution of these alone can be used to calculate $F_{c,z}$. In PK fibers, the azimuthal intensity distribution of 002 peak will directly give the value of $\langle \cos^2 \phi_{c,z} \rangle$.

Unfortunately, there is a strong 2θ overlap of the 002 reflection with the 200 reflection. This creates a problem in unoriented or poorly oriented samples as the azimuthal intensity distribution of the 002 reflection is affected by that of the 200 reflection. Thus the 002 reflection is not satisfactory for measuring low degrees of orientation. At high degrees of orientation this overlap no longer causes any problem in determining the chain axis orientation function as the 002 is concentrated on the equator and the 200 is 90° away on the meridian. On the Rigaku x-ray diffractometer, the fibers are held parallel in the holder and the detector is set at the 002 2θ peak position to obtain azimuthal distribution of intensity ranging from $\alpha = 0^\circ$ to $\alpha = 90^\circ$. Prior to this, a 2θ scan was done to ascertain the exact peak position.

For lower draw ratios the 110 & 210 (Figure 3.7) peak intensity distribution can be used to estimate the $F_{c,z}$ values, as explained in the following discussion. For any crystal system, Wilchinsky has modified the treatment to determine a $\langle \cos^2 \phi \rangle$ function even in the absence of planes normal to the chosen crystallographic direction [47]. If Z be the reference direction, a , b & c are the crystallographic axes, $N(hkl)$ is the normal to the reflecting planes with intercepts m , n , p and U , V , c are the Cartesian coordinate axes, then Z and N , unit vectors in the Z and N directions are given by.

$$\mathbf{Z} = (\cos \phi_{U,Z}) \mathbf{i} + (\cos \phi_{V,Z}) \mathbf{j} + (\cos \phi_{c,Z}) \mathbf{k} \quad (3.8)$$

$$\mathbf{N} = e\mathbf{i} + f\mathbf{j} + g\mathbf{k} \quad (3.9)$$

Their scalar product is

$$\mathbf{N} \cdot \mathbf{Z} = \cos \phi_{hkl,z} = e \cos \phi_{U,Z} + f \cos \phi_{V,Z} + g \cos \phi_{c,Z} \quad (3.10)$$

From which the mean-square cosine of $\phi_{hkl,z}$ is given by:

$$\begin{aligned} \langle \cos^2 \phi_{hkl,z} \rangle &= e^2 \langle \cos^2 \phi_{U,Z} \rangle + f^2 \langle \cos^2 \phi_{V,Z} \rangle + g^2 \langle \cos^2 \phi_{c,Z} \rangle \\ &\quad + 2ef \langle \cos \phi_{U,Z} \cos \phi_{V,Z} \rangle \\ &\quad + 2fg \langle \cos \phi_{V,Z} \cos \phi_{c,Z} \rangle \\ &\quad + 2eg \langle \cos \phi_{c,Z} \cos \phi_{U,Z} \rangle \end{aligned} \quad (3.11)$$

In Equation 3.11, the quantity of primary interest is $\langle \cos^2 \phi_{c,z} \rangle$, which expresses the degree of alignment of the crystallographic direction c (by convention parallel to the molecular chains) with the reference direction. In PK-C₂ & PK-C₂/C₃, which is an orthorhombic system, type $hk0$ reflections obtained in the 2θ wide-angle x-ray diffraction scan are used to determine $\langle \cos^2 \phi_{c,z} \rangle$. Using the unit

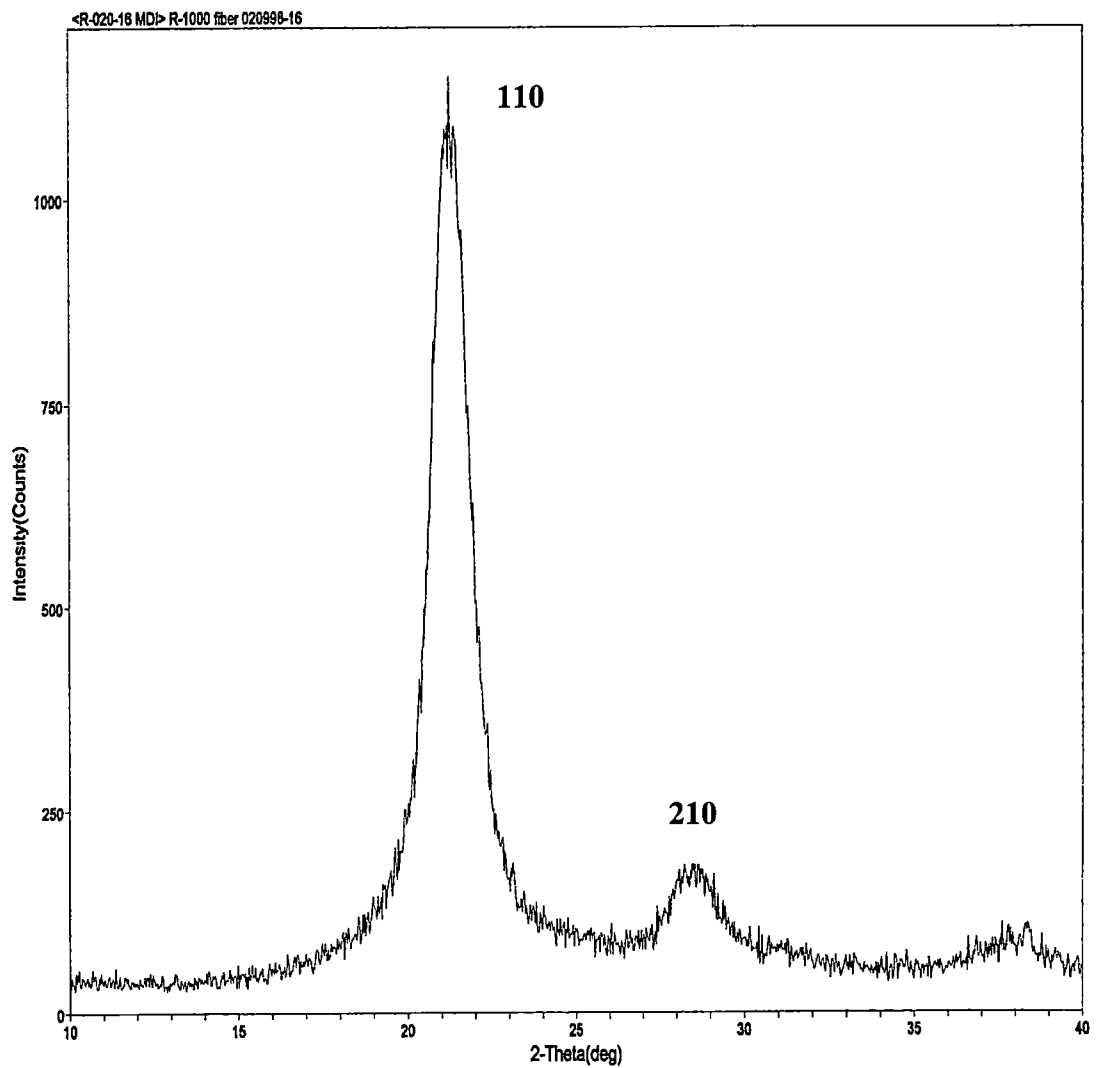


Figure 3.7 Equatorial 2θ scan of an oriented PK-C₂/C₃ fiber ($\alpha = 0^\circ$)

cell dimensions of the β -form, the following relationship was derived for calculating

$\langle \cos^2 \phi_{c,z} \rangle$ from the (110) & (210) reflecting planes (Appendix 2):

$$\langle \cos^2 \phi_{c,z} \rangle = 1 - 0.54 \langle \cos^2 \phi_{110,z} \rangle - 1.46 \langle \cos^2 \phi_{210,z} \rangle \quad (3.12)$$

For the determination of background, the azimuthal intensity distribution was taken at two other positions (where no peaks were detected in a 2θ scan), and then by interpolation the background intensity was calculated at the respective peak position for each α . This was then subtracted from the observed peak intensity to determine the corrected intensity for each α in the azimuthal scan. The corrected intensity distribution was used to determine the orientation functions.

3.3.2.2 Birefringence

Birefringence is a measure of the total molecular orientation of a system. It is defined as the difference in the principal refractive index parallel n_{\parallel} and perpendicular n_{\perp} to the stretch direction for a uniaxially oriented specimen. The refractive index in turn is the measure of the velocity of light in the medium and is related to the polarizability of the chains. Thus, the final measured birefringence is a function of contributions from the polarizabilities of all the molecular units in the sample.

$$\Delta_T = n_{\parallel} - n_{\perp} \quad (3.13)$$

Optical birefringence measurements were made on a Olympus microscope with a Leitz 30 order Berek Compensator. Tables provided in the Leitz compensator manual were used for determination of retardation. The fiber diameter was measured

using a television monitor attached to the microscope by a video camera. The calibration was done using a slide that had graduations marked with a least count of 0.01mm Both the 10X and 40 X objective lens was used for calibration. Using the relationship given below the birefringence was determined:

$$\Delta_T = \Gamma/d \quad (3.14)$$

Where,

Γ is the retardation and

d is the diameter.

A sample population of 6 for each fiber-specimen was tested and the average results were reported

3.3.3 Thermal Analysis

The thermal analysis was done on a Perkin-Elmer series 7 differential scanning calorimeter (DSC) using Indium with a melting point of 156.5 °C as the calibration standard. Thermal scans were done at a scan rate of 20 °C for the determination of melting point, α to β phase transition temperature (in copolymers), onset of melting and heat of fusion. Using 227 J/g as the heat of fusion for a 100 % crystalline PK-C₂/C₃ [48], and 239 J/g for PK-C₂, the % crystallinity of the samples was obtained.

The samples were chopped using scissors and placed into aluminum DSC pans The sample mass in the pans was kept between 5 to 10 mg Three specimen weights representative of a sample were taken and their averaged values were reported

3.3.4 Tensile Testing

Tensile testing was done on a Table Model 1122 Instron at a strain rate of 50mm/min with a gauge length of 25 mm. A short gauge length was used because specimens at low draw ratios have high elongations at break. Tensile samples of the filament tow were mounted on paper sample holders. The paper holders were prepared with a 25x10 mm rectangular window. The fibers were attached to one side of the holder with scotch tape. After mounting the samples between the jaws of the INSTRON, the paper holder strips were cut so that when the test started, the entire load was taken by the fibers.

From the engineering stress-strain curve, the initial modulus (slope of the initial linear part of the curve), tenacity (maximum engineering stress borne by the specimen), % strain at break, breaking stress and toughness were determined.

3.3.4.1 Elevated Temperature Tensile testing

Elevated temperature tensile measurements were performed on MTS 10/GL equipped with a 50 lbf load cell. A gage length of 120 mm and strain rate of 50 mm/min was used. Tensile testing was done at four different temperatures – 20 (room temperature), 100, 125 & 150 °C. The samples were enclosed in a heating chamber or oven and sufficient time was allowed to let them come to equilibrium with their surroundings. Ten specimens were tested per sample and the average values were reported.

The data was fed into a computer and Testworks 4.0 software was used to calculate the tenacity, % strain at break and modulus (all from the engineering stress-strain curve).

3.3.5 Thermal Shrinkage

Shrinkage upon annealing is generally a result of the relaxation of the amorphous phase. The degree of crystallinity, amorphous orientation and the time and temperature of annealing are the decisive factors. The higher the shrinkage, the higher is the orientation of the amorphous regions before annealing. Whereas a low level of shrinkage indicates that there is less amorphous orientation or a high degree of crystallinity. By definition, it is the change in the length of the fiber after annealing:

$$\% \text{ Thermal Shr.} = (\Delta l/l_0) \times 100 \quad (3.15)$$

where l_0 is the original length

Shrinkage gives an approximate indication of the level of amorphous orientation and any concrete inferences should not be made based on this

Annealing of the samples was done in a temperature range of about 165 ± 5 °C, in an oven, for about 10 minutes, in a perfectly relaxed state. The initial sample length was taken to be 20 cm. After annealing the samples were allowed to cool down to room temperature, and measured for any change in length. The % shrinkage values were reported as averages of three sample readings

3.3.6 Electron Microscopy

Scanning electron microscopy was done on a Cambridge Stereoscan 360 SEM[®] with a tungsten filament and a resolution capability of 2.5 nm. Pictures of peeled surfaces and fractured surfaces of the fibers were taken at 1000X and 2-3000 X respectively.

To observe the peel surfaces, the samples were given a thin cut using a sharp scalpel and then peeled using a fine pair of tweezers under a microscope. Two or more than two samples were thus prepared for any given specimen and then mounted on the holder over the black carbon background. The fractured fiber samples from the tensile testing were mounted in a similar way to observe the type of the fracture.

After mounting the samples, gold plating was done using a Technics Hummer I gold plating apparatus under a 100-millitorr vacuum. A current of 10mA was set for 1 minute to gold plate the samples.

3.3.7 Sonic Modulus

The sonic modulus for a long, thin, rod like sample is given by the expression[49]:

$$E = \rho C^2 \quad (3.16)$$

Where E is the sonic modulus, ρ is the density and C is the sonic velocity. The sonic velocity is usually determined by measuring the transit time of sound pulse between two transducers coupled to a test specimen. Figure 3 8 represents schematically the general features of an experimental apparatus for measuring the sonic velocity of a

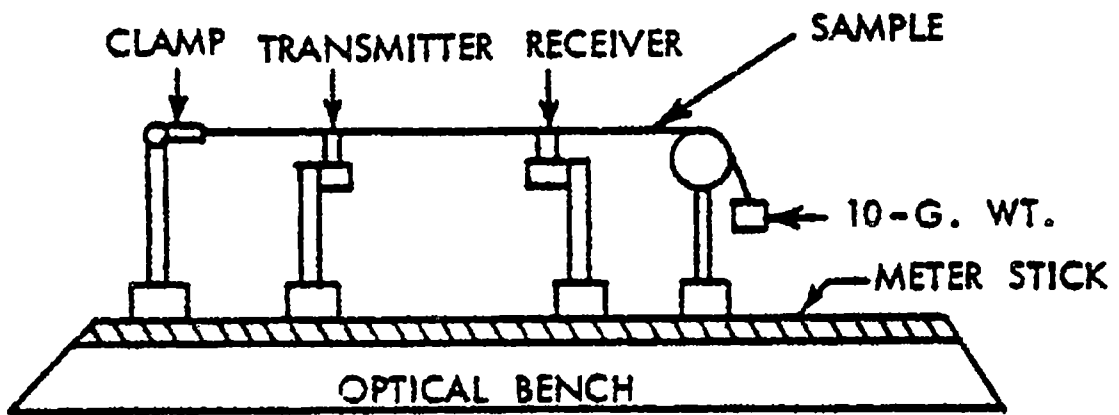


Figure 3.8 Schematic representation of Sonic modulus apparatus.

Source Samuels, R. J., "Structured Polymer Properties", John Wiley & Sons, NY, 46 (1974).

polycrystalline specimen. The filament tow is clamped at one end, passed over a pulley and kept taut by a 10-g weight (for light tension) at the other end. The transmitter and the receiver transducers can be moved along the bench and the distance between the probes can be measured using a meter scale, attached to the bench. A pulse propagation meter supplies the sound pulse. The transducers are kept at a given distance apart in contact with the specimen and the transit time is read directly in microseconds on the panel meter. This is measured at several distances (at least ten) between the probes and a plot of distance vs time is obtained. The slope of the line gives the sonic velocity. Once the velocity is calculated the sonic modulus can be calculated by the expression given above. At least four sets of readings per sample were taken and the average results were reported.

CHAPTER 4

RESULTS AND DISCUSSION

4.1 Temperature Dependence of Drawing

The first phase of this study was to find the optimum drawing conditions of PK-C₂ and PK-C₂/C₃ filaments. For this the as-spun filaments were drawn at different temperatures (as described in chapter 3) and the maximum draw ratio that a filament tow could be drawn to was recorded. This was done at different temperatures for each grade of the polyketone fibers provided. Figure 4.1 shows the temperature dependence of the drawing process. It appears that the fibers could be drawn over a broad range of temperatures but there appears to be an optimum temperature range in which each of the co and terpolymer grades could be drawn. Table 4.1 lists these optimum temperatures for each of the different polyketone polymer grades.

Among the terpolymers the high MW (THMW) grade has a higher optimum draw temperature than the low MW grade (TLMW), though the low MW (TLMW) grade attains a higher draw ratio. Again, the copolymer (CLMW) and the higher melting terpolymer (THMP) have substantially higher optimum draw temperatures than the others. The optimum temperature for different grades varies in accordance to their melting temperatures, with the copolymer (CLMW) having the highest and TLMW the lowest. In case of the copolymer, there is high % crystallinity to start with, so that this also accounts for its substantially high optimum draw temperature and a lower maximum draw ratio.

Table 4.1 Optimum temperatures and maximum draw ratios for different polyketone grades.

Polyketone grade	Optimum Draw Temp.	Maximum DR
TLMW	130 °C	8.5
THMW	170 °C	7.5
THMP	175 °C	8.6
CLMW	190 °C	7.4

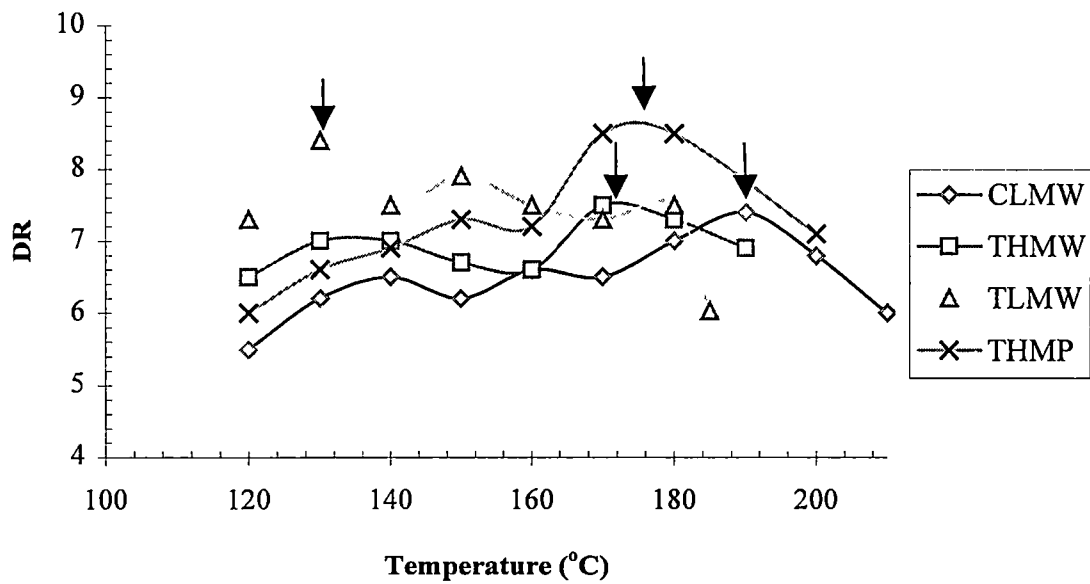


Figure 4.1 Plot of DR Vs Temperature for different PK grades.

4.2 Crystal Phases

As discussed in chapter 2, at room temperature the predominant crystal phases in the copolymer and the terpolymer are usually α and β , respectively. In the fibers, however, this may not be always true. Figure 4.2 shows the equatorial 2θ scans of the as-spun filaments of copolymer, CLMW and the high molecular weight terpolymer, THMW on the same plot. The respective peaks corresponding to each crystal phase are marked for clarity. In the terpolymer, all the peaks correspond to the β form, however in the copolymer, peaks from both phases are present. In particular, the 210 peaks from both α and β -phases are clearly observed. This is a strong indication that in the as-spun filaments of copolymer, there are two crystal forms present at room temperature.

Interestingly, with increasing draw ratio the relative amount of the two phases changes. In the as-spun sample, the proportion of the β component in the copolymer is the maximum and decreases gradually with increasing draw ratio, as reflected by the intensity of the 210 β peaks in Figure 4.3, where equatorial 2θ scans of copolymer fibers drawn at different draw ratios are plotted. At the same time, the proportion of the α component increases, as reflected by the increasing intensity of the 200 & 210 α peaks. Table 4.2 lists the ratio of the volume and weight fractions of α/β phases. These have been calculated from taking the ratio of the measured peak intensities of 210 α to 210 β . In this calculation it was assumed that the ratio of the calculated intensities, i.e., the structure factors of these phases is $I_{\alpha}^0/I_{\beta}^0 = 0.95$, so that the volume fraction of

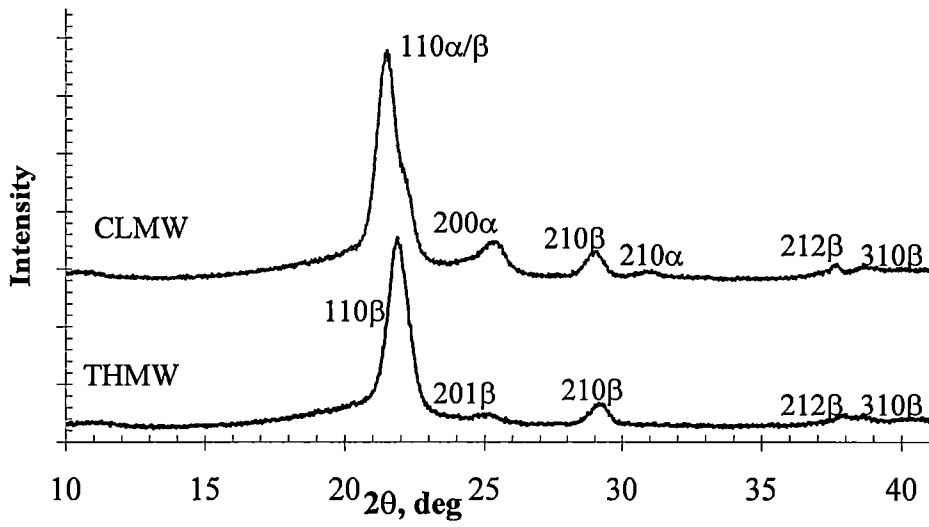


Figure 4.2 Equatorial 2θ scans of CLMW and THMW.

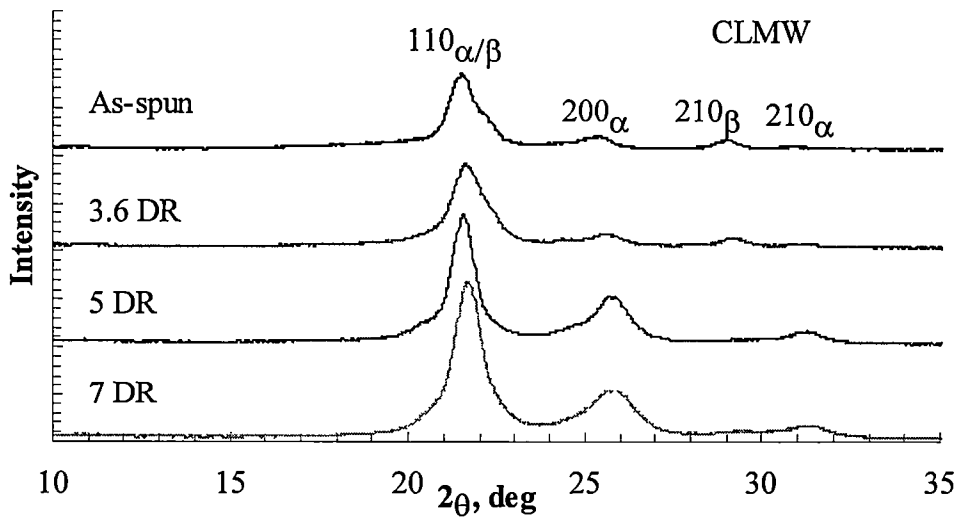


Figure 4.3 Equatorial 2θ scans of different draw ratio samples of CLMW.

Table 4.2 Volume and Weight fractions of α and β phases in CLMW.

DR	I _{total}	I _{210β}	I _{210α}	V _{α}	W _{α}	V _{β}	W _{β}
1	577	454	123	0.22	0.23	0.78	0.77
3.6	975	668	307	0.33	0.34	0.67	0.66
5	1187	159	1028	0.87	0.88	0.13	0.12
7	1475	281	1194	0.82	0.83	0.18	0.17

the α phase relative to the total crystalline fraction is given by:

$$V_{\alpha} = \frac{I_{\alpha}}{I_{\alpha} + 0.95I_{\beta}} \quad \dots(4.1)$$

Since we know the densities of the two phases we can obtain the relative weight fractions as follows:

$$W_{\alpha} = \frac{1.382I_{\alpha}}{1.382I_{\alpha} + 1.297I_{\beta} \cdot 0.95} \quad \dots(4.2)$$

where, the densities of the α and β phases taken are 1.382 & 1.297 g/cc. The as-spun sample has the highest amount of β phase whereas the high draw ratio oven drawn samples (5 & 7 draw ratios) have the lowest amount of β form. During melt spinning, which is conducted at temperatures well above the α to β phase transformation temperature (90-100 °C), the predominant form in the as-solidified fibers is β . And because of the rapid quenching, the β form has insufficient time to completely

transform back into the α phase. Hence we find both the α and β phases in the as-spun filaments at room temperature. However, after drawing, that is again performed at temperatures higher than 90-110 °C, the cooling is much slower thereby giving time for the β to α phase transformation to take place. The axial stresses coupled with the heat may also drive the structure into the more compact α form. Hence we see the gradual increase in the weight fraction of the α form and a simultaneous decrease in the weight fraction of the β form.

Figures 4 4-5 show the equatorial 2θ scans of THMW and THMP respectively with the respective peaks marked on the plots for clarity. With increasing draw ratio the intensity of the 110β and 210β peak increases in both the samples. This indicates that the proportion of these planes aligned along the fiber axis increases with increasing draw ratio. Similar trend was also observed in the copolymer for the 110 planes in Figure 4 3.

Figure 4.6 shows the WAXD flat plate patterns of the highly drawn samples of all the four polymeric grades. Comparing the copolymer (CLMW) with the rest of the terpolymer grades, it can be seen that both the 011 & 111 peaks occur in terpolymer, whereas 011 is missing in the copolymer flat plate film pattern (characteristic double arcs in the film that can be seen as we go radially outward at 45° angle from the center, see Figure 3.3). Another difference is the distance between the 200 & 210 peaks. Both these observable differences are due to the different types of crystal structures present in the system. At room temperature, α & β forms are present predominantly in the

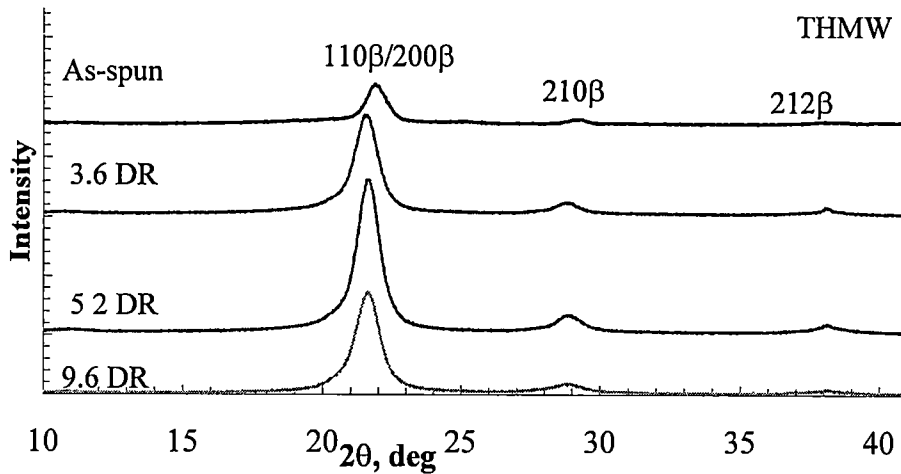


Figure 4.4 Equatorial 2θ scans of different draw ratio samples of THMW.

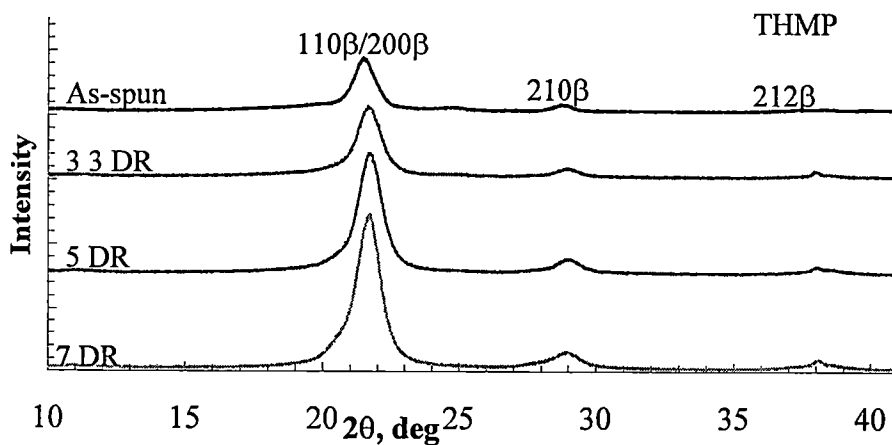
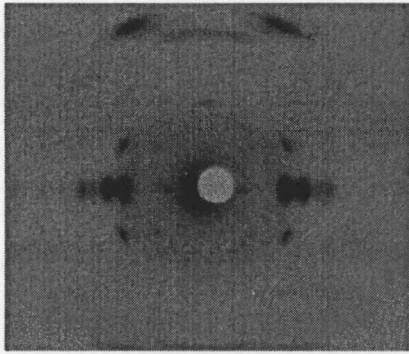
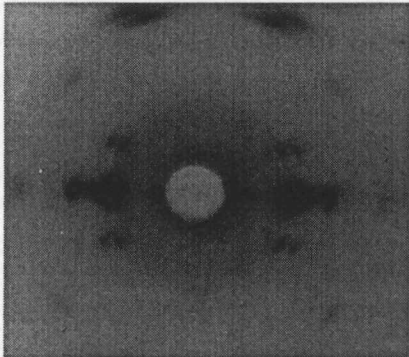


Figure 4.5 Equatorial 2θ scans of different draw ratio samples of THMP.



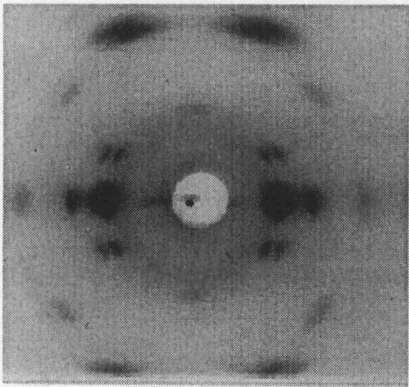
CLMW, 7 DR

Oven Drawn, 250 °C.



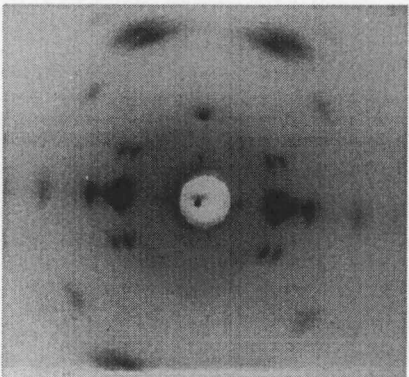
TLMW, 9.6 DR

Oven Drawn, 235 °C



THMW, 9,6 DR

Oven Drawn, 235 °C



THMP, 9,6 DR

Oven Drawn, 250 °C

Figure 4.6 WAXD Flat Plate Patterns of high draw ratio fibers.

highly drawn fibers of copolymer and terpolymer respectively. Thus, looking at the flat film pattern, an idea about the type of crystal phase can be assessed.

4.3 Thermal Properties

Figure 4.7 shows the variation of the melting point with draw ratio. The melting point increases slightly with draw ratio, though very gradually. Based on the results obtained from the small angle scattering, described later in another section, it was found that the lamellar thickness increases with draw ratio. This result is true for both the copolymer and the terpolymer fibers. Hence, the increase in melting point can be attributed to the increase in the lamellar thickness with draw ratio. The copolymer, CLMW, and the high melting point terpolymer, THMP have higher values, as expected, than the corresponding low melting-point terpolymer grades (TLMW & THMW)

Figure 4.8 shows the DSC scans of as-spun fibers of the copolymer and the terpolymer. All the scans display bimodal melting peak behavior. This could be due to a number of possibilities. The first one being that the packing of the fibers in the DSC pans is non-uniform so that during melting two melting endotherms occur. The second possibility might be that there are two different crystalline forms present. And the third is that there are two different populations of the same type of crystalline form differing only in lamellar thickness. Yet another could be that the first peak represents the crystals as they are at room temperature and the second peak occurs due to the lamellar thickening during the DSC scan itself.

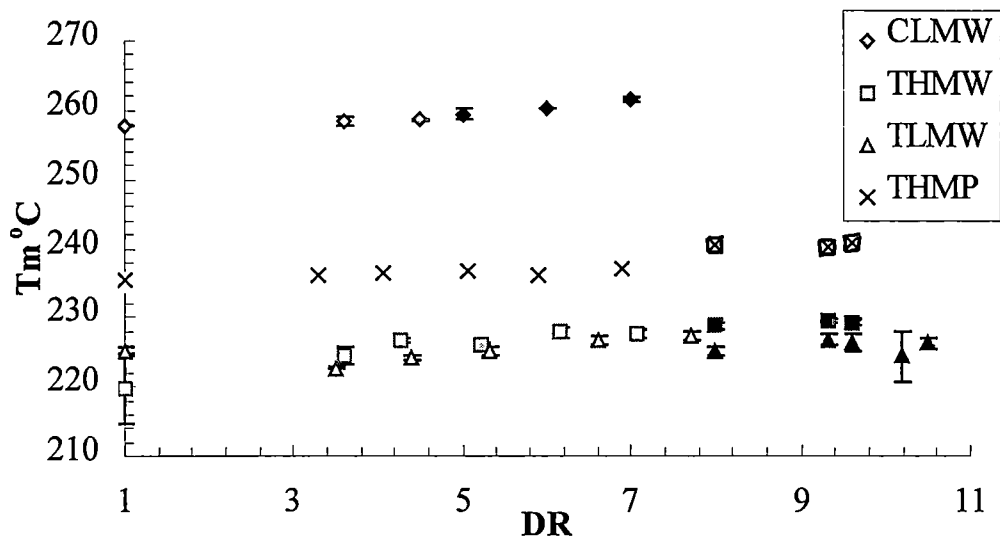
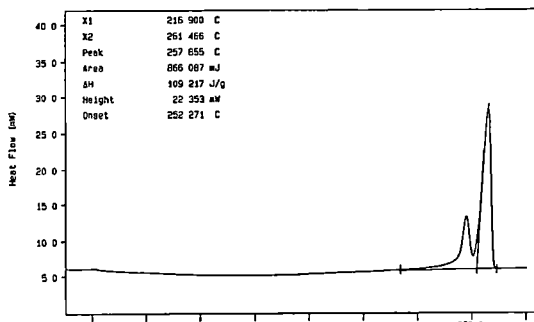
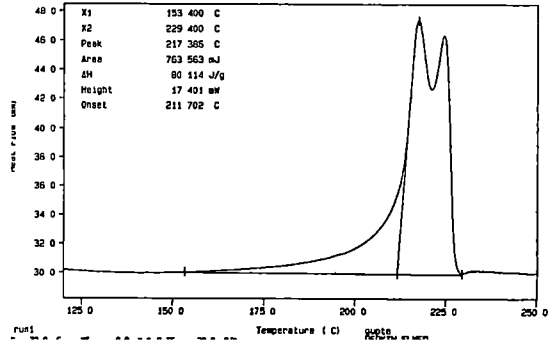


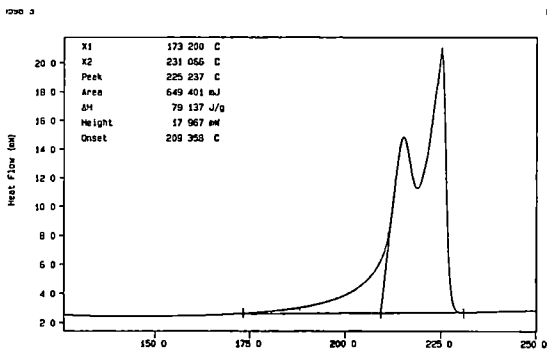
Figure 4.7 Variation of Melting point, T_m , with Draw ratio, DR.
 (data points in black represent oven-drawn samples)



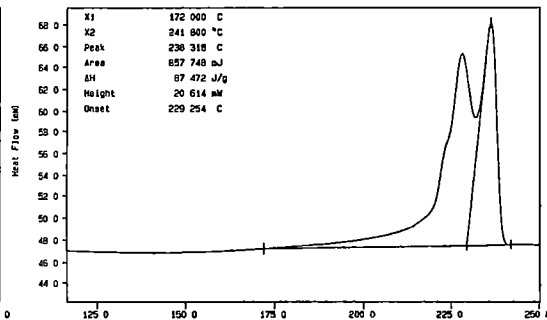
As spun filament, CLMW



As spun filament, THMW



As spun filament, TLMW



As spun filament, THMP

Figure 4.8 DSC scans of as-spun filaments.

Samples of as-spun fibers were run with and without alumina powder to investigate the effects of packing in the pans. There was no significant change in the peak shape or peak positions with respect to the temperature, hence the first possibility of poor thermal conductivity was eliminated.

By the discussion in the preceding sections, it was concluded that the terpolymer as-spun or drawn samples had only the β crystal form present (Figures 4 2-5) Hence the possibility of having two crystal forms in the terpolymer samples is ruled out. However, in the case of the as-spun copolymer, both α and β phases are present. But we know that a phase transformation of α to β takes place in the temperature range of 90-110 °C, so that during the DSC scan itself, any α phase in the sample will transform into the β . Accordingly we should observe a small endotherm in that temperature range marking such a transformation. In Figure 4.8, however, we do not observe such a phenomenon. This is because of the low weight fraction (~ 0.2 , Table 4 2) of the α phase in the as-spun copolymer fibers, at room temperature, to start with. The heat changes accompanying the transformation are so low that we do not observe any appreciable endothermic peak in the scan. Whereas in the high draw ratio samples, where the α phase is more predominant, this transformation is much more prominent. This is depicted by the marked endotherms (at around 90-100 °C temperature range) in the high draw ratio copolymer fibers in Figure 4.9.

Based on this discussion, the possibility of having two crystal forms that might attribute to bi-modal melting behavior was ruled out. This leaves us with the

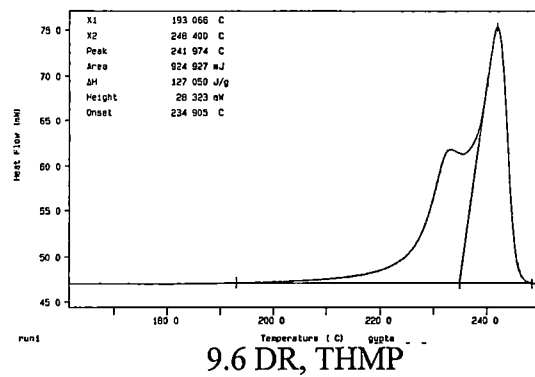
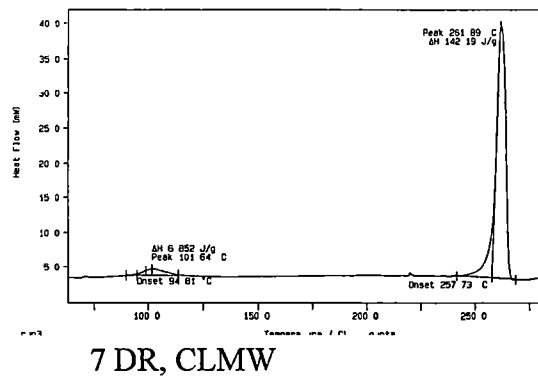
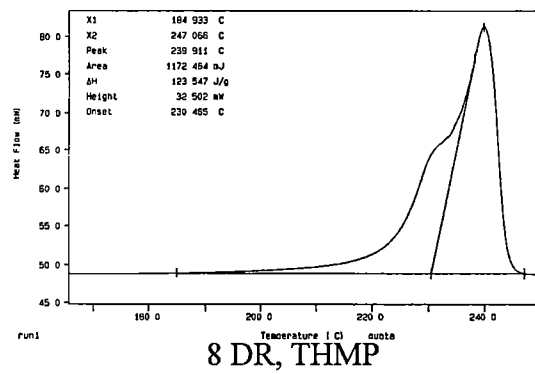
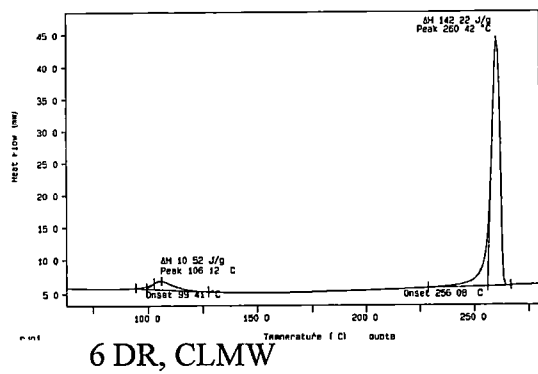
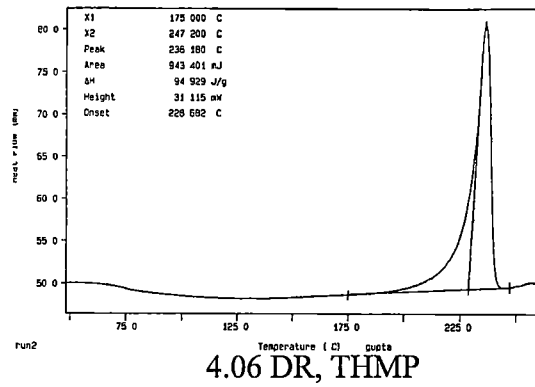
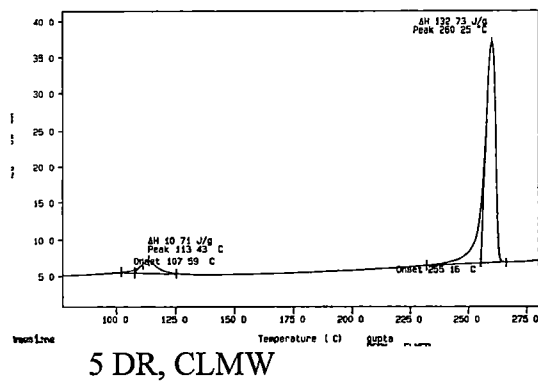


Figure 4.9 DSC scans of CLMW and THMP

explanation of having two distinct populations of the same crystalline form but with different lamellar thicknesses or the possibility of lamellar thickening during the DSC run.

With increasing draw ratio, the bimodal melting behavior gradually disappears in the case of the copolymer. It is most pronounced in the as-spun filaments which fades into a shoulder in the lower draw ratio samples and finally disappears completely at higher draw ratios, indicating that at higher draw ratios there is perhaps only one distinct population of a unique crystalline form having a fixed lamellar thickness.

For the terpolymers, however, the bimodal melting peak behavior is more pronounced for as-spun and the highly drawn fibers. As shown in Figure 4 9, the high draw ratio samples of THMP (8 & 9 6 DR), that were oven drawn at a temperature of 250 °C, display a marked bi-modal melting behavior. In the low draw ratio sample (4 06 DR), which was drawn on heated rollers at a temperature of 175 °C there is only one melting peak, indicating that there is only one distinct population of a unique crystalline form having a fixed lamellar thickness. On observing the other intermediate draw ratio samples of THMP (not shown in Figure 4 9), that were drawn on the heated rollers, we found that the bi-modal melting peak behavior is absent at low draw ratios. This is true for all the three terpolymer grades. With increasing draw ratios, the melting peak starts to broaden (intermediate draw ratios of 4-5.5) leading eventually to the appearance of a low temperature shoulder at somewhat higher draw ratios (6-8

DR) However, the bi-modal melting behavior is more prominent in the oven drawn samples.

Figure 4.10 shows the DSC scans of THMW as-spun filaments run at different scan rates. It can be seen that with increasing scan rates the bi-modal melting peak behavior disappears and at extremely high scan rates we find only one peak. This may be an indication that recrystallization during the DSC scan takes place but is not a conclusive observation. Figure 4.11 shows the variation of heat of fusion, ΔH , and melting temperature, T_m (for both the peaks) with increasing scan rate for the same sample, THMW as-spun. The heat of fusion rises steadily and then levels off at higher scan rates. The peak melting temperatures for both the peaks, however, keep rising steadily in a linear progression. We have not been able to understand this phenomena perfectly well and further investigations need to be done to be able to understand the bi-modal melting behavior of terpolymer fibers. From these results, it can be concluded that the bi-modal melting phenomena could be due to either of the two possibilities: 1) presence of two distinct populations of the same crystal form with different lamellar thicknesses and 2) occurrence of recrystallization during the DSC scan itself. The latter possibility seems more plausible looking at the DSC scans run at different scan rates but it is not conclusive.

Lommerts [6] conducted DSC studies on oriented polyketone fibers that had varying amounts of propylene in them. The data in Figure 4.12 is adapted from his results, which shows the plot of T_m , the melting point temperature, with wt % of

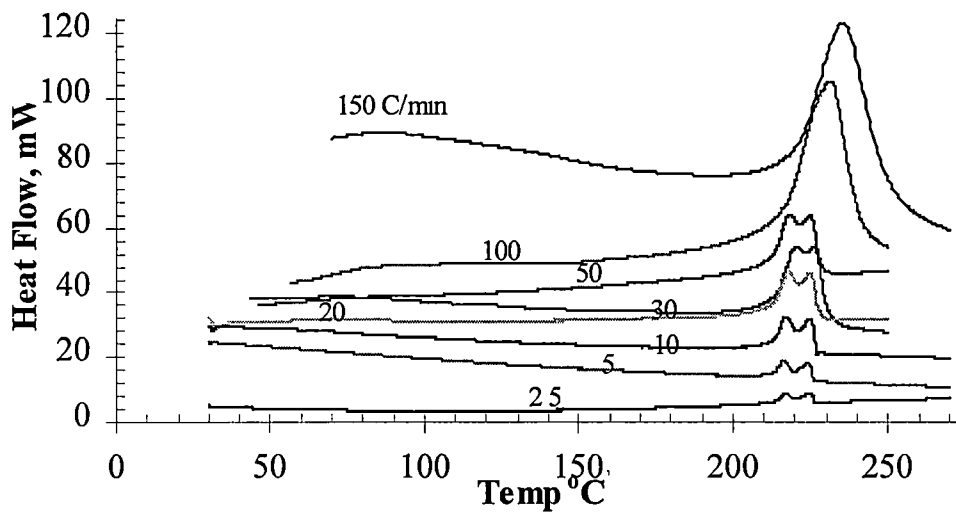
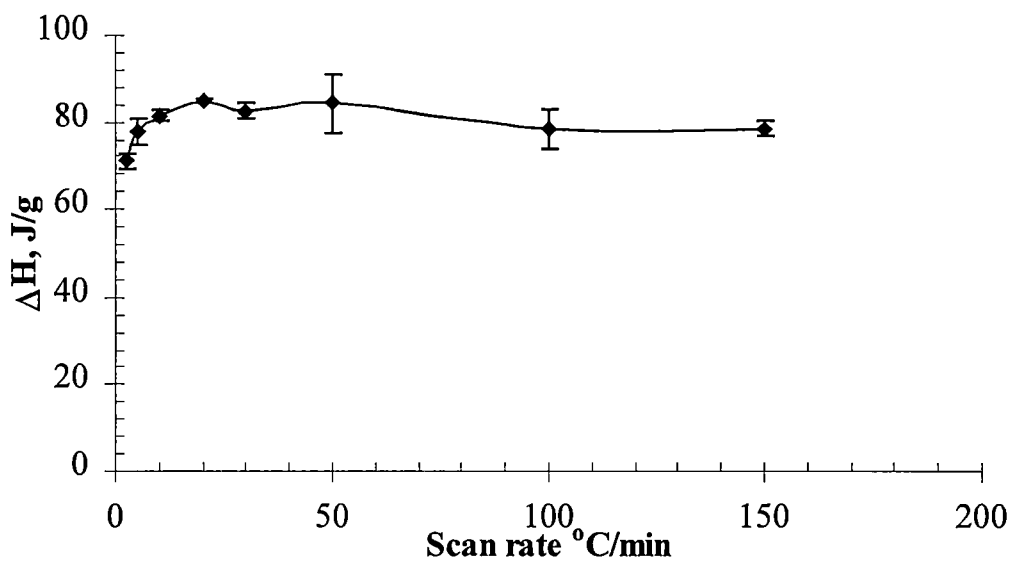
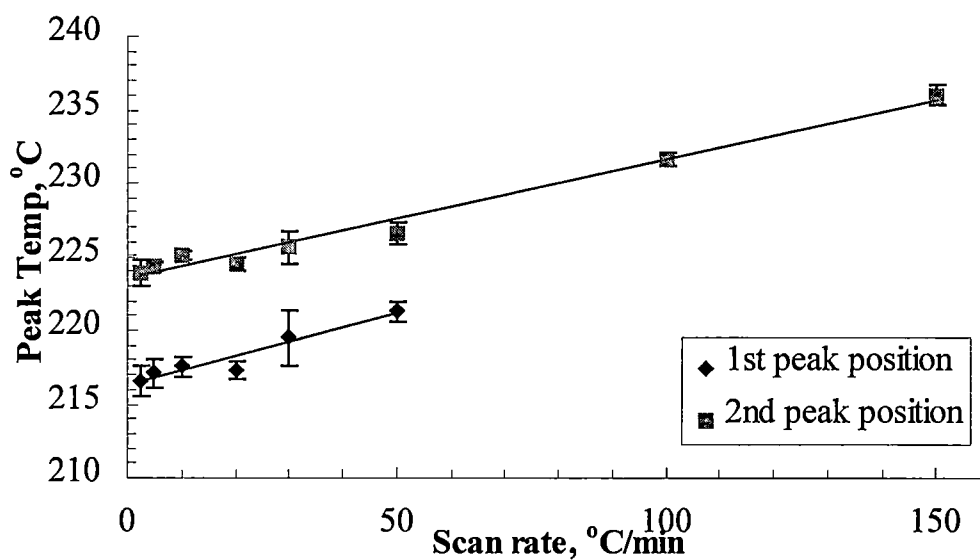


Figure 4.10 DSC scans of THMW as-spun filaments at different scan rates showing the disappearance of b₁-modal melting behavior at higher scan rates.



a)



b)

Figure 4.11 Variation of a) ΔH and b) peak temperatures with DSC scan rates, THMW.

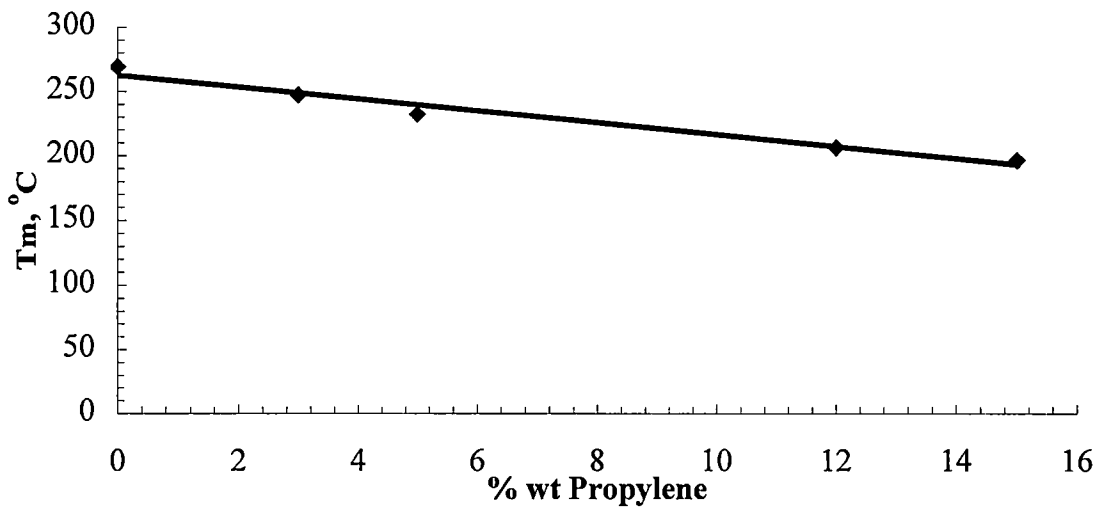


Figure 4.12 Plot of Tm Vs % Propylene.

Adapted from Lommerts, B J., “ Structure Development in polyketone & polyalcohol fibers”, Ph.D Dissertation, University of Groningen, 109 (1994).

propylene content. From the DSC results, the melting point temperatures of our terpolymer samples were compared with Lommerts' data to get an estimate of the concentration of propylene in the terpolymer fibers. Table 4.3 lists the average melting temperatures of oriented TLMW, THMW and THMP fibers along with their estimated values of % wt propylene.

The low melting point terpolymers (TLMW & THMW) have higher wt % propylene, about 7-9 wt %, than the high melting point terpolymer (THMP) which has only 5-6 wt % propylene by weight.

4.4 Crystallinity

Copeland [47] studied the development of density of low and high molecular weight terpolymer fibers with draw ratio and related that to their % crystallinity. From the DSC scans of as-spun low and high molecular weight fibers (TLMW & THMW respectively), we found the % crystallinity to be 34-36 % Copeland reported 36-37 %

Table 4.3 Estimation of % Propylene in Terpolymer samples.

Grade	T_m range (°C)	Propylene wt %	Propylene mol %
THMP	236-240	4.9-5.8	3.9-4.6
THMW	224-229	7.2-8.3	5.8-6.6
TLMW	222-226	7.9-8.7	6.3-6.9

for the same sample fibers. This agreement of the data suggests that even if there is any recrystallization occurring, it does not affect the overall % crystallinity of the fibers.

The percentage crystallinity values were calculated based on the heats of fusion obtained from the DSC scans. For a 100 % crystalline PK-C₂ & PK-C₂/C₃, the heats for fusion were taken as 227 J/g and 239 J/g [48]. Figure 4.13 shows the variation of crystallinity with draw ratio. With increasing draw ratio, the crystallinity of the samples increases. The effect is more pronounced in the copolymer than in the terpolymer grades, where not only the crystallinity values are significantly higher but also they respond at a faster rate to the draw ratio than the terpolymer grades.

Maximum % crystallinity in the range of 58-60 % for the copolymer and 52-56 % for the terpolymers were obtained for highly drawn fibers. The as spun crystallinity values were around 45 and 35 %, respectively for the co and terpolymer.

Amongst the terpolymer grades, the variation at low draw ratios is more or less the same with all of them having the same amounts of crystallinity. However, at higher draw ratios, the high melting point terpolymer, THMP, has higher crystallinity than the lower melting point grades. Further the crystallinity values of the low and high molecular weight, low melting point terpolymers, TLMW & THMW respectively, are more or less the same. Their variation with draw ratio is also the same.

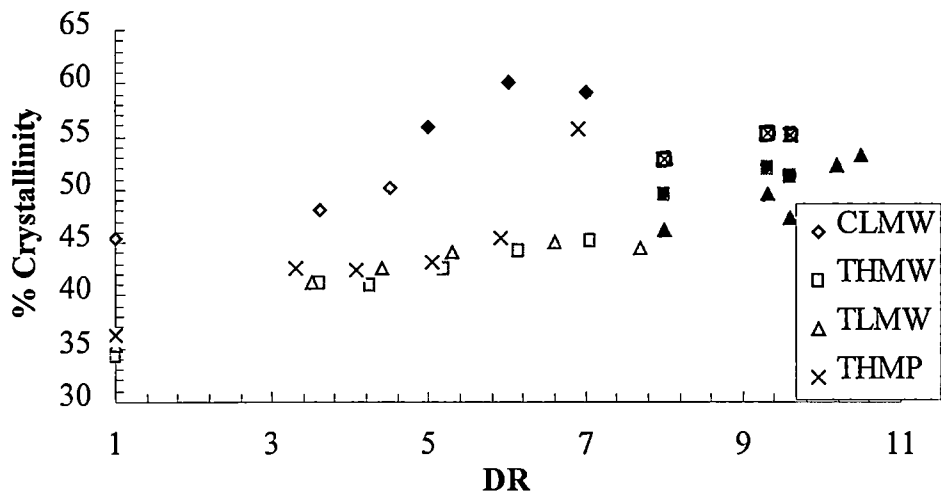


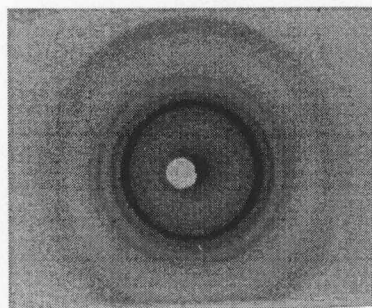
Figure 4.13 Variation of % crystallinity with draw ratio, DR
 (data points in black represent oven-drawn samples)

4.5 Crystalline Orientation

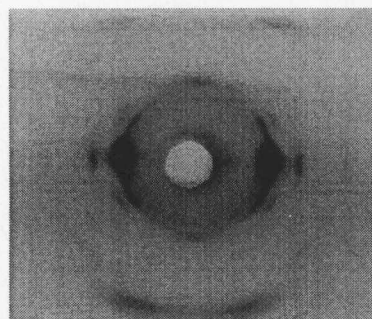
Based on the wide-angle flat plate x-ray diffraction patterns of different grades of polyketone fibers (Figures 4.14-15), the as spun filaments have little or no orientation. This is probably due to the fact that fibers spun at slow spinning speeds develop little or no orientation because of the low axial stresses that are not sufficient to align the molecules along the fiber axis. However, during the post spinning draw operation, the axial stretching of the filaments tends to align the chains along the fiber axis, which reflects as an increase in the orientation. This is reflected in the flat plate patterns where the concentric rings, in the as-spun filaments, are reduced to small discontinuous arcs, for smaller draw ratios and spots for higher draw ratios.

Since the high draw ratio samples were oven drawn, they are marked as "OD" beneath each pattern along with the temperature at which they were drawn. Similarly, the low draw ratio samples that were drawn on heated rollers are marked as "RD" along with their draw temperature. It can be concluded from these photographs that the crystalline orientation increases with increasing draw ratio.

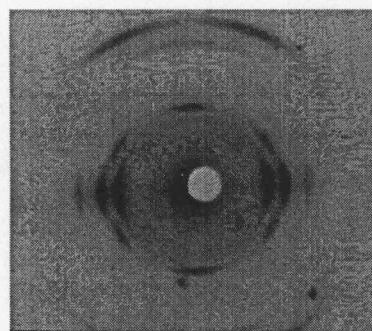
The crystalline orientation functions also corroborate this fact. As described in chapter 3, we had calculated the orientation functions by two methods: one by using the 110 & 210 peak intensity distribution data and the other by 002 peak intensity distribution data. Figures 4.16-17 show the $F_{c,z}$ values of the four grades, calculated by different methods. The values calculated by using the 110 & 210 peak intensity distribution data is lower than those calculated by the 002 peak data. The difference in



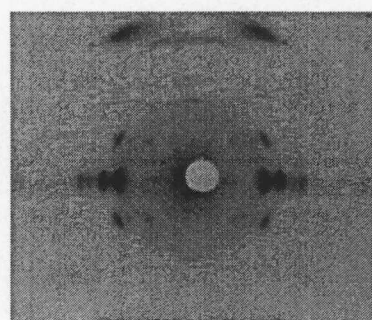
As-spun



3.6 DR, RD, 130 °C

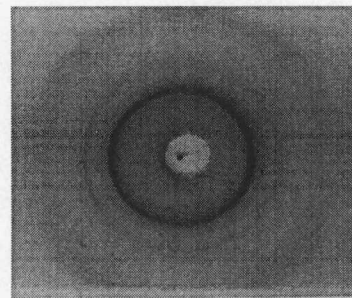


5 DR, OD, 250 °C

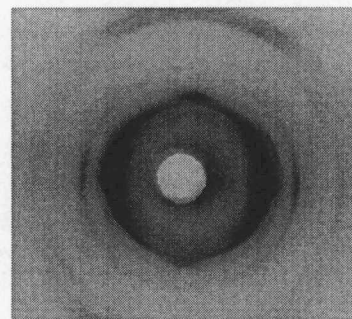


7 DR, OD, 250 °C

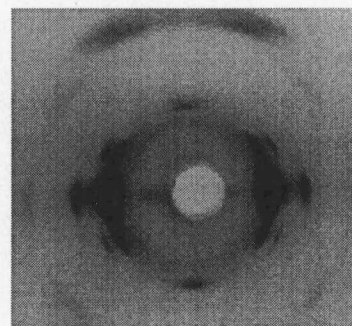
CLMW



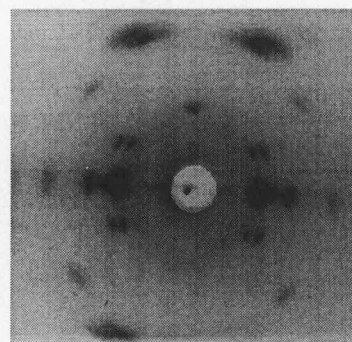
As-spun



3.3 DR, RD, 175 °C



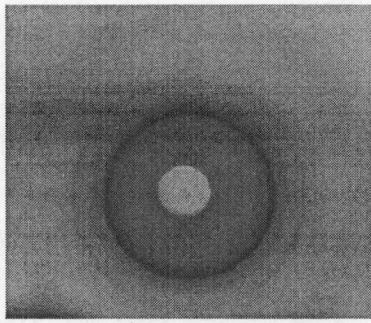
5 DR, RD, 175 °C



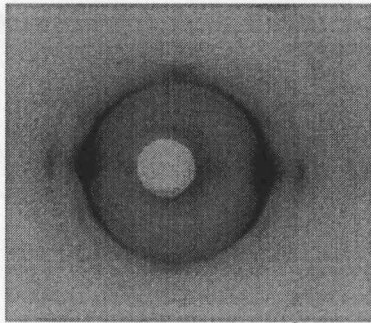
8 DR, OD, 250 °C

THMP

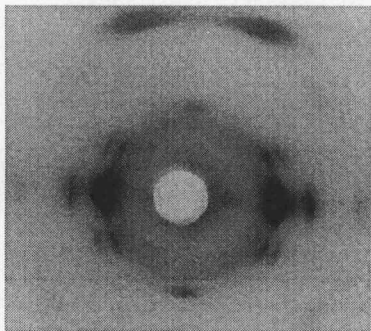
Figure 4.14 WAXD Flat plate patterns of CLMW & THMP
(Where RD stands for “fibers drawn on heated rollers” and OD for “oven drawn”)



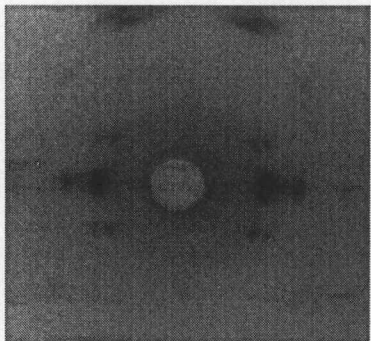
As-spun



3.5 DR, RD, 130 °C

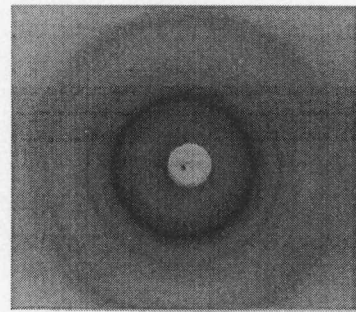


5.3 DR, RD, 130 °C

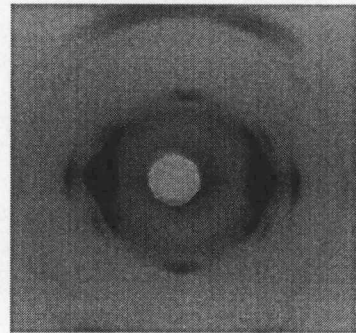


9.6 DR, OD, 235 °C

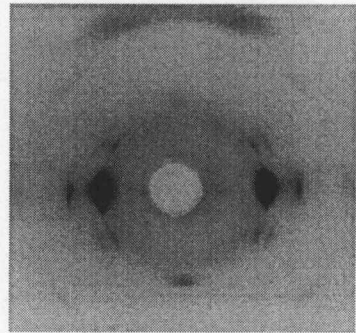
TLMW



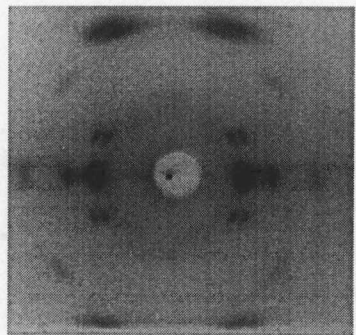
As-spun



3.6 DR, RD, 170 °C



5.2 DR, RD, 170 °C



9.6 DR, OD, 235 °C

THMW

Figure 4.15 WAXD Flat plate patterns of TLMW & THMW
(Where RD stands for “fibers drawn on heated rollers” and OD for “oven drawn”)

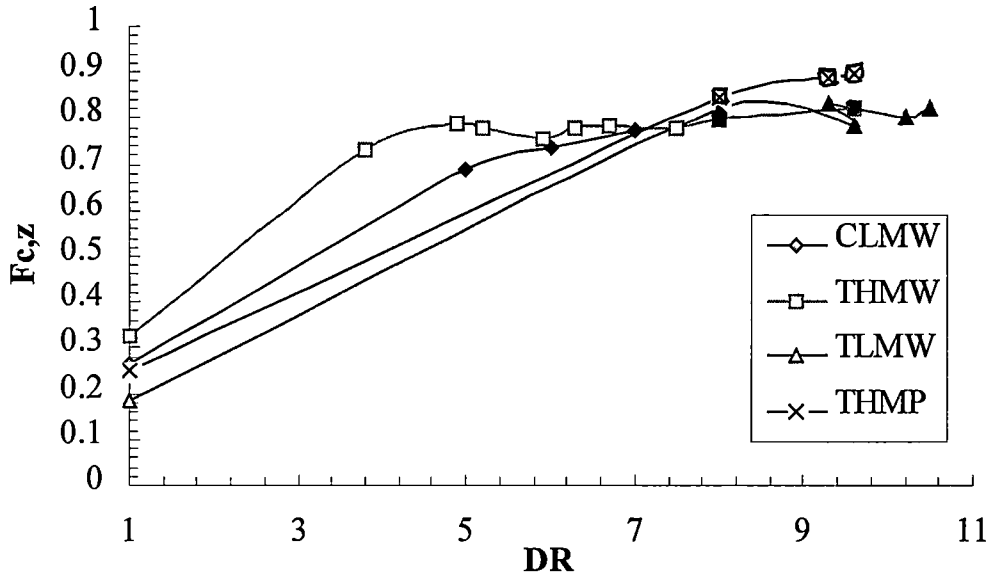


Figure 4.16 $F_{c,z}$ Vs DR, calculated using 110 & 210 peak intensity distribution. (data points in black represent oven-drawn samples)

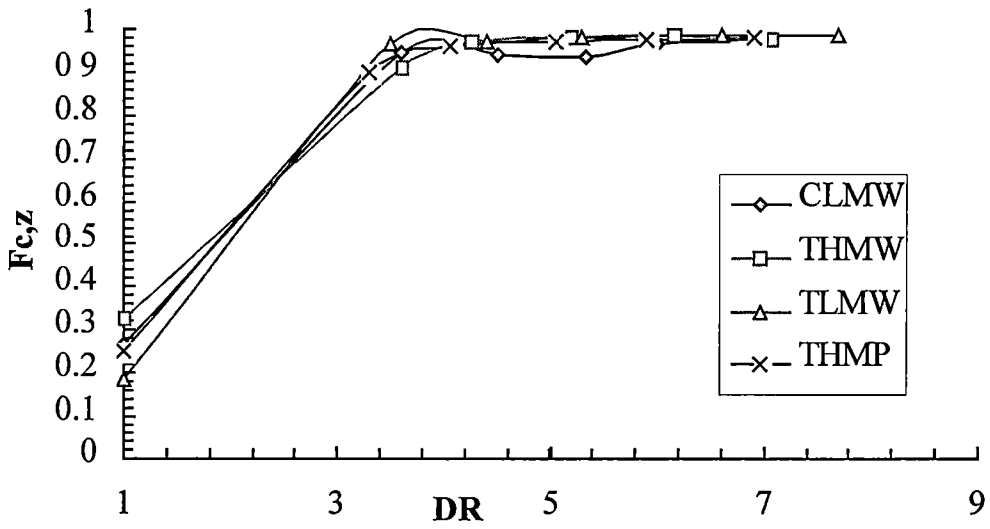


Figure 4.17 $F_{c,z}$ Vs DR, calculated using 002 peak intensity distribution.

the two sets of values is because that while taking the azimuthal intensity distribution scans of 110 & 210 peaks, there is an additional peak, 011, in the immediate vicinity of 110. Hence not only the 110 intensity distribution gets recorded but also we get some interference from the 011 peak, going from $\alpha = 0^\circ$ to 90° .

Figure 4.18 shows the α Vs 2θ scan of a highly oriented (DR 9.6) THMP fiber. Looking at around $2\theta = 20-23^\circ$, we find that there is an additional peak distribution (011), at low α , that will interfere with the 110 scan because of its proximity to the 110 peak. The data obtained from the 002-peak intensity distribution is therefore more accurate, as there is no interference in the immediate vicinity of the peak at small angles.

However, in both the plots, we see a similar trend of increasing orientation function values with draw ratios. The interesting observation here to be made is that around a draw ratio of four, the values level off. At this draw ratio the drawing forces are probably sufficient enough to cause a substantial orientation of the crystals along the fiber axis. Any further increase in draw ratio tends to increase the crystalline orientation slightly. A maximum $F_{c,z}$ value of 0.98 was recorded for both the highly drawn PK-C₂ and PK-C₂/C₃ grades and values of 0.91 were recorded at draw ratios as low as 3.5.

4.6 Birefringence & Amorphous Orientation

Figure 4.19 shows the development of optical birefringence with draw ratio. The Δn values for as-spun filaments could not be measured because the filaments did

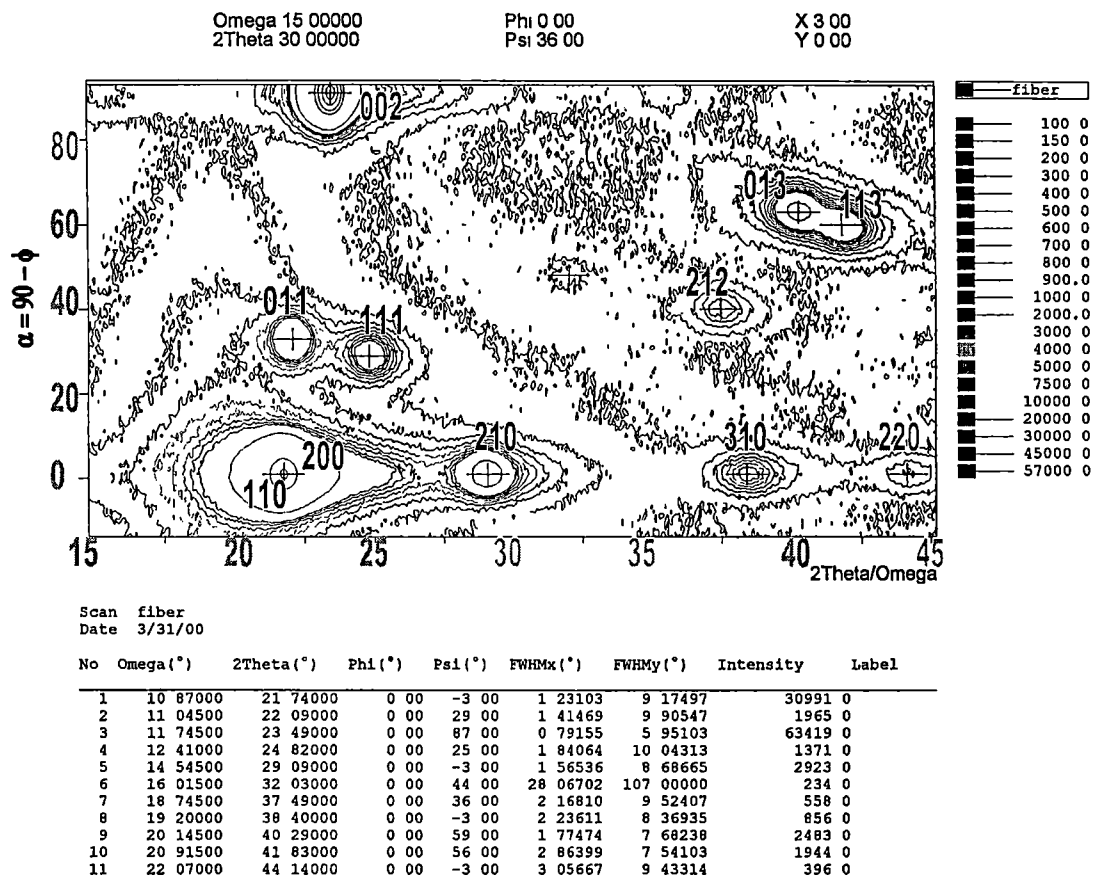


Figure 4.18 α Vs 2θ diffraction scan of an oriented PK-C₂/C₃.

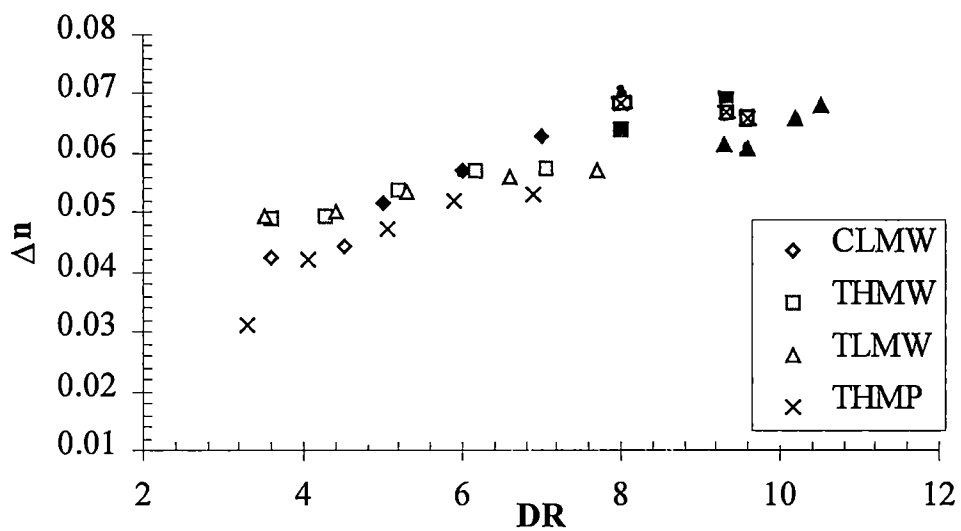


Figure 4.19 Development of orientation with draw ratio.

(data points in black represent oven-drawn samples)

not pass enough light to allow a measurement of retardation. With increasing draw ratio the orientation of the samples increases consistently. A maximum value of 0.065-0.067 for the highly drawn PK-C₂/C₃ and 0.062 for PK-C₂ was recorded. As birefringence or Δn values are a measure of the total orientation in a sample, an estimate of the amorphous orientation can be ascertained [49] by subtracting the contribution due to the crystalline orientation.

The values of amorphous orientation function, F_a , were back calculated after calculation of % crystallinity values from the DSC results. For the terpolymer, the intrinsic birefringences of the amorphous and crystalline phases were taken to be 0.0604 and 0.2446 and their densities taken were 1.206 and 1.296 g/cc, respectively, from the literature [44]. Figure 4.20 shows the plot of amorphous orientation Vs draw ratio. The values of amorphous orientation, like the birefringence, increases monotonically with draw ratio. Unlike the trend in the F_c, z Vs DR, we don't observe a plateau at any point. This is an indication that after a draw ratio of four, even though the crystal orientation is more or less complete, the amorphous orientation keeps on increasing. Apparently, the non-crystalline regions get oriented at higher draw ratios and they are responsible for the increase in the overall orientation.

Figure 4.21 shows the plot of thermal shrinkage versus draw ratio. The undrawn fibers showed 0% shrinkage whereas slightly drawn fibers showed maximum shrinkage, suggesting that the amorphous chains are pulled taut immediately upon drawing. However, the birefringence results show that at low draw ratios the fibers have developed only modest amorphous orientation relative to the fiber axis. The

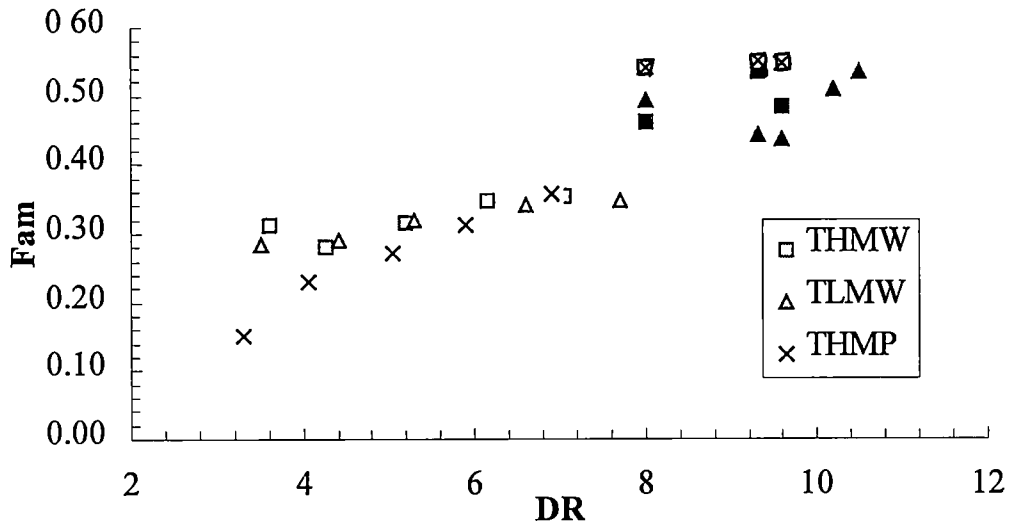


Figure 4.20 Plot of Amorphous orientation, Fam, with draw ratio, DR. (data points in black represent oven-drawn samples)

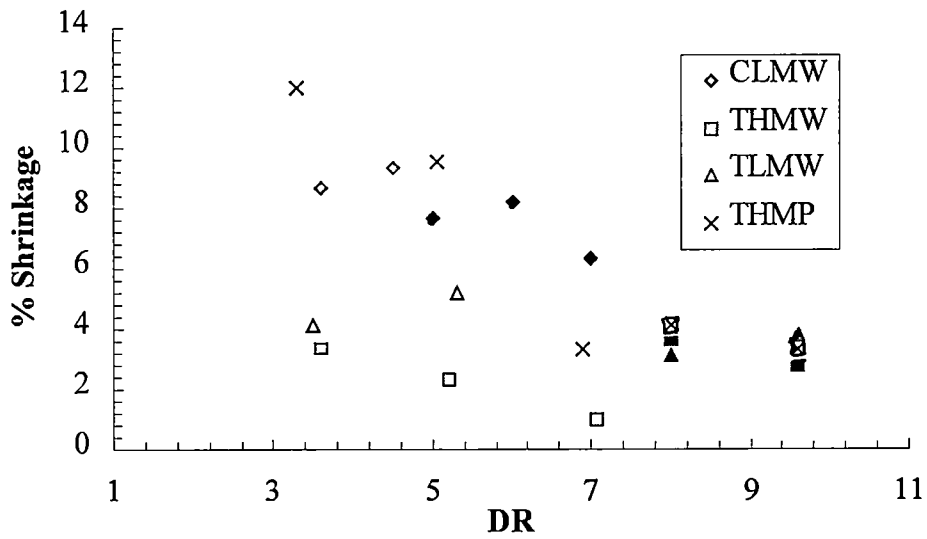


Figure 4.21 Thermal Shrinkage of fibers Vs Draw Ratio for different grades. (data points in black represent oven-drawn samples)

decrease in shrinkage at higher draw ratios, while amorphous orientation is increasing, suggests that some of the amorphous material may be crystallizing during the draw process. Note that the decrease in shrinkage occurs primarily for the THMP and CLMW fibers. Figure 4.13 clearly showed a marked increase in crystallinity for fibers produced from these two resins beginning at about DR = 5 for CLMW fibers and about DR = 7 for the THMP fibers. These are the same conditions that result in low shrinkage for these resins according to Figure 4.21. On the spot crystallization may occur that may lead to the formation of a rigid-truss like structure. Because of this the amorphous phase is constrained and its relaxation is prevented.

4.7 Lattice Cell Parameters

Based on the data in Figure 4 18 for oriented THMP, the unit cell dimensions were calculated. For the different peak positions the corresponding d-spacing values were calculated using the Braggs Law. For each reflecting plane, indexed by comparing our data with that of Chatani [30] and Lommerts [6], a relationship involving the d-spacing and the lattice constants (a , b , & c) was obtained. Solving any three of these simultaneously gives the values of a , b & c , the unit cell dimensions. Detailed calculations are provided in Appendix 3. The following values were obtained: $a = 8.09 \text{ \AA}$, $b = 4.74 \text{ \AA}$ and $c = 7.59 \text{ \AA}$. Table 4.4 compares the unit cell parameters to those reported by Chatani and Lommerts.

Table 4.4 Comparison of unit cell parameters as with Lommerts and Chatani's values.

Experimenter	Material	% C ₃	Process/Physical Form	a Å	b Å	c Å
This work	PK-C ₂ /C ₃	5.5	Melt Spun/ Fiber	8.09	4.74	7.59
Lommerts	PK- C ₂ /C ₃	5	Gel Spun/Fiber	8.05	4.75	7.61
Lommerts	PK- C ₂ /C ₃	12	Gel Spun/Fiber	8.23	4.75	7.58
Lommerts	PK- C ₂ /C ₃	0	Gel Spun/Fiber	8.24	4.74	7.58
Chatani	PK- C ₂ /C ₃	0	Solution Cast/Umaxially oriented film	7.97	4.76	7.57

4.8 SEM Results

A lot of polymeric fibers develop microfibrillar morphologies upon drawing. For example, fibers produced from PE [58], PP [57] and PET [61, 62] all develop microfibrillar morphologies at high draw ratios. This is usually accompanied by a rise in modulus, tenacity and optical birefringence. The microfibrils consist of highly oriented folded chain crystals that are connected by many tie molecules with the amorphous layers which separate the crystals.

Figure 4.22 shows the development of the structure of the copolymer fibers. At low draw ratios, about 3.5, the crystals are still aligning and the structure has not yet subdivided into microfibrils. Therefore the peel surface has a smooth texture. With increasing draw ratios, the fibrillar structure develops as reflected in the peel surface micrographs. According to previous authors [49, 57, 65-68], the drawing stresses shear the crystalline segments from the pre-existing lamellae and a restacking of crystals takes place leading to the formation of microfibrils. At a draw ratio of 5, the

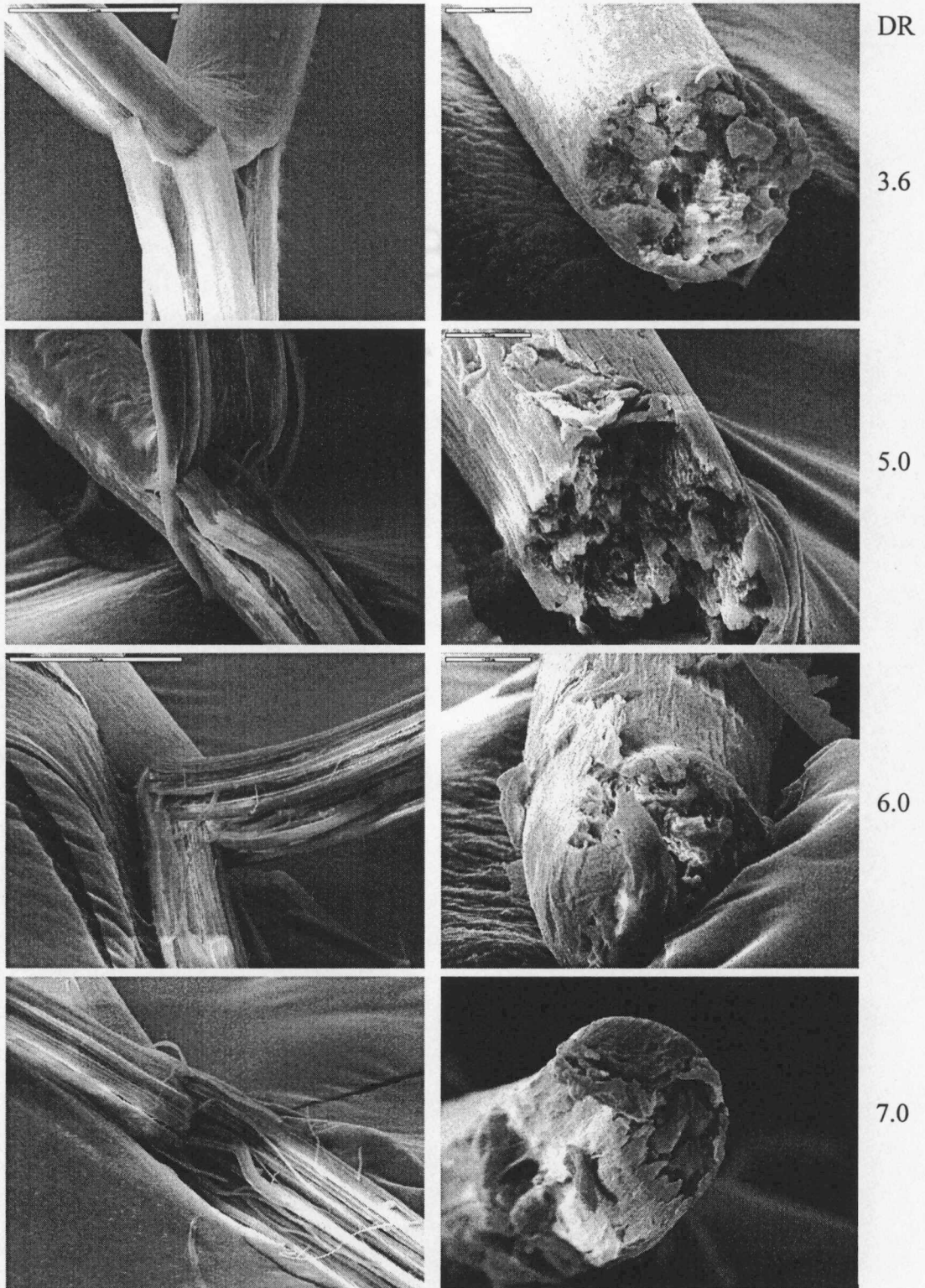


Figure 4.22 SEM photographs of peel and fracture surfaces of CLMW.

presence of fibrils becomes apparent. This is also marked by the characteristic jagged fracture surface. Further increase in draw ratio leads to extensive fibrillation and microfibrillar structure and by a draw ratio of 7, distinct and well defined microfibrils can be seen in the micrograph.

Figures 4.23-25 show the peel and fracture surface micrographs of the terpolymer fibers. The low melting point grades, THMW & TLMW, have a faster development of structure than the higher melting point grade, THMP, with respect to draw ratio. The microfibrillar morphology starts appearing as early as at a draw ratio of 3.5 in THMW & TLMW, whereas in THMP, the microfibrils can be seen at around a draw ratio of 5. Possibly the content of propylene has a role to play. TLMW & THMW have higher propylene content that may cause early chain slippage and crystal shearing, so that the microfibrillar morphology forms at lower draw forces.

Looking at the fracture surfaces, it appears that the lower draw ratio samples have a ductile failure and a more highly structured fibrillar appearance at higher draw ratios. At high draw ratios, the fracture surfaces appear jagged with deep cavities where fractured microfibrils exited.

4.9 SAXS Results

Figures 4.26-27 display SAXS contour plots of different grades. The as-spun filaments (draw ratio = 1) already exhibit some equatorial diffuse scattering and a two-point pattern on the meridian (which may be used to calculate long period spacing). Drawing produces an increase in the equatorial diffuse scattering and a tendency for

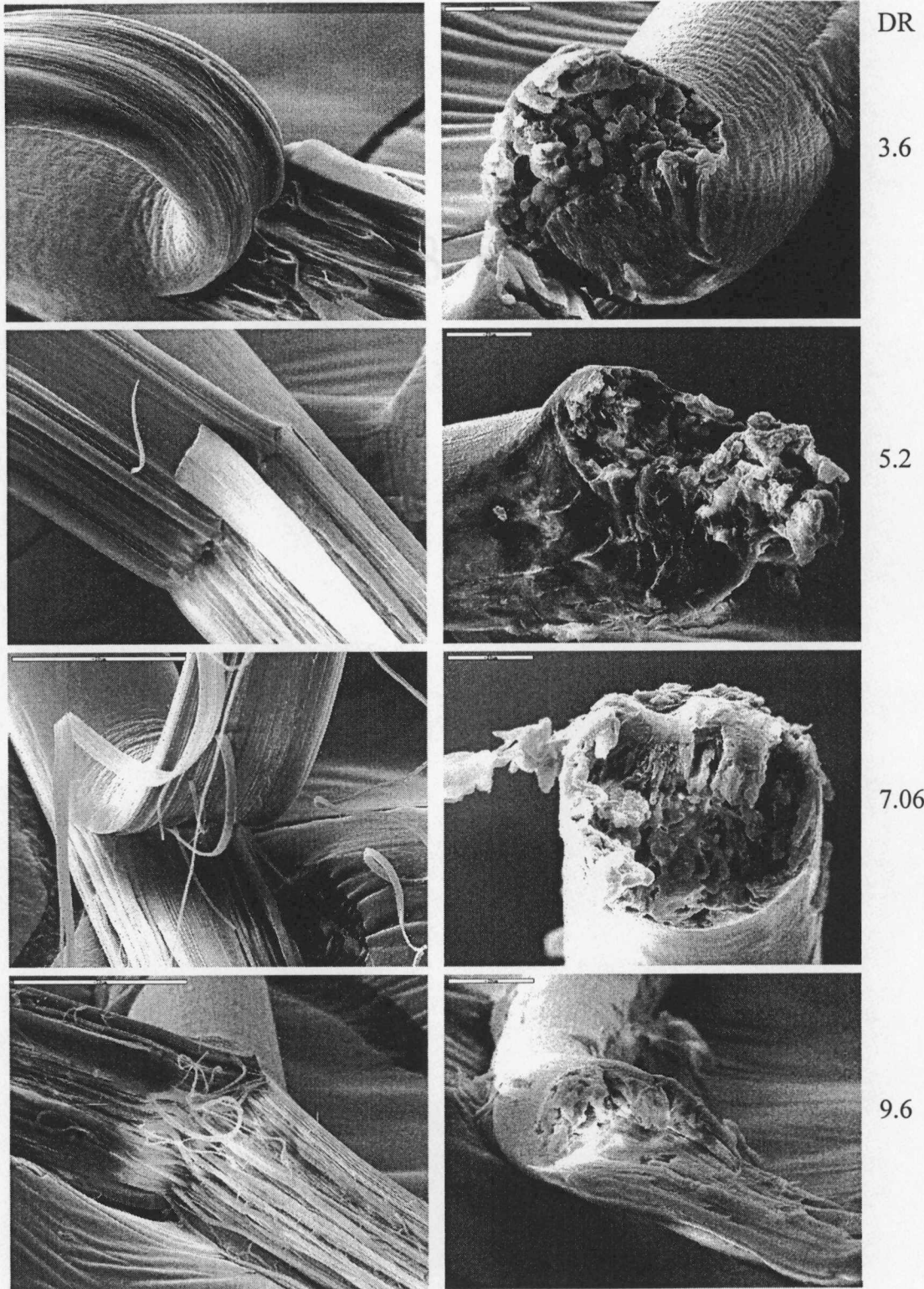


Figure 4.23 SEM photographs of peel and fracture surfaces of THMW.

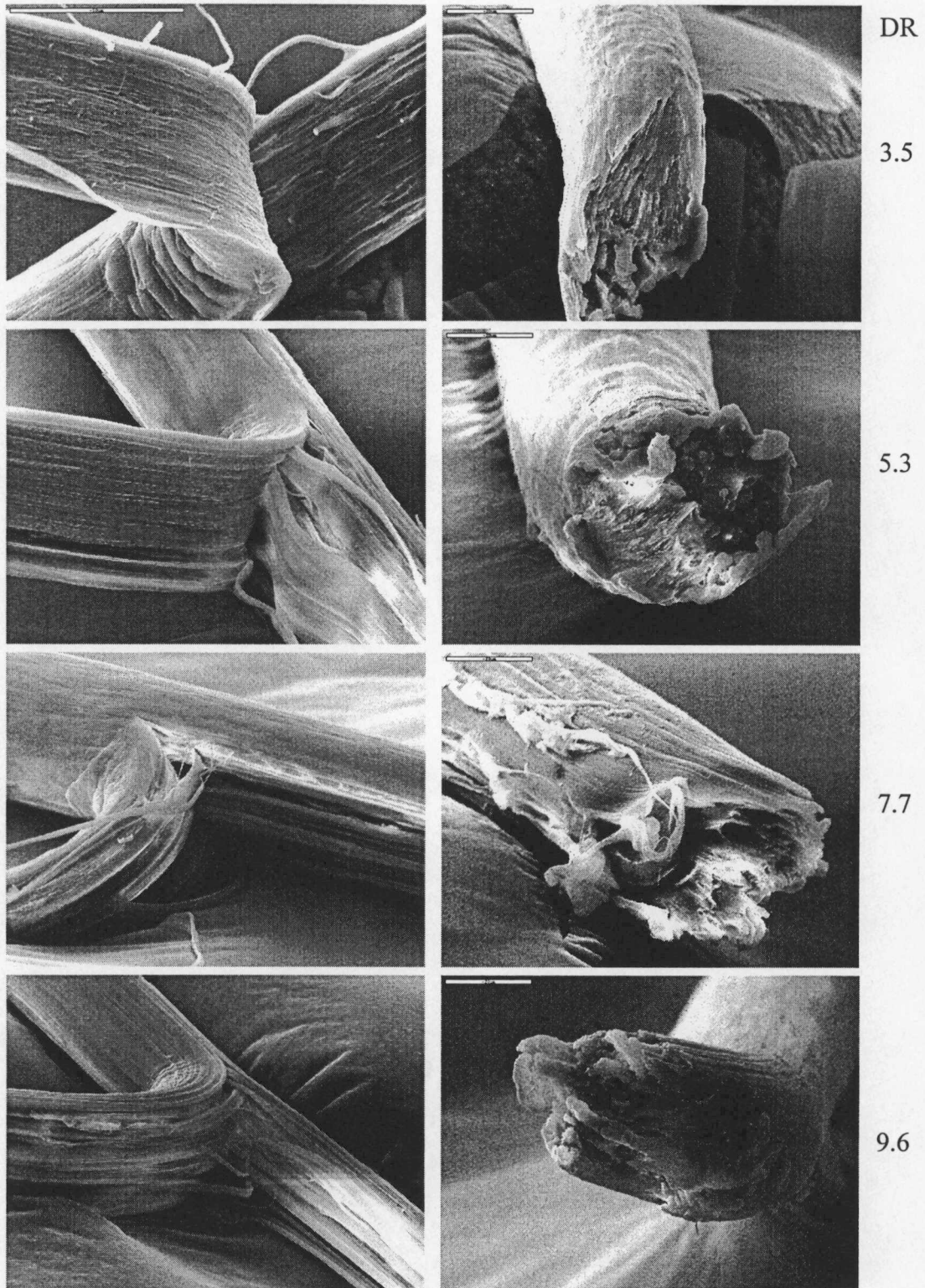


Figure 4.24 SEM photographs of peel and fracture surfaces of TLMW.

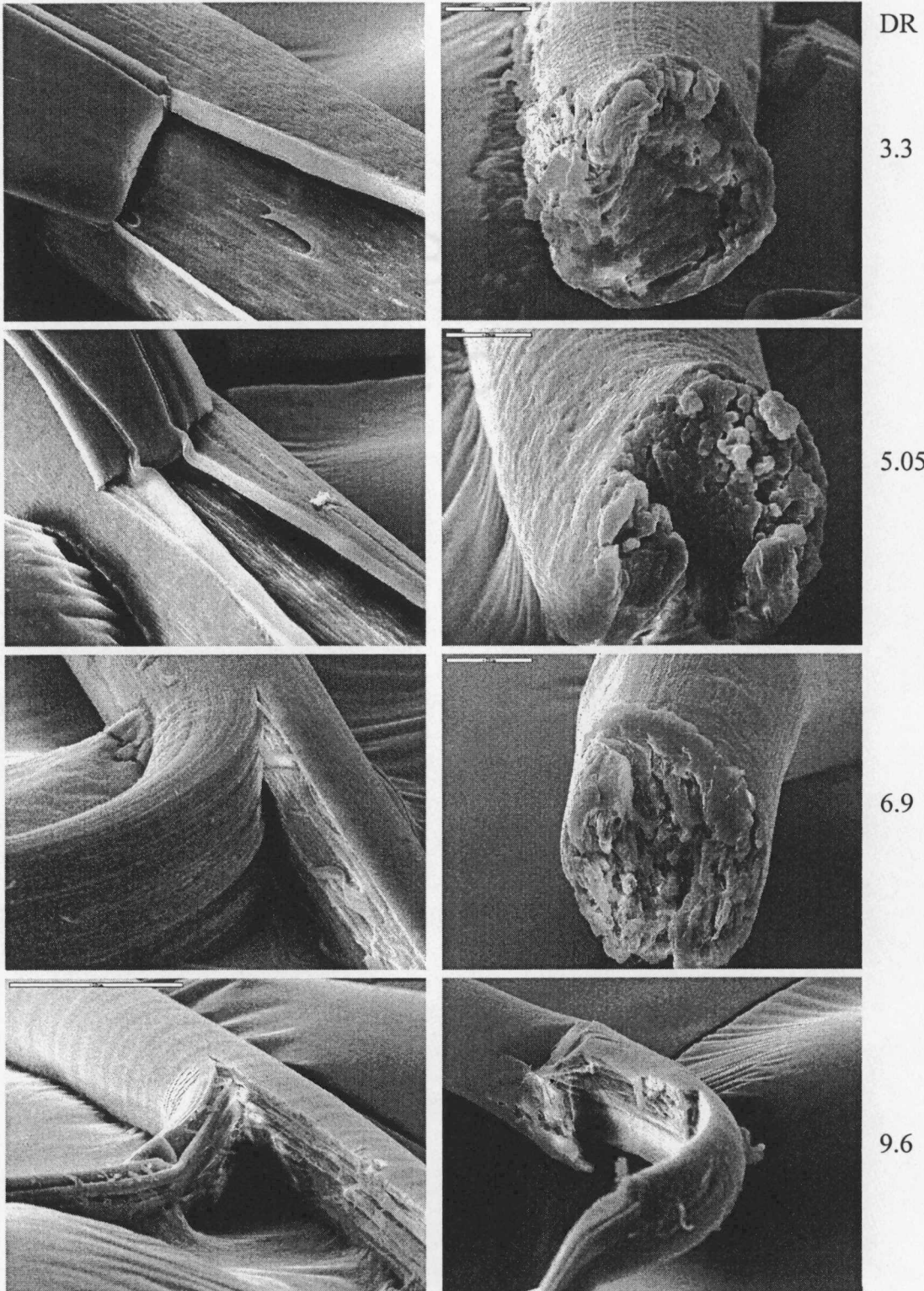
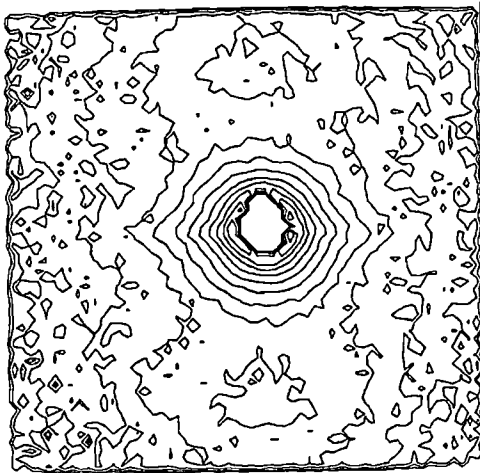
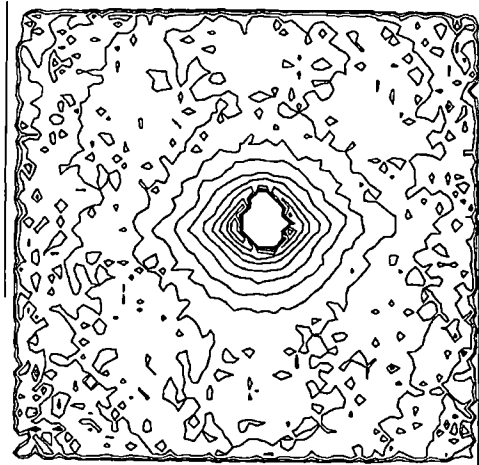


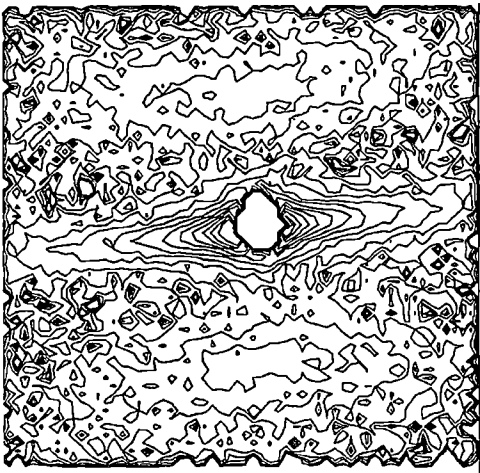
Figure 4.25 SEM photographs of peel and fracture surfaces of THMP.



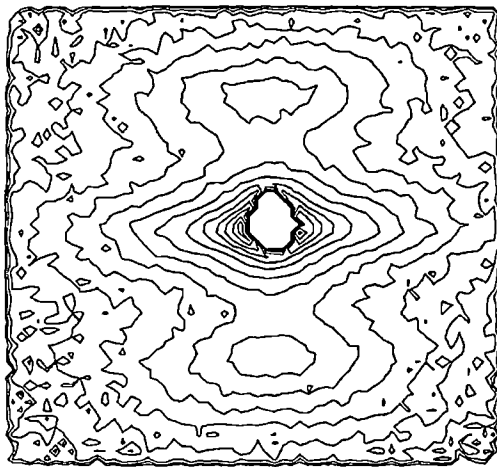
As-spun THMW



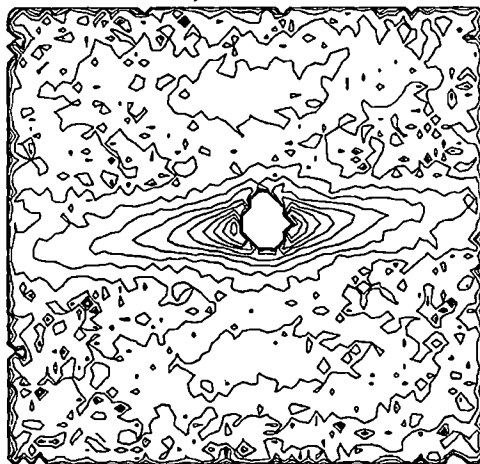
As-spun, TLMW



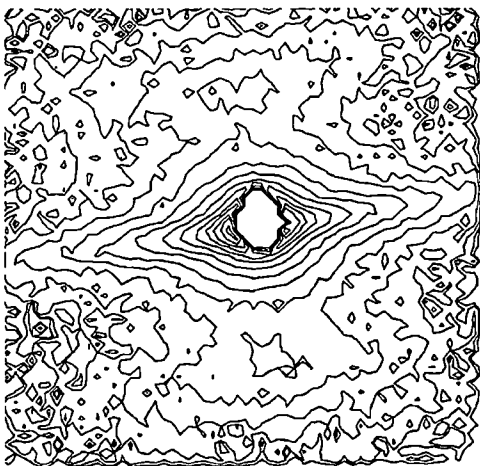
8 DR, THMW



8 DR, TLMW

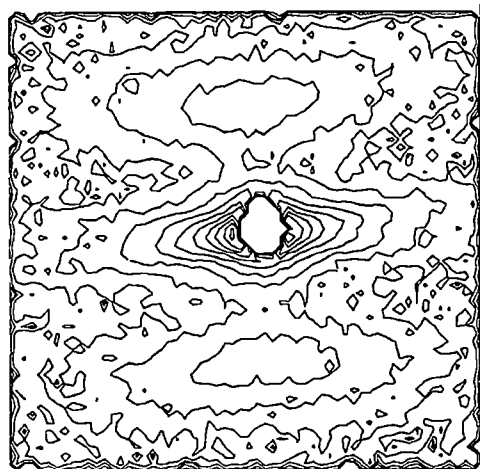


9 6 DR, THMW

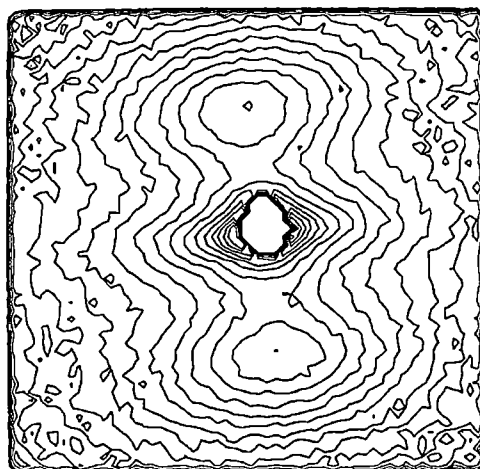


10 5 DR, TLMW

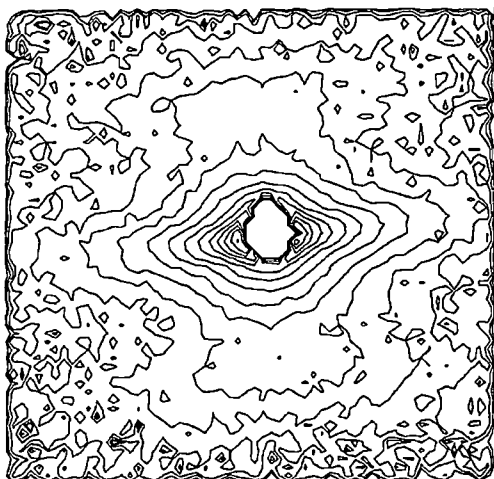
Figure 4.26 SAXS Contour plots of THMW & TLMW



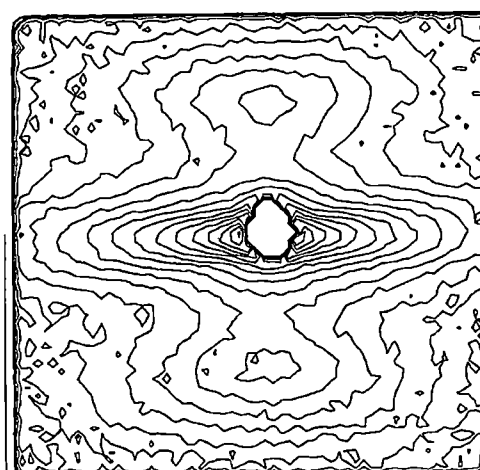
8 DR, THMP



5 DR, CLMW



9.6 DR, THMP



7 DR, CLMW

Figure 4.27 SAXS Contour plots of THMP & CLMW

the maximum on the meridian to develop a “tear drop shape”. At higher draw ratios the peaks on the meridian weaken and broaden in the direction parallel with the equator. This is a consequence of a change in volume ratio and/or in density difference between the crystal core of the lamellae and the amorphous region between the lamellae. The higher the deformation is, the more irregular the blocks are - as far as the fold containing surface and the interior of the crystal blocks are concerned and more folds of subsequent blocks interpenetrate- so that with the concurrently increasing number of tie molecules, the electron density difference markedly decreases. These features suggest the classical development of a microfibrillar structure during drawing. The development of the diffuse equatorial scattering indicates the presence of voids elongated in the direction of the fiber axis [55, 58-60].

As discussed above, the peaks along the meridian weaken in high draw ratio samples of all the terpolymer grades excepting the copolymer, CLMW, where we see a prominent 2-point pattern at high draw ratios (5 & 7). Interestingly, the as-spun copolymer does not show any noticeable peaks along the meridian, whereas they can be noticed in the as-spun, THMW. Therefore, in the copolymer, the electron density difference is substantial at high draw ratios to give peaks along the meridian, indicating that there are distinct crystalline and non-crystalline regions. This could be attributed to the development of microfibrillar morphology that starts to appear as early as a draw ratio of 3.5, as concluded by the SEM pictures in the preceding section. However, in the high draw ratio terpolymer fibers, the electron density difference decreases leading to the weakening of meridional peaks. This could be due

to the weak microfibrils getting transformed into a strong, highly ordered non-crystalline inter-microfibrillar phase. Occurrence of some on-the-spot crystallization in the inter-fibrillar region is another possibility.

The long period was calculated directly from Bragg's law and the lamellar thickness was calculated by multiplying the long period by the percent crystallinity of the fiber. Table 4.5 lists the long period along with the lamellar thickness for different fibers. The drawn fibers have a higher long period than the as-spun filaments. The as-spun filaments have a very low crystallization temperature as compared to the draw temperature of the drawn samples. In the drawn filaments, the long period and lamellar thickness appear to be a function of the draw temperature rather than the crystallization temperature. Hence the observed marked difference in the values of long period and lamellar thickness for as-spun and drawn filaments. At high draw ratios the long period either increases slightly or stays the same. For the relaxed samples, we find that the long period actually decreases a bit for TLMW and THMP. This is because during relaxation process the amorphous regions shrink more causing the inter-fibrillar regions to decrease in size.

Table 4.6 compares the long period and lamellar thickness to crystallite size computed from the 002 reflection for THMW. The 002 planes are perpendicular to the fiber axis, hence their crystallite size, computed from a 2θ scan along the meridian, gives a reasonable estimate of the thickness of the crystals in the direction along the fiber axis. It is interesting to note that the 002-plane crystallite size is more or less the

Table 4.5 Long Period and Lamellar Thickness with Draw Ratio.

Polymer	DR	Long period (nm)	Lamellar thickness (nm)
THMW	1	12.93	4.46
THMW	8	14.93	7.44
THMW	9.3*	14.89	7.88
THMW	9.6	14.81	7.63
TLMW	1	12.67	4.5
TLMW	8	16.89	7.84
TLMW	9.6	16.95	8.21
TLMW	9.3*	15.97	7.95
TLMW	10.2*	14.9	7.82
TLMW	10.5	15.94	8.53
THMP	1	13.42	4.93
THMP	8	15.91	8.72
THMP	9.3*	16.74	9.48
THMP	9.6	18.96	10.82
CLMW	1	-	-
CLMW	5	16.97	9.48
CLMW	6	-	-
CLMW	7	15.52	9.27

*Fibers relaxed in oven (THMP at 250 °C and TLMW & THMW at 235 °C).

Table 4.6 Long Period, Lamellar thickness and 002 crystallite size data of THMW.

DR	Long period nm	Lamellar thickness (nm)	002 crystallite size (nm)
3.6		-	84
5.2	-	-	8.5
8	14.93	7.44	-
9.3*	14.89	7.88	8.6
9.6	14.81	7.63	7.8

* Fibers relaxed in oven at 235 °C

same as the lamellar thickness computed from a combination of long period and crystallinity

4.10 Variation in Crystallite size with Draw Ratio

Table 4.7 lists the crystallite size in the direction perpendicular to the fiber axis measured by conducting equatorial 2θ scans on the 210 reflections from the fibers. In the copolymer, since both α and β phases are present in low draw ratio fibers, both the 210 α and 210 β crystallite sizes are listed. Irrespective of the type of phase present, the 210 crystallite size decreases with increasing draw ratio.

4.10 Structure Development on drawing

In a spherulite, the crystallites aligned along the equatorial region have their a axis oriented perpendicular to the force direction and their c axis in the force direction.

Table 4.7 Crystallite size data for the 210 crystal planes.

Polymer	DR	210β crystallite size (Å)	210α crystallite size (Å)
CLMW	1	144	132
CLMW	3.6	112	114
CLMW	5	-	84
CLMW	7	-	69
THMW	1	137	-
THMW	3.6	84	-
THMW	5.2	75	-
THMW	9.6	73	-
THMP	1	114	-
THMP	3.3	91	-
THMP	5	84	-
THMP	8	70	-

Application of a force to these crystals causes them to separate from each other such that the distance between them increases. With continuing deformation of the spherulite, crystal reorganization proceeds by the processes of lamellar slip, orientation, and separation, until the crystal lamellae in all regions of the spherulite become aligned with their c-axis (chain axis) direction nearly parallel to the deformation direction.

As the large crystals become more highly oriented, crystal orientation becomes exceedingly difficult and further deformation must occur by crystal cleavage. Ultimately, as deformation continues (at draw ratios > 4), the entire sample becomes highly oriented, crystal cleavage leads to the loss of spherulitic structure, and a new microfibrillar structure evolves. The microfibrils consist of highly oriented folded chain crystals that are connected by many tie molecules with amorphous layers that separate the crystals

In the previous section, we had found a decrease in the crystallite size in a direction perpendicular to the axis of the fiber with increasing draw ratio. This is in consonance with Pervorshek's folded chain "Swiss-Cheese" model [66] where the folded chain segments are interconnected with highly ordered non-crystalline regions. In this model, with increasing draw ratio, the size of the folded chain segments or crystals decreases and the increase in strength is attributed to the strengthening of the weaker inter-fibrillar phase that gets transformed into a highly ordered non-crystalline region. The overall % crystallinity, should therefore, decrease a little as the new ordered regions are formed at the expense of the shrunken folded chain segments

However, the % crystallinity of the polyketone fibers actually increases a little with the draw ratio. Also, the weakening of the 2-point pattern in high draw ratio fibers of terpolymer indicates an increase of order in the inter-fibrillar region and a possibility of formation of new crystal centers cannot be ruled out. This aspect is in agreement with Taylor & Clark's model [57], which states that with increasing draw ratio new crystals form at the expense of the non-crystalline phase. The increase in %

crystallinity of the fibers is thus responsible for the increase in tensile strength and modulus. The super drawn fibers (only theoretically possible) then, are supposed to be continuous crystal matrix interspersed with small amorphous regions.

Based on the preceding discussion, the following Model as shown in Figure 4.28 is proposed. The stacks of folded chain segments interconnected with interfibrillar tie molecules are placed uniformly in the non-crystalline matrix. With increasing draw ratio these crystal blocks shrink in size in a direction perpendicular to the fiber axis and new crystal blocks are formed as well. The overall % crystallinity is not affected significantly, however it may increase marginally. At high draw ratios the tie molecules in the inter-fibrillar region become increasingly oriented and ordered, which is responsible for the increase in the axial strength of the fibers. Also formation of voids along the meridian takes place. The microstructure becomes increasingly uniform with a decrease in the density difference between the crystalline and non-crystalline phases. This accounts for the weakening of the peaks along the meridian in the SAXS contour plot.

4.12 Mechanical Properties

4.12.1 Tensile Properties at room temperature

Many flexible chain polymers experience increase in tenacity on drawing. Some of them are PE, PP, PA6, PA12, PVA, PET, PLLA, PK-C₂ and PK-C₂/C₃ [6, 34, 42, 50-55].

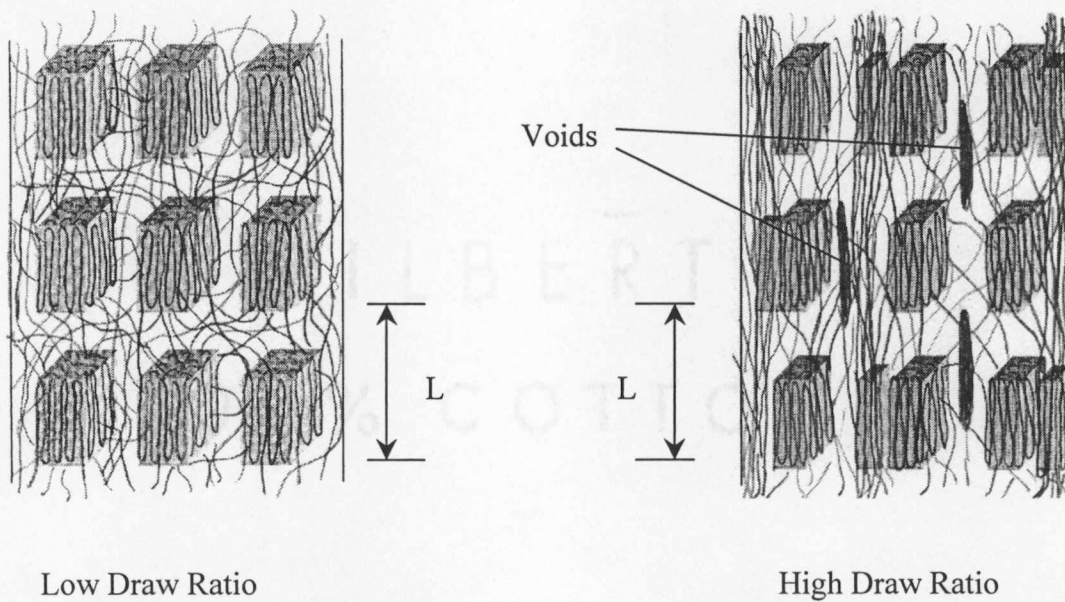


Figure 4.28 Proposed fiber model for polyketone terpolymer fibers.

Figure 4.29 shows a typical stress-strain curve for two samples of THMW polyketone. One sample was drawn to a high draw ratio while the other was given a low draw ratio. The low draw ratio sample has a high % elongation at break, about 90 %, whereas it is only 20 % for the high draw ratio sample. The slope of the initial linear region of the stress strain curve gives the initial modulus. The low draw ratio sample has a lower modulus and a very high extension indicating its ductile nature. However, the highly drawn fibers have a near perfect linear curve with a high initial modulus and very low extension at break. Also the maximum load or tenacity that the fibers can bear, increases with draw ratio. Thus, with increasing draw ratio, the filaments become stronger, more rigid and less ductile.

Figure 4.30 shows the development of tenacity with draw ratio. As expected, the increase in tenacity with draw ratio is almost linear. This follows for both the copolymer and the terpolymer grades. However, it appears that the low molecular weight terpolymer, TLMW, and the copolymer, CLMW, tenacity values attain a plateau. This could be due to the fact that at higher draw ratios (above 9 in TLMW and 6 in CLMW), the tie molecules are fully extended and taut. Any further increase in draw ratio does not extend them any more. Hence the strength or the tenacity values level off.

Figure 4.31 shows the variation of tenacity of polyketone fibers with birefringence. The tenacity increases slowly up to a birefringence of 0.045, whence it rises more rapidly. This rapid increase corresponds to the draw ratio where the crystal orientation reaches its semi-plateau. As described later, this transition point,

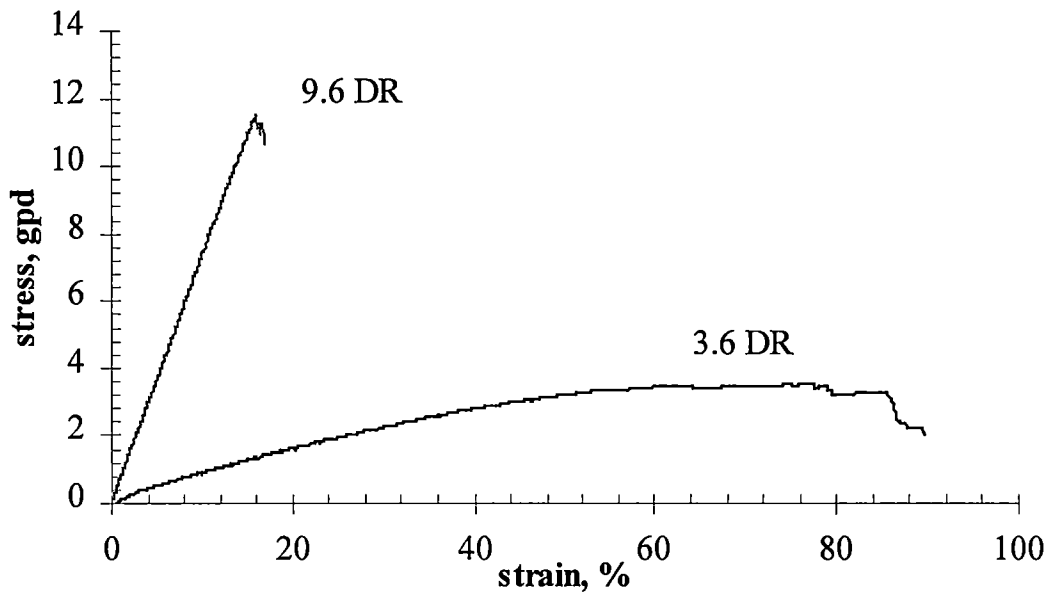


Figure 4.29 A typical stress strain curve of polyketone fibers (THMW)

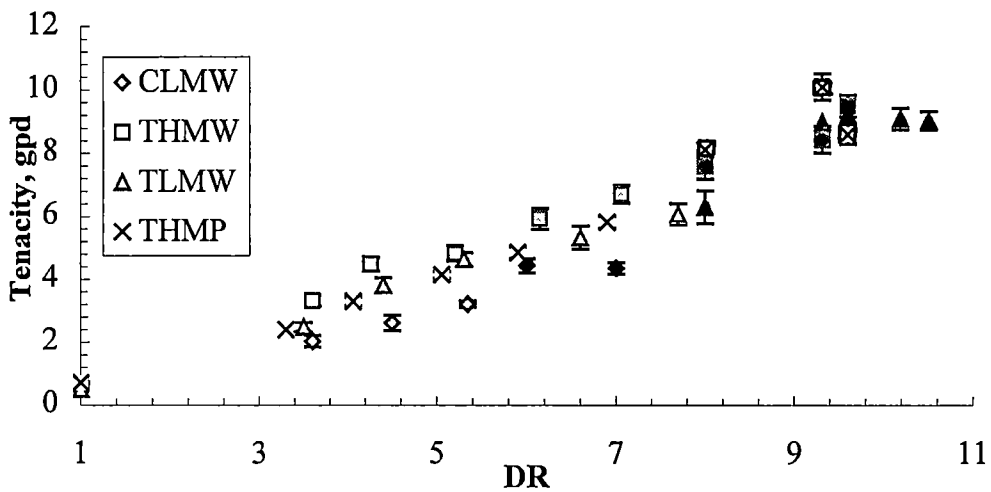


Figure 4.30 Development of Tenacity with Draw ratio (data points in black represent oven-drawn samples)

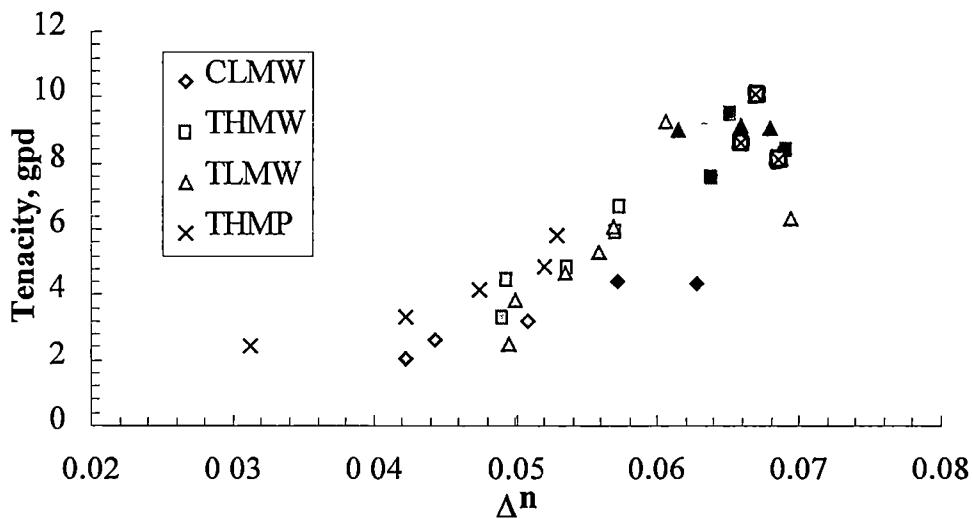
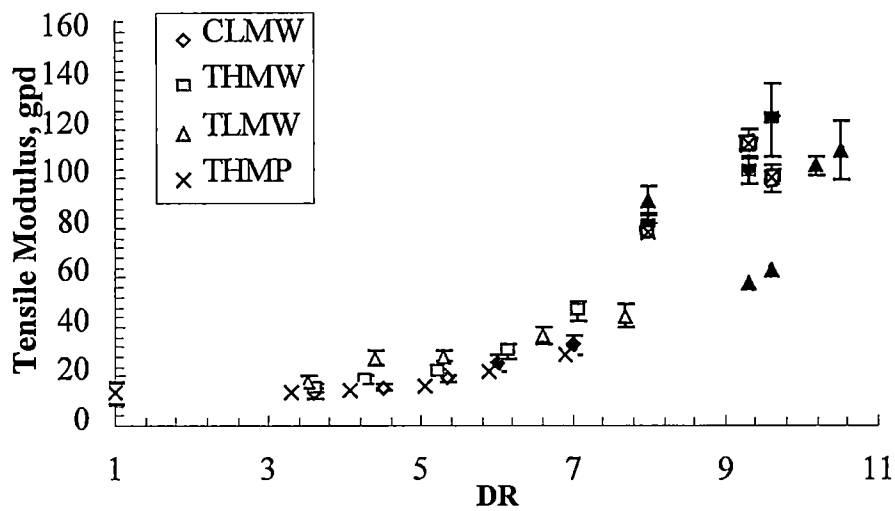


Figure 4.31 Variation of tenacity with orientation as measured by optical birefringence. (data points in black represent oven-drawn samples)

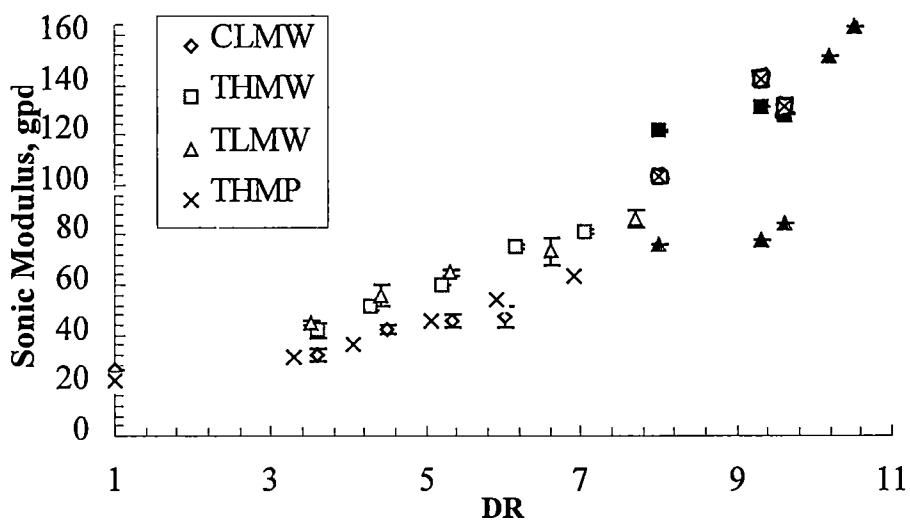
corresponding to a draw ratio of 5, is probably where the development of the microfibrillar structure is more or less complete. At higher draw ratios, the microfibrils slide past each other, generating more inter-fibrillar tie molecules, which is reflected in the increase of crystallinity, elastic modulus and tensile strength.

A similar trend was observed for the tensile and sonic modulus of these fibers. Figure 4.32 (a & b) show the variation of modulus with draw ratio. Clearly the modulus increases steadily with draw ratio. Again, there appears to be a change in slope of the modulus versus draw ratio curves above a draw ratio of about 5. This further suggests that this draw ratio represents a major transition point in the way the morphology of the fiber is developing. Comparing the sonic moduli with the tensile modul, the sonic moduli are higher than the tensile moduli by about 10-15 gpd. This is true for both the copolymer and the terpolymer samples. The observed difference is likely due to the fact that the two measurements do not measure the same quantity. The sonic modulus measurements measure the fiber's response to a much higher frequency stimulus than does the tensile test [56]. There does not appear to be any significant difference in modulus with change in material composition at a given draw ratio with the possible exception of the TLMW sample at higher draw ratios.

Elongation of filaments accompanied by structural development normally results in a reduction of % strain at break. Figure 4 33 shows the reduction in % strain at break with draw ratio, indicating that at higher draw ratios the fiber becomes less ductile. This is also confirmed by observing the type of fracture, described in another section. The highly drawn PK-C₂/C₃ fibers had lower elongation at break (10-15%)



a)



b)

Figure 4.32 Development of a) Tensile modulus and b) Sonic Modulus with Draw ratio. (data points in black represent oven-drawn samples)

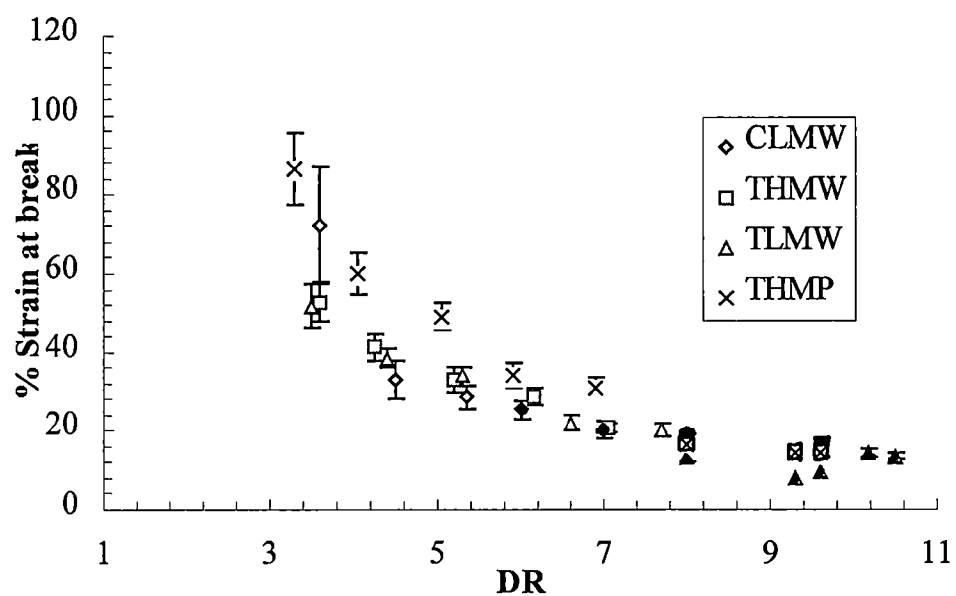


Figure 4.33 Plot of % Strain at break with Draw ratio.
 (data points in black represent oven-drawn samples)

than the oriented PK-C₂ fibers (20-25%), but the copolymer was drawn to a lower draw ratio. At the same draw ratio the elongation of all samples are comparable with the possible exception of the THMP sample that appears to be a bit higher than the others. Table 4.8 compares the mechanical properties of PK-C₂/C₃ to industrial grade fibers of Nylon 66 and PET that are used for tire cord applications. The PK-C₂/C₃ fibers have equal or better tenacities and modulus values than nylon and polyester. In addition, its low thermal shrinkage (5-8 %) should be an advantage for tire cord applications.

4.12.2 Tensile Properties at Elevated Temperatures

Another interesting aspect about the PK fibers is their retention of mechanical properties at elevated temperatures. Figures 4.34-36 show the variation of tenacity, modulus and % strain at break, with temperature. The values at room temperature are also compared. For each polymeric grade two high draw ratio samples were selected and tensile testing was conducted at elevated temperatures. As can be seen the tenacity

Table 4.8 Comparison of high-strength tire cord fibers with PK-C₂/C₃.

Fiber	Tenacity* (gpd)	Modulus* (gpd)
PA66	10	60
PET	9	90
PK-C ₂ /C ₃	9-11	80-100

* Data for PA66 and PET are from references 63 and 64.

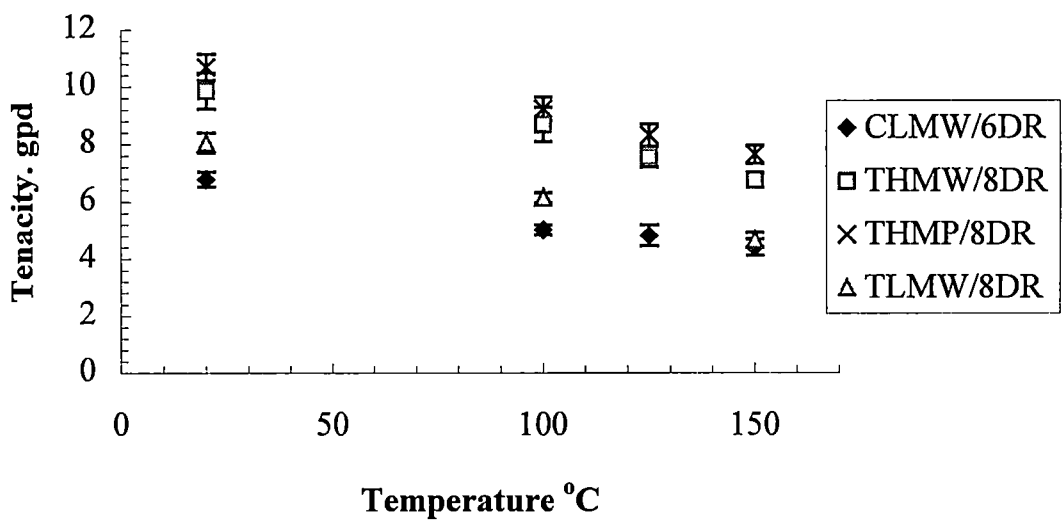
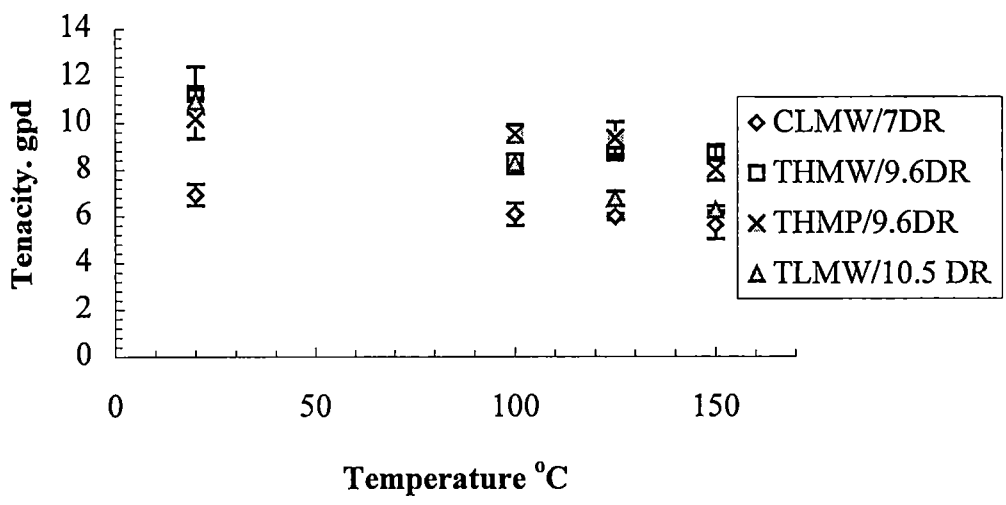


Figure 4.34. Plot of Tenacity Vs Temperature (all oven-drawn samples)

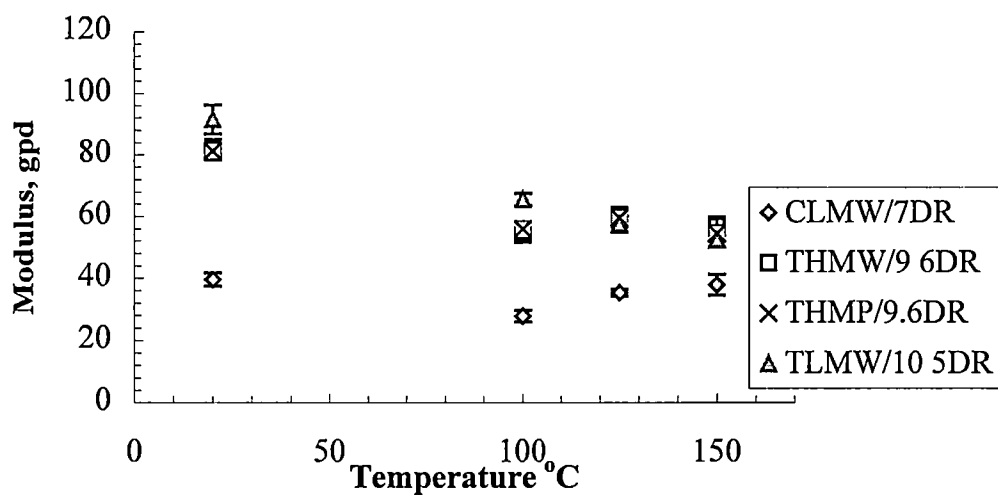
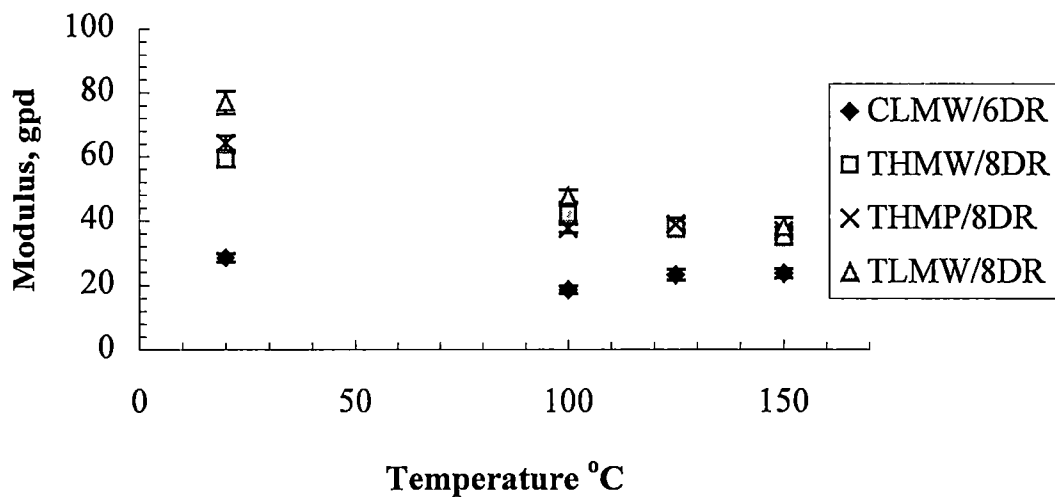


Figure 4.35 Plot of Modulus with Temperature (all oven-drawn samples)

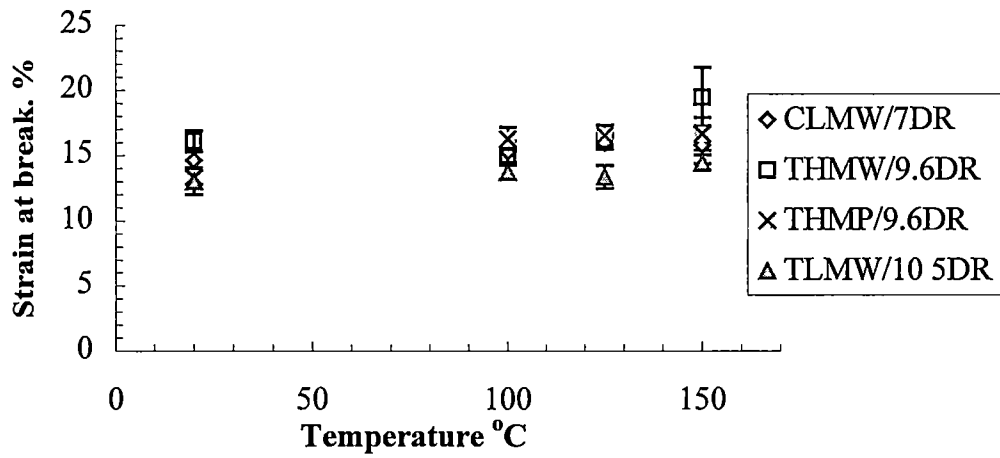
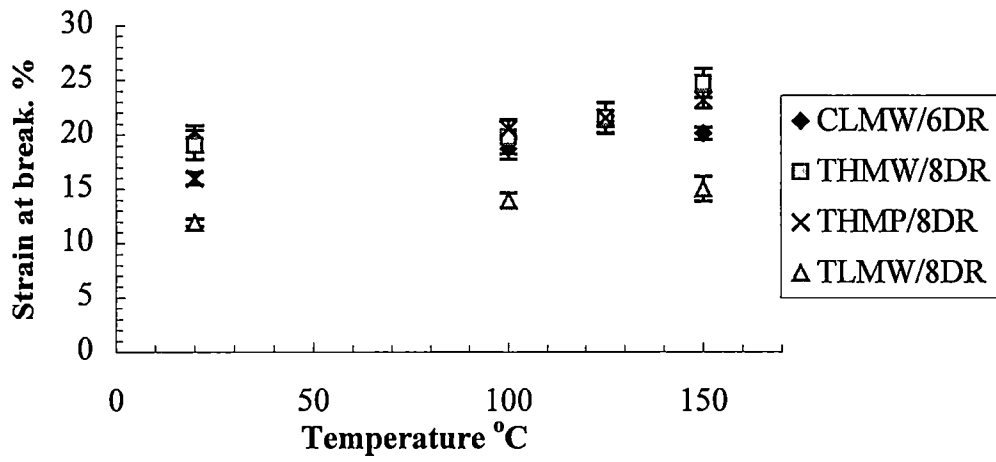


Figure 4.36 Plot of % Strain at break with temperature. (all oven-drawn samples)

drops with increasing temperature. At a temperature of 150°C the drop in the strongest terpolymer fiber (THMW, 9.6 DR) was only 25 %. It had recorded 11.26 gpd at room temperature and at 150 °C it was a very satisfactory 8.6 gpd. The higher melting point terpolymer, THMP behaves extremely well till a temperature of 125 °C with only a 9 % drop in tenacity. Further increase, however, causes a significant drop by about 21 %. Similar trends are observed for the copolymer, CLMW and the low molecular weight terpolymer, TLMW

The modulus behaves in a similar manner to the tenacities. With increasing temperature the modulus drops. There is significant drop in modulus between 25 and 100 °C, but there is little change thereafter. The copolymer, CLMW, actually appears to increase slightly. Between 25 and 150 °C, the drop for terpolymer fibers is about 30-40 %.

The % strain at break increases with temperature. For all the PK fibers, the % strain at break increases to about 14-20 % at 150 °C from 10-15 % at room temperature. With increasing temperature, the plastic flow increases, as a result of which the maximum stress or the tenacity drops. Further, with increasing chain movement at higher temperatures, the modulus decreases. Molecular weight too plays a role here. Higher molecular weight samples (THMW) definitely show less decrease in strength as against lower molecular weights (TLMW) with increasing temperature. The modulus decrease is more or less the same for both the grades.

In general, it can be concluded that the retention of mechanical properties of the PK fibers is extremely good till a temperature of 125 °C. Further increase in

temperature causes significant drops in tenacity, though % strain at break values are not that much affected. Considering the relatively small amount of effort placed so far in trying to improve the properties of PK fibers, it suggests that it may be possible to obtain fibers that are better than the current Nylon 66 and PET fibers used for tire cords.

It may be noted here that the elevated temperature tensile test measurements were done on MTS tensile testing equipment. The tensile testing results previously reported were conducted on INSTRON.

There was a slight difference in the modulus values reported by the two systems, especially for high draw ratio samples. The INSTRON reported higher modulus values than the MTS system. This is perhaps because of the difference in the gripping assembly in the two systems.

The pneumatic grip, used with the INSTRON system, consisted of two flat plates with a rubber lining on the inner gripping surface. Whereas, in the purely mechanical grips of MTS, the fibers were gripped between two steel blocks, that could be tightened mechanically, after being passed over a small pulley. There were two pulleys in all, one for the lower and the other for the upper jaw. Here, an additional fiber length, Δl , as depicted in Figure 4.37, was not accounted for in the gage length although the fibers in this region also participated the tensile test. Hence the actual strain was larger and thus the modulus, which is a ratio of the stress and strain, was smaller than the values reported on the INSTRON.

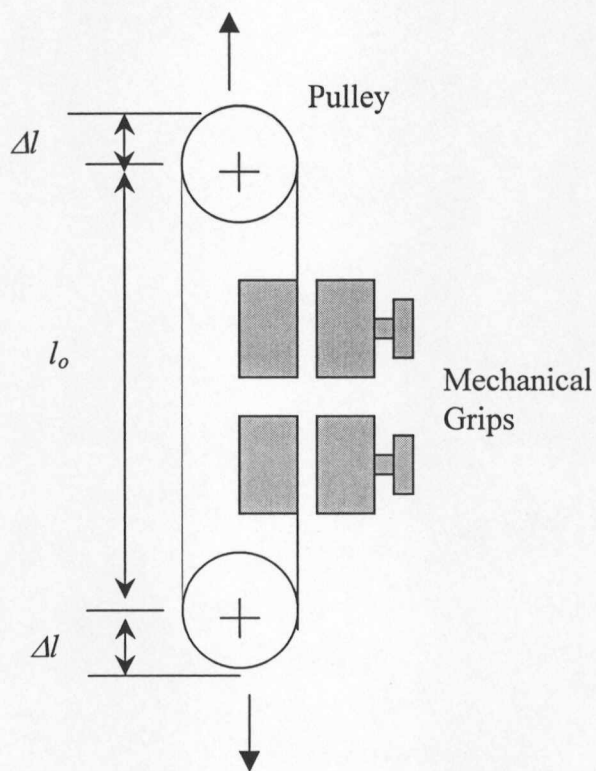


Figure 4.37 MTS Gripping system showing the extra Δl that goes unaccounted in the tensile test.

CHAPTER 5

CONCLUSIONS

PK-C₂ & PK-C₂/C₃ fibers were prepared by melt spinning and drawing techniques to yield high strength fibers that have tenacity in the range of 9-11 gpd and moduli of 80-100 gpd. The mechanical properties of these filaments and their good thermal and chemical stability suggest that they may be quite useful in a variety of industrial applications such as tire cords.

A broad draw temperature window makes their post spinning processing feasible over a range of temperatures. However there appears to be an optimum temperature range in which each of the co and terpolymer grades could be drawn. These vary with the molecular weight and propylene content. When drawn on heated rollers, the copolymer, CLMW and the high melting point terpolymer, THMP are best drawn in the temperature range of 170-190 °C, whereas the low melting point terpolymers, TLMW & THMW have an optimum temperature range of about 130-170°C.

The only detectable crystalline phase present in the terpolymer was the β phase at all temperatures and preparation conditions. The copolymer consisted of a mixture of α and β phases in the as-spun fibers at room temperature. Highly drawn fibers of the copolymer were largely α -phase at room temperature. A phase transformation from α to β takes place in the temperature range of 90-110 °C. The α form has a smaller unit cell volume as compared to the β form. The addition of termonomer

reduces the melting point and crystallinity compared to the copolymer. The % crystallinity values for as-spun co and terpolymer fibers were 45 and 34-36 % respectively. The % crystallinity increases with the draw ratio and for high draw ratio fibers of co and terpolymers it was 60 and 53-57 % respectively.

The crystal orientation increases rapidly up to a draw ratio of 4, and then it levels off at a high value. $F_{c,z}$ values of 0.98 were observed for highly drawn terpolymer samples. The amorphous orientation, on the other hand, steadily increases with draw ratio. This indicates that the orientation of the non-crystalline regions constituted mainly by the interfibrillar tie molecules increases with increasing draw ratios even though the crystal orientation is complete at around a draw ratio of ~ 4 .

The unit cell dimensions of THMP were calculated and were found to be $a = 8.09 \text{ \AA}$, $b = 4.74 \text{ \AA}$ and $c = 7.59 \text{ \AA}$. This is in good agreement with the values reported by Chatani and Lommerts.

The as-spun filaments display a bi-modal melting peak behavior. This phenomenon disappears at higher draw ratios in the copolymer samples but persists in the terpolymer samples. This is because of the presence of two different populations of the same crystal forms with different lamellar thicknesses or due to the lamellar thickening that takes place during the DSC run itself. It was observed that the heat of fusion and the peak temperatures change with the scan rate of the DSC run. This has not been understood properly and it is recommended that more studies be conducted to investigate this phenomenon fully.

The SEM and SAXS analysis show the development of microfibrillar morphology with increasing draw ratio. At high draw ratios the 2-point pattern in the SAXS contour plots weakens indicating the increase in order of the non-crystalline regions. This reflects as an increase in the strength and modulus of the fibers. Due primarily to the ability to reach higher draw ratios it was possible to achieve higher strength and moduli in the terpolymers as compared to the copolymer. Among the terpolymers the high melting point terpolymer, THMP and high molecular weight terpolymer, THMW have better mechanical properties than the low molecular weight, TLMW. Another notable feature is the retention of strength at elevated temperatures. It was observed that these fibers retain about 85-90 % of their original strength till a temperature of 125 °C. At 150 °C, the fibers retain only 70-75 % of their room temperature strength. Once again the terpolymer fibers THMP and THMW behave better when compared to CLMW and TLMW. It is perhaps worth noting that high strength polyethylene fibers would be melted at 150 °C and have no measurable strength.

Based on the WAXS, SAXS, birefringence and crystallinity measurements a modified fiber model was proposed where with increasing draw ratio, new crystals originate at the expense of the inter-fibrillar matrix in between the shrunken crystallites. The % crystallinity remains the same or increases marginally. The overall orientation of the tie molecules in the inter-fibrillar region increases and is responsible for the increase in tenacity and modulus of the fiber.

REFERENCES

REFERENCES

1. Okajima, K., Yamane, C. & Ise F., *Polymeric Materials Encyclopedia*, 7, 5387 (1996)
2. Drent, E., European Patent: 121,965 (Shell), (1984).
3. Drent, E., van Broekhoven, J. A. M. & Doyle, M. J , *J Organomet Chem.*, 417, 235 (1991)
- 4 Nobile, M. A. Del., Mensitieri, G. & Sommazzi, A., *Polymer*, 36, 26, 4943 (1995).
5. Sommazzi, A. & Garbassi, F., *Prog Polym Sci* , 22, 1547 (1997).
6. Lommerts, B. J , “Structure development in polyketone & polyalcohol fibers”, Phd dissertation, University of Groningen, Reading (1994).
7. Danforth, R L , Machado, J M & Jordaan, J C. M., *Plastics Engineering*, March, 77 (1996).
8. Ballauf, F., Bayer, O & Liechmann, L., G Patent: 863,711 (1941).
9. Reppe, W. & Mangini, A., US Patent. 2,577,208 (1951).
10. Brubaker, M. M., US Patent: 2,495,286 (1950)
- 11 Brubaker, M M., Coffman, D. D. & Hoehn, H. H., *J Am Chem Soc.*, 74, 1509 (1952)
- 12 Russo, S & Munari, S. & Baigini, E , *J Phys Chem.*, 73, 378 (1969).
13. Hartley, G. H. & Gulliet, J. E., *Macromolecules*, 1, 165 (1968).
14. Heskins, M & Gulliet, J. E., *Macromolecules*, 3, 224 (1970)
- 15 Van Broekhoven, J. A. M. & Drent, E., European Patent: 235, 865 (1987).
- 16 Keijsper, J. J , European Patent: 512, 647 (1992).

17. Sen, A., *Chemtech* , 48 (1986)
18. Jiang, Z., Dahlen, G. M & Sen, A., *New Advances in Polyolefins*, Plenum Press, NY, 47 (1993)
19. Sen, A., *Acc Chem Res* , 26, 303 (1993).
- 20 Sen, A., *Adv Polym Sci.*, 73/74, 125 (1986).
21. Lai, T. W. & Sen, A., *Organomet.*, 3, 866 (1984).
- 22 Brumbaugh, J S., Wittle, R. R., Parvez, M. A. & Sen, A., *Organomet.*, 9, 1735 (1990)
23. Chen, J. T. & Sen, A., *J. Am Chem Soc.*, 106, 1506 (1984).
- 24 Vetter, W. M & Sen, A., *J Organomet Chem.*, 378, 485 (1989)
25. Yamamoto, A., *Organo Transition Metal Chemistry*, Wiley Interscience Press, 246 (1986).
26. Toth, I., Elsevier, C. J , Vrieze, K & van Leeuwen, P. W N M., *Organomet.*, 11, 1598 (1992)
- 27 Zhao, A. X. & Chien, J C W , *J Polym Sci Polym Chem* , 30, 2735 (1992)
28. Batistini, A. & Consiglio, G , *Organomet.*, 11, 1766 (1992)
- 29 Wong, P. K , van Doorn, J A , Drent, E , Sudmeyer, O. & Stil, H A., *Ind Eng Chem Res* , 32, 986 (1993)
30. Chatani, Y., Takizawa, T , Murahshi, S , Sakatia, Y. & Nishimura, Y., *J Polym Sci* , 55, 811 (1961).
31. Lommerts, B. J., Klop, E. A. & Aerts, J., *J Polym Sci Part B Polym Phys* , 32, 1319 (1993).

32. Walter, E. R. & Reding, F. P., *J Polym Sci.*, 21, 561 (1956).
33. Flood, J. E., Wienkauf, D. H. & Londa M., Proceedings of the Soc. Of Plastics Eng (ANTEC), XLI, 2336 (1995)
34. Klop, E. A., Lommerts, B. J., Veurink, J, Aerts, J. & Van Puijenbroek, R. R., *J Polym Sci Part B Polym Phys*, 33, 315 (1995).
35. Ash, C. E. & Flood, J. E., Proceedings of the ACS division of Polym. Mats. Sci. & Eng, 76, 110 (1997).
36. Danforth, R. L. & Machado, J M., Proceedings of the Soc. Of Plastics Eng. (ANTEC), XLI, 2316 (1995)
37. Ash, C. E. & Waters, D. G., Proceedings of the Soc. Of Plastics Eng. (ANTEC), XLI, 2319 (1995)
38. Weinkauf, D. h., Kinneberg, P. A. & Ash, C. E., Proceedings of the Soc. Of Plastics Eng. (ANTEC), XLI, 2340 (1995).
39. Gingrich, R P., Machado, J M & Londa, M., Proceedings of the Soc Of Plastics Eng. (ANTEC), XLI, 2345 (1995)
40. Machado, J. M. & Londa, M., Proceedings of the Soc. Of Plastics Eng. (ANTEC), XLI, 2335 (1995).
41. Chien, J. C. W & Zhao, A. X., *Polym Degr Stab.*, 40, 257 (1993).
42. Copeland, C. C & Spruiell, J. E., Proceedings of the Soc. Of Plastics Eng. (ANTEC), 1800 (1997).
43. Cullity, B. D., "Elements of X-Ray Diffraction", second ed., Addison –Wesley Pub. Company, Inc., Reading (1978)

44. Copeland, C. C., "The structure-property-processing relationship for a melt spun and drawn aliphatic polyketone terpolymer fiber", M. S. Thesis, University of Tennessee, Reading (1997).
45. Kamf, G., "Characterization of Plastics by Physical Methods", Hanser Pub., Macmillin, NY, 107 (1986).
46. Desper, C.R. & Stein R. S., *J. App. Phys.*, **37**, 3990 (1966).
47. Alexander, L. E., "X-Ray Diffraction Methods in Polymer-Science", Robert E. Krieger Pub. Company, NY, Reading (1969).
48. Holt, G. A., personal communication.
49. Samuels, R. J., "Structured Polymer Properties", John Wiley & Sons, NY, Reading (1974).
50. Smith, P. & Lemstra, P. J , *Polymer*, **21**, 1342 (1980).
51. Barham, P. J. & Keller, A., *J Mat Sci* , **20**, 2281 (1985).
52. Nadella, P. H., Spruiell, J. E. & White, J. L. , *J Appl Poly Sci* , **22**, 3121 (1978).
53. Bodaghi, H. , Spruiell, J. E. & White, J. L., *Intern Poly Proc* , **3**, 100 (1988).
54. Cho, W. J., Lee, W. J. & Chun, B. C. , *J Appl Poly Sci* , **62**, 771 (1996).
55. Smook, J. , Vos., G. J. H. & Doppert H. L. , *J Appl Poly Sci* , **41**, 105 (1990).
56. Bhatt, G., personal communication.
57. Taylor, W. N. & Clark, E. S., *Poly Eng & Sci* , **18**, 518 (1978).
58. Sze, G. M., Spruiell, J. E. & White J. L., *J Appl Poly Sci* , **20**, 1823 (1976).
59. Kitao, T. Spruiell, J. E. & White J. L., *Poly Eng & Sci* , **19**, 761 (1979).
60. Statton, W. O., *J Poly , Sci* , **41**, 143 (1959).

61. Pakula, T. & Fischer, E. W., *J Poly Sci . Poly Phys* , 19, 1705 (1981).
- 62 Fu-Min, L., Goswami, B. C. & Duckett, K. E., *J Appl Poly Sci* , 30, 1859 (1985).
63. Encyclopedia of Polymer Science, John Wiley & Sons, 11, 425 (1988).
- 64 Encyclopedia of Polymer Science, John Wiley & Sons, 11, 427 (1988).
- 65 Prevorsek, D. C., Harget, P. J. & Sharma, R. K., *J Macromol Sci - Phys* , **B-8** (1-2), 127 (1973)
- 66 Prevorsek, D. C , *Ibid* , **C, 32**, 343 (1971).
67. Peterlin, A., *J Macromol Sci* , **B6** (4), 583 (1972).
- 68 Peterlin, A., *J Polym Sci* , **C, 32**, 297 (1971).

APPENDICES

APPENDIX 1

CALCULATION OF THE RESIDENCE TIME

Randcastle Microtruder

Screw diameter: $\frac{1}{4}$ "

Channel width: $\frac{1}{4}$ "

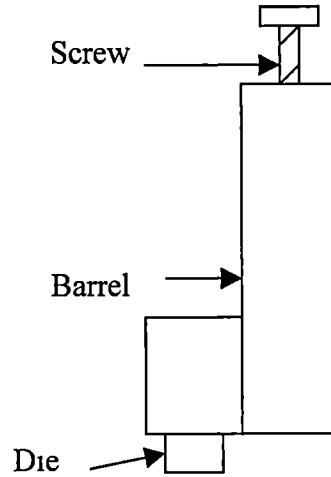
Channel depth: 0.03"

Number of turns: 12

Melt has to travel some additional distance

From the barrel to the die through a zone

That has a diameter of $\frac{1}{4}$ " and is 3.5" long.



$$\therefore \text{Total volume, } V = 0.03 \times \frac{1}{4} \times \left(\pi \times \frac{1}{4} \right) \times 12 + 3.5 \times \pi \times \left(\frac{1}{8} \right)^2 = 0.242 \text{ m}^3 \quad (\text{A2.1})$$

Taking $\rho = 0.88 \text{ g/cm}^3$ (for PE) and $Q = 3.5 \text{ g/min}$

we get $Q = 3.972 \text{ cm}^3$

$$\therefore t = \frac{V}{Q} = \frac{0.242 \times 2.54^3}{3.972} = 0.998 \text{ min} \quad (\text{A2.2})$$

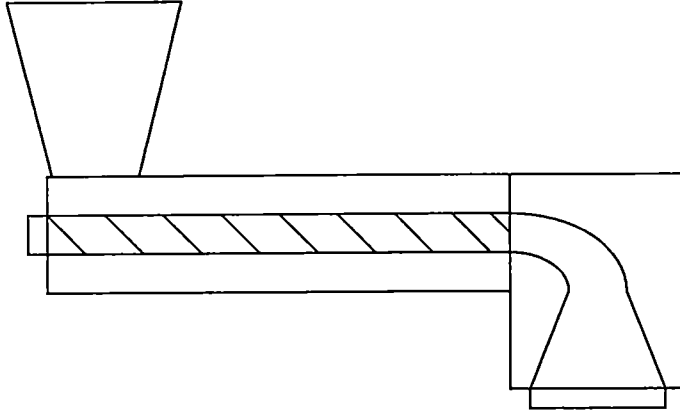
Residence time for regular melt spinning equipment with a 1" diameter screw.

Screw inner diameter: 0.99"

Barrel length: $23 \frac{5}{16}$ "

Square pitched angle: 17.6°

Channel Height: 0.1825" for first 8 turns and 0.047" for the next 7 turns.



$$\therefore H_{av} = \frac{0.1825 \times 8 + 7 \times 0.047}{15} = 0.11926'' \quad (\text{A2.3})$$

$$\text{Channel width} = \left(1 - \frac{1}{8}\right) \cos \theta = 0.833'' \quad (\text{A2.4})$$

$$\text{Volume of the melt in the barrel} = 15 \times 0.833'' \times 0.1196 \times \pi \times 0.99'' = 4.635 \text{ in}^3 \quad (\text{A2.5})$$

For the diverging section at the end of the extruder tip:

$$V_{\text{div}} = \pi \times \left(\frac{1.252}{2}\right)^2 \times \frac{19}{32} + \left(\frac{3}{8 \times 2}\right)^2 \times \pi \times \frac{11}{4} + \text{Volume of the conic section, } V_{\text{conic}} \quad (\text{A2.6})$$

$$V_{\text{conic}} = \int_{11/16}^{0.626} \pi \left(0.6378y + \frac{3}{16}\right)^2 dy \quad (\text{A2.7})$$

$$= \int_{11/16}^{0.626} \pi \left(0.4068y^2 + 0.239y + \frac{9}{256}\right) dy$$

$$= \pi \times 0.4068 \times y^3 \Big|_{3/8}^{0.626} + \pi(239) \times y^2 \Big|_{3/8}^{0.626} + \frac{9\pi}{256} \times y \Big|_{3/8}^{0.626}$$

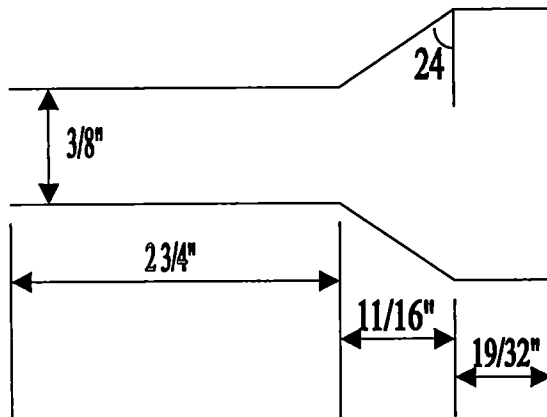
$$= 0.204 \text{ in}^3$$

$$V_{\text{div}} = 1.805 \text{ in}^3$$

$$V = 4.635 + 1.805 = 6.44 \text{ in}^3$$

At a mass throughput rate of 30 g/min and a melt density of 0.85 g/cm³

$$T = \frac{V}{Q} = \frac{6.44 \times (2.54)^3}{\frac{30}{0.85}} = 2.99 \text{ min} \quad (\text{A2.8})$$



APPENDIX 2

CALCULATION OF $\langle \cos^2 \phi_{c,z} \rangle$ FROM THE INTENSITY DISTRIBUTION OF (110) & (210) PEAKS (WHEN $\alpha = 0^\circ$)

Polyketone fiber: β -form

$$a = 7.97 \text{ \AA}$$

$$b = 4.76 \text{ \AA}$$

$$c = 7.57 \text{ \AA}$$

Reflections at 110 and 210 planes

For (hk0) planes,

$$g = 0; \text{ so that } e^2 + f^2 = 1 \quad (\text{A1.1})$$

Thus,

$$\langle \cos^2 \phi_{hk0,z} \rangle = e^2 \langle \cos^2 \phi_{u,z} \rangle + f^2 \langle \cos^2 \phi_{v,z} \rangle \quad (\text{A1.2})$$

Or, on solving for two reflections and using the orthogonality relationship (e_1, f_1 for 110 and e_2, f_2 for 210 peak)

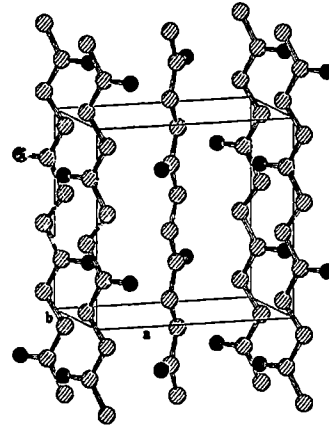
we get,

$$\langle \cos^2 \phi_{c,z} \rangle = 1 + \frac{(2e_2^2 - 1) \langle \cos^2 \phi_{1,z} \rangle - (2e_1^2 - 1) \langle \cos^2 \phi_{2,z} \rangle}{e_1^2 - e_2^2} \quad (\text{A1.3})$$

calculation of e_1 and e_2 :

e_1 & e_2 are the direction cosines between (110) and (210) with 'a' axis respectively.

To evaluate these we need to find the cosine of the angle between the normal to the reflecting plane and the respective axis. In the reciprocal lattice system:



β

$\bar{r}^* \perp$ reflecting plane

For orthorhombic system;

$$\bar{r}^*_{hkl} = h \bar{a}^* + k \bar{b}^* + l \bar{c}^* \quad (\text{A1.4})$$

$$\bar{r}^*_{hkl} = \frac{h}{a} \left(\frac{\bar{a}}{|\bar{a}|} \right) + \frac{k}{b} \left(\frac{\bar{b}}{|\bar{b}|} \right) + \frac{l}{c} \left(\frac{\bar{c}}{|\bar{c}|} \right) \quad (\text{A1.5})$$

if unit vectors along \bar{a} , \bar{b} & \bar{c} axes be \bar{i} , \bar{j} & \bar{k} ,

we get:

$$\bar{r}^*_{hkl} = \frac{h}{a} \left(\frac{\bar{a}}{|\bar{a}|} \right) + \frac{k}{b} \left(\frac{\bar{b}}{|\bar{b}|} \right) = h \frac{\bar{i}}{a} + k \frac{\bar{j}}{b} \quad (\text{A1.6})$$

$$n^*_{110} = \frac{\frac{\bar{i}}{a} + \frac{\bar{j}}{b}}{\sqrt{\frac{1}{a^2} + \frac{1}{b^2}}} \quad \text{and} \quad (\text{A1.7a})$$

$$n^*_{210} = \frac{\frac{2\bar{i}}{a} + \frac{\bar{j}}{b}}{\sqrt{\frac{4}{a^2} + \frac{1}{b^2}}} \quad (\text{A1.7b})$$

$$\text{or } e_1 = e_{110} = n^*_{110} \cdot \bar{i} = \frac{\frac{\bar{i}}{a}}{\sqrt{\frac{1}{a^2} + \frac{1}{b^2}}} = \frac{b}{\sqrt{a^2 + b^2}} = 0.5127 \text{ or } \theta = 59.15^\circ \quad (\text{A1.8a})$$

$$e_2 = e_{210} = n^*_{210} \cdot \bar{i} = \frac{\frac{2\bar{i}}{a}}{\sqrt{\frac{4}{a^2} + \frac{1}{b^2}}} = \frac{2b}{\sqrt{a^2 + 4b^2}} = 0.7667 \text{ or } \theta = 39.94^\circ \quad (\text{A1.8b})$$

$$\therefore \langle \cos^2 \phi_{c,z} \rangle = 1 + \frac{(2e_2^2 - 1) \langle \cos^2 \phi_{1,z} \rangle - (2e_1^2 - 1) \langle \cos^2 \phi_{2,z} \rangle}{e_1^2 - e_2^2}$$

$$\text{or } \langle \cos^2 \phi_{c,z} \rangle = 1 - 0.54 \langle \cos^2 \phi_{110,z} \rangle - 1.46 \langle \cos^2 \phi_{210,z} \rangle \quad (\text{A1.9})$$

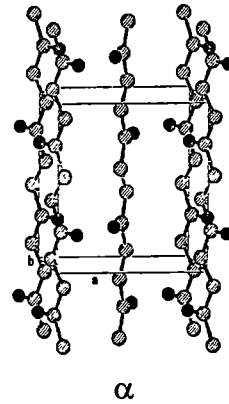
Likewise, for the α form, taking different values of a, b & c, an expression similar to given by A1.9 can be obtained:

For α form

$$a = 6.91 \text{ \AA}$$

$$b = 5.12 \text{ \AA}$$

$$c = 7.6 \text{ \AA}$$



$$e_1 = \frac{2b}{\sqrt{a^2 + 4b^2}} = 0.595 \text{ and} \quad (\text{A1.10})$$

$$e_2 = \frac{2b}{\sqrt{a^2 + 4b^2}} = 0.829 \quad (\text{A1.11})$$

This gives,

$$\langle \cos^2 \phi_{c,z} \rangle = 1 - 1.125 \langle \cos^2 \phi_{110,z} \rangle - 0.875 \langle \cos^2 \phi_{210,z} \rangle \quad (\text{A1.12})$$

APPENDIX 3

CALCULATION OF UNIT CELL DIMENSIONS OF THMP, 9.6 DR FIBERS.

The d-spacing of any crystal plane with indices hkl , is given by:

$$d = \frac{1}{\sqrt{\frac{h^2}{a^2} + \frac{k^2}{b^2} + \frac{l^2}{c^2}}} \quad (\text{A3.1})$$

Taking $\lambda_{\text{mean}} = 1.541838 \text{ \AA}$, and using bragg's law, the following data is generated:

Table A3.1 X-ray data for different crystal planes in oriented THMP fiber

$2\theta^*$	θ	$\sin \theta$	$d = \lambda/(2 \sin \theta)$ A	hkl	$(1/d)^2$
21.74	10 87	0 188581	4.087993	110	0.059838
22 09	11 045	0.191579	4.024007	011	0.061756
23 49	11 745	0.203556	3.787251	002	0 069719
24 82	12.41	0 214905	3.587241	111	0 077710
29 09	14.545	0.251140	3 069674	210	0.106124
32 03	16 015	0.275889	2.794308	112	0.128071
37.49	18.745	0.321356	2.398950	212	0 173763
38 4	19.2	0.328866	2 344169	310	0.181979
40 29	20 145	0.344397	2 238459	013	0.199572
41 83	20 915	0.356982	2.159542	113	0.214425
44 14	22 07	0.375739	2 051740	220	0 237550

*Note · The 2θ value for the 200 reflection was not used as it was significantly overlapped with the 110 and could not be determined accurately

The above data was obtained after running the 2θ scan of the L1000 filaments on a Philips x-ray scan apparatus. The indexing of the peaks is done by comparing our data with the corresponding 2θ angles obtained by Chatani and Lommerts From the d-spacing values above and Equation A3.1, we get the following relationships:

$$(110) \cdot 0.059838 = \frac{1}{a^2} + \frac{1}{b^2} \quad f$$

$$(011) \cdot 0.061756 = \frac{1}{b^2} + \frac{1}{c^2} \quad g$$

$$(002) \cdot 0.069719 = \frac{4}{c^2} \quad h$$

$$(111) \cdot 0.07771 = \frac{1}{a^2} + \frac{1}{b^2} + \frac{1}{c^2} \quad i$$

$$(210) \cdot 0.106124 = \frac{4}{a^2} + \frac{1}{b^2} \quad j$$

$$(212) \cdot 0.173763 = \frac{4}{a^2} + \frac{1}{b^2} + \frac{4}{c^2} \quad k$$

$$(310) \cdot 0.181979 = \frac{9}{a^2} + \frac{1}{b^2} \quad l$$

$$(013) \cdot 0.199573 = \frac{1}{b^2} + \frac{9}{c^2} \quad m$$

$$(113) \cdot 0.214426 = \frac{1}{a^2} + \frac{1}{b^2} + \frac{9}{c^2} \quad n$$

$$(220) \cdot 0.23755 = \frac{4}{a^2} + \frac{4}{b^2} \quad o$$

Solving any three equations simultaneously will give the values of a , b & c , the unit cell dimensions. For instance, the combination of equations f, g & h gives $a = 8.029 \text{ \AA}$, $b = 4.749 \text{ \AA}$ and $c = 7.5745 \text{ \AA}$. Similarly other equations are used and solved for real values of a , b & c . Non-real and negative values were rejected. Table A3.2 lists all possible combinations of the above relationships and tabulates the computed values of a , b & c . The equation solver Maple was used for solving the simultaneous equations. The values obtained are $a = 8.09 \text{ \AA}$, $b = 4.74 \text{ \AA}$ and $c = 7.59 \text{ \AA}$.

Table A3.2 Computed lattice cell constants for oriented, THMP fiber.

Combination	a Å	b Å	c Å
<i>fgh</i>	8.02915	4.7497	7.5745
<i>fhi</i>	-	-	-
<i>fij</i>	8 050740011	4.745291251	7.480203656
<i>fjk</i>	8.050740011	4.745291251	7.690089717
<i>flk</i>	8 093087909	4.73671065	7 662771975
<i>flm</i>	8.093087909	4.73671065	7.619943097
<i>fmn</i>	8.205270625	4.714831079	7 63015509
<i>fno</i>	-	-	-
<i>fgj</i>	8 050740011	4.745291251	7.592625574
<i>fgk</i>	8 116679912	4.732008357	7.647862024
<i>fgl</i>	8 093087909	4.73671065	7.628116804
<i>fgm</i>	8 082111087	4.738917395	7.618923229
<i>fgn</i>	8 095522229	4 736222894	7.63015509
<i>fgo</i>	-	-	-
<i>fhj</i>	8.050740011	4.745291251	7.574507868
<i>fhk</i>	8.237966427	4.708676889	7.574507868
<i>fhl</i>	8 093087909	4.73671065	7.574507868
<i>fhm</i>	7.639878663	4 839041712	7.574507868
<i>fhn</i>	-	-	-
<i>fho</i>	-	-	-
<i>fij</i>	8 050740011	4.745291251	7.480203656
<i>fik</i>	8 407914564	4 678195122	7.480203656
<i>fil</i>	8 093087909	4.73671065	7 480203656
<i>fin</i>	-	-	-
<i>fio</i>	-	-	-
<i>fjl</i>	-	-	-
<i>fjm</i>	-	-	-
<i>fjn</i>	8.050740011	4.745291251	7 615987767
<i>fjo</i>	8 050740011	4 745291251	7.63015509
<i>fkm</i>	-	-	-
<i>fkn</i>	8 152833252	4.724908048	7 625429077
<i>fko</i>	8.145149937	4.726406435	7.63015509
<i>fln</i>	-	-	-
<i>flo</i>	8 093087909	4.73671065	7.63015509
<i>fmo</i>	-	-	-
Average	8.088094966	4.738530895	7.593298731

VITA

Pankaj Gupta was born on November 21, 1977 in Rohtak, in the state of Haryana, India. He attended public schools in Haryana and graduated from Apeejay Public School, Faridabad in June 1994. He entered the Indian Institute of Technology, Delhi, India where he graduated with a Bachelor of Technology (B. Tech) in Textile Technology in June 1998. During his undergraduate training he did his internship at Winsome Textile Industries, Baddi, HP, India. Thereafter, in Fall 1998, he joined University of Tennessee, Knoxville for his M S degree in Polymer Engineering.

The author is a member of the Society of Plastics Engineers and the American Society of Materials